Synthesis of glycerol carbonate from glycerol and urea by using gold-supported catalysts.

Marilien Van Oudenhove

Supervisors: Prof. Pascal Van Der Voort, Prof. An Verberckmoes
Counsellor: Dr. Willinton Yesid Hernández Enciso

Master's dissertation submitted in order to obtain the academic degree of Master of Science in de industriële wetenschappen: chemie

Vakgroep Anorganische en Fysische Chemie
Chairman: Prof. dr. Isabel Van Driessche

Department of Industrial Technology and Construction
Chairman: Prof. Marc Vanhaelst

Faculty of Engineering and Architecture
Academic year 2014-2015

UNIVERSITEIT GENT

Synthesis of glycerol carbonate from glycerol and urea by using gold-supported catalysts.

Marilien Van Oudenhove

Supervisors: Prof. Pascal Van Der Voort, Prof. An Verberckmoes
Counsellor: Dr. Willinton Yesid Hernández Enciso

Master's dissertation submitted in order to obtain the academic degree of Master of Science in de industriële wetenschappen: chemie

Vakgroep Anorganische en Fysische Chemie
Chairman: Prof. dr. Isabel Van Driessche

Department of Industrial Technology and Construction
Chairman: Prof. Marc Vanhaelst

Faculty of Engineering and Architecture
Academic year 2014-2015

UNIVERSITEIT GENT

Admission to loan

Ghent, May 2015

The author,

Marilien Van Oudenhove

Foreword

A master's dissertation is often interpreted as a piece of evidence that the student is capable of fulfilling a research, related to his or her field of study, with success. I think this perception is true, however, the social aspect of bringing a master thesis to completion is also a significant factor. For example, the cooperation between colleagues or the professional relationship between the student and the mentor are at least two very important aspects of working on a master thesis that have to be taken into account. This because those two social aspects provide the input of new ideas and the constructive search for solutions. Herewith, I would like to thank the people who contributed to all of this.

To begin with, I would really like to thank my mentor, Dr. Willinton Yesid Hernández Enciso. He was always around if I had a question or a problem. He also gave advice when it was necessary and he guided me through this assignment until the end. With the support of Yesid, I was sure that I would finish this thesis with success.

Besides, I would like to thank my supervisors Prof. Dr. Pascal Van Der Voort and Prof. Dr. Ir. An Verberckmoes for giving me the chance to be able to cooperate with this project. With their critical view on things they provided the necessary adjustments, but also new insights during the four thesis meetings.

I also want to give thanks to the COMOC group in general. In the coffee room, in the office, in the lab and even in the hallway the atmosphere was always cheerful. This is certainly one of the reasons that I liked to be present in the S3 every day.

Finally, I want to thank my parents, my closest friends, in particular Peter Van Puyvelde, and my boyfriend for the moral support during the academic year. They gave me the courage to carry on and they were always there for me when I needed them to.

Marilien Van Oudenhove

Abstract

Gold nanoparticles supported on magnesium oxide (MgO) are reported as efficient catalysts for the synthesis of glycerol carbonate from glycerol and urea. The catalytic transformation of glycerol into glycerol carbonate is an interesting reaction that uses two cheap and easily available products, since glycerol is a by-product of the production of biodiesel and urea represents a source of carbon dioxide (CO_2).

Magnesium oxide is applied as basic support material. The support is synthesized by a hydrothermal dissolution-recrystallization method. The goal of this soft templating technique is to obtain magnesium oxide support materials with a surface area as high as possible, since this property is partially responsible for the amount of Lewis basic places, situated on the support, which are necessary to catalyze the reaction.

Once the mesoporous magnesium oxide supports are synthesized and characterized, the most promising supports are impregnated with gold through a deposition-precipitation method using urea as precipitation agent. Gold is used because it acts as a Lewis acid and therefore it shows good activities for the glycerolysis of urea. With this deposition method, very small gold nanoparticles on the surface of the supports are acquired.

Before and after the catalytic reaction, the catalysts are characterized with different instrumental techniques, such as XRD, XRF, TEM and nitrogen adsorption, in order to know something about the changes the catalyst goes through regarding its crystal structure, its porosity, the leaching of gold and the size of the gold nanoparticles. Furthermore, the best performing gold catalyst in terms of conversion of glycerol, yield of glycerol carbonate and selectivity towards glycerol carbonate, is tested again by a second run to investigate the reusability of the catalyst.

Extended abstract

Goud beladen op magnesiumoxide (MgO) staat bekend als een effectieve katalysator voor de bereiding van glycerolcarbonaat uitgaande van glycerol en urea. De omzetting van glycerol naar glycerolcarbonaat is een boeiende katalytische reactie die gebruik maakt van twee goedkope en gemakkelijk verkrijgbare grondstoffen, want glycerol is een bijproduct van de productie van biodiesel en urea doet zich voor als bron voor koolstofdioxide (CO_2).

Magnesiumoxide wordt gebruikt als basisch dragermateriaal. Het dragermateriaal wordt gemaakt via een hydrothermale oplossings-herkristallisatie methode. Het doel van deze *soft templating* techniek is het verkrijgen van magnesiumoxide dragermaterialen met een zo hoog mogelijk specifiek oppervlak. Dit is nodig omdat een hoog specifiek oppervlak mede zorgt voor een grote hoeveelheid aan Lewis basische plaatsen op het oppervlak. Deze basische plaatsen zijn eveneens verantwoordelijk voor het katalyseren van de reactie.

Wanneer de mesoporeuze magnesiumoxide dragermaterialen bereid en gekarakteriseerd zijn, worden de meest veelbelovende dragers beladen met goud via een depositie-precipitatie methode waarbij urea gebruikt wordt als precipitatieagens. Goud wordt aangewend omdat het handelt als Lewis zuur en bijgevolg vertoont het een goede activiteit voor de bereiding van glycerolcarbonaat uitgaande van glycerol en urea. Met behulp van deze depositiemethode worden zeer kleine gouden nanopartikels op het oppervlak van het dragermateriaal verkregen.

De katalysatoren worden gekarakteriseerd zowel voor als na de reactie met verschillende instrumentele technieken zoals XRD, XRF, TEM en stikstof adsorptie met als doel informatie te bekomen over de veranderingen die de katalysator ondervindt betreffende de kristalstructuur; de porositeit, het uitlogen van het goud en de afmetingen van de goud nanopartikels. Bovendien wordt de katalysator die de beste resultaten vertoont omtrent de conversie van glycerol, de opbrengst van glycerolcarbonaat en de selectiviteit naar glycerolcarbonaat toe opnieuw getest aan de hand van een tweede run, om de herbruikbaarheid ervan te achterhalen.

Table of contents

List of abbreviations

Au/MgO(CTAB)	Gold deposited on MgO synthesized with CTAB
Au/MgO(P123)	Gold deposited on MgO synthesized with P123
BET	Brunauer, Emmet and Teller
BJH	Barrer, Joiyner and Halenda
CCD	Charge-coupled device
CMC	Critical micelle concentration
CMT	Critical micelle temperature
CommMgO	Commercial magnesium oxide
CPB	Cetylpyridinium bromide
CTAB	Cetyltrimethylammonium bromide
DDAO	Dimethyldodecylamine oxide
DEGME	Diethyleneglycolmonomethylether
DP	Deposition-precipitation
DRIFTS	Diffuse reflectance infrared Fourier transform spectroscopy
EISA	Evaporation-induced self-assembly
F127	$PEO_{106}PPO_{70}PEO_{106}$
FT-IR	Fourier transform infrared spectroscopy
GC	Glycerol carbonate
GC	Gas chromatography
GC-MS	Gas chromatography and mass spectrometry
HAP	Hydroxyapatite
HAS	High surface area
IR	Infrared
IUPAC	International Union of Pure and Applied Chemistry
LDHs	Layered double hydroxides
LSA	Low surface area
MgO(CTAB)	Magnesium oxide synthesized with the surfactant CTAB
MgO(P123)	Magnesium oxide synthesized with the surfactant P123
NMR	Nuclear magnetic resonance
ODO	2-oxo-1,3-dioxolane
P123	$PEO_{20}PPO_{70}PEO_{20}$
PEO	Polyethylene oxide
PID	Proportional-integral-derivative

PPO	Polypropylene oxide
RF	Response factor
SDS	Sodium dodecyl sulfate
SEM	Scanning electron microscopy
TCD	Thermal conductivity detector
TEM	Transmission electron microscopy
TPD	Temperature-programmed desorption
UPS	Ultraviolet photoelectron spectroscopy
UV-VIS	Ultraviolet-visible
XPS	X-ray photoelectron spectroscopy
XRD	X-ray diffraction spectroscopy
XRF	X-ray fluorescence spectroscopy

PART I

Literature survey

1 General concepts

1.1 Introduction

Glycerol carbonate (GC) is a valuable raw chemical. This small molecule, with a molar weight of 118.09 g/mol, is one of the glycerol derivatives that attract more scientific and industrial interest as a result of its excellent physical and chemical properties and of its variety of potential end uses due to its wide reactivity. The reaction of glycerol with urea provides a sustainable route to become glycerol carbonate.

The synthesis of glycerol carbonate grants an alternative way to revalue waste glycerol produced in large quantities during the production of biodiesel. Biodiesel is a familiar term for the fatty acid methyl esters formed from the transesterification of vegetable oils with methanol. Biodiesel can be produced from many feedstocks, but its production typically leads to the same by-product of glycerol with an amount at one-tenth of biodiesel production. At the present, the quantity of glycerol produced for industrial utilization globally is around 160 000 tonnes per year and this amount is increasing at an annual rate of 2,8%. Moreover, the production of biodiesel is growing at an annual rate of 5,5%. So an overflow of glycerol is expected in the near future. Due to the rapid decrease in its price, new methods for converting glycerol into high value-added chemicals, such as 1,2-propanediol, dihydroxyacetone, acrolein, hydroxyaceton and glycerol carbonate, are being developed. Among these products, glycerol carbonate is one of the most attractive derivatives of glycerol because of its high reactivity with alcohols, amines, ketones, carboxylic acids and isocyanates.

The reaction of glycerol with urea to form glycerol carbonate (also glycerin carbonate or 4-hydroxymethyl-2-oxo-1,3-dioxolane) is a very interesting process that utilizes two cheap and readily available raw materials. After all, urea represents an activated form of carbon dioxide (CO_2). The reaction between CO_2 and ammonia (NH_3) producing urea is the most important process involving the chemical utilization of CO_2.

The use of CO_2 as a platform chemical is an elegant and sustainable way to face the challenge of reducing the effect of CO_2 emissions. During the glycerolysis of urea, glycerol carbonate and also NH_3 are formed. This ammonia can be easily converted back to urea by reaction with carbon dioxide. Thus, this reaction is very important since it is a chemical cycle that, overall, results in the chemical fixation of CO_2. [1-4]

1.2 Applications of glycerol carbonate

In the last few years, research in the synthesis of glycerol carbonate has increased. GC has excellent properties such as low toxicity, low flammability, good biodegradability, water-soluble, a high boiling point and a high flash point. Fig. 1 shows the structural formula of glycerol carbonate.

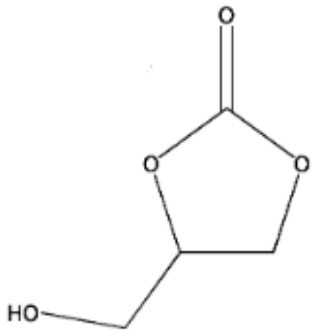

Fig. 1. Structural formula of glycerol carbonate. [7]

Combination of bio-based origin and wide reactivity has made GC a very promising green chemical in a variety of both direct and indirect applications. GC can be used as a protic solvent for general purpose, for nuclear magnetic resonance (NMR) analysis and for soluble enzymatic systems. GC is used in lithium-ion batteries as well due to its high dielectric constant. This high dielectric constant supplies better lithium solvation properties. In other words, glycerol carbonate permits the dissolution of larger quantities of lithium salts that are mostly used in lithium-ion batteries. In addition, GC is utilized as nail lacquer gel remover, as emulsifier, as plasticizer or as wetting agent in cosmetics. Because of its low flammability and bio-based origin GC doesn't cause drying and cracking of the nails or skin irritation. Other important direct applications where glycerol carbonate is used are in detergents, as plant vitalizer, as a component in membranes for gas separation, etc.

GC has an almost unique number of reactive sites: the three carbon atoms of the dioxolane ring and the pendant hydroxyl moiety. GC can react both as a nucleophile through its hydroxyl group, and as an electrophile through its ring carbon atoms. These reactive sites open numerous possibilities for using glycerol carbonate as a raw material that can be converted in chemical intermediates, which are then useful in the production of surfactants and polymers. This is an indirect approach to synthesize polymers which can be used in manufacturing useful materials such as coatings, adhesives, foams and so on. [5-7]

1.3 Different synthesis routes forming glycerol carbonate

The interest for developing synthetic procedures for glycerol carbonate manufacturing is growing parallel with its applications. Whatever the selected synthetic strategy for industrial manufacturing, it is obvious that it has to meet some basic criteria to be industrially achievable:

- If catalytic, a cheap and easily separable and recyclable catalyst must be used.
- The separation and purification methods have to be uncomplicated.
- The use of solvents has to be avoided or minimized.
- A high conversion and selectivity has to be obtained to increase productivity and to minimize capital investment.
- A low reaction time is required.
- The reaction has to be intrinsically safe. Therefore, both highly inflammable and toxic chemicals must be avoided.

According to these criteria not all the synthesis methods will be discussed herein. Only the most relevant synthesis routes starting from glycerol will be presented in this manuscript. [7]

1.3.1 Carbonation of glycerol with CO or CO_2

Several research groups have been investigating the direct synthesis of glycerol carbonate by conversion of glycerol with carbon monoxide or carbon dioxide.

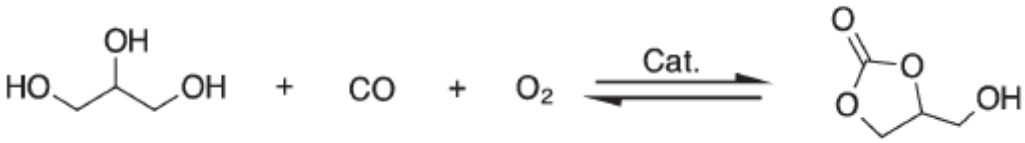

Fig. 2. Synthesis of glycerol carbonate from glycerol and carbon monoxide. [6]

Glycerol carbonate can be synthesized through the reaction of glycerol with carbon monoxide and oxygen in the presence of a catalyst or additional reactants (fig. 2). This synthetic route has limited uses because of the toxicity of carbon monoxide and the inherent difficulty to handle it safely both at laboratory and industrial scales.

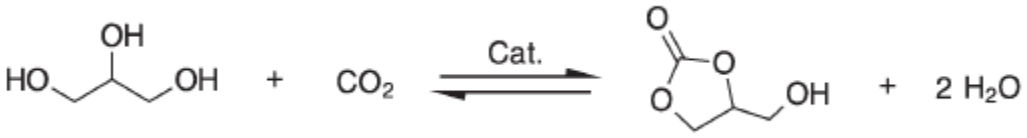

Fig. 3. Synthesis of glycerol carbonate from glycerol and carbon dioxide. [6]

Glycerol carbonate can be obtained by reacting glycerol with carbon dioxide as well, in the presence of a catalyst (fig. 3). This reaction seems to be the obvious choice to synthesize glycerol carbonate given that both are green chemicals commercially available at a low price. However, this synthesis method is currently not realizable because of its very low conversions since carbon dioxide is a highly stable molecule. Therefore, a significant amount of energy and very active catalysts are required for the conversion of CO_2. [5-7]

1.3.2 Transcarbonation of glycerol and a carbonate source

Transcarbonation is a chemical reaction similar to transesterification. It is the carbonate exchange reaction between alcohols and carbonate sources. A nucleophile attack of the carbon atom of the carbonate group by the oxygen atom of the hydroxyl group of the alcohol takes place. This leads to the conversion from one carbonate to another. Therefore, glycerol carbonate can be acquired by the transcarbonation of a carbonate source with a 1,2-diol such as glycerol (fig. 4). There are three main types of carbonate sources: phosgene, alkylene carbonate (in particular ethylene carbonate) and dialkyl carbonate (in particular dimethyl carbonate). [6]

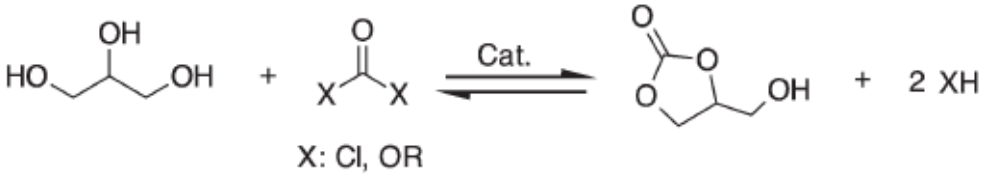

Fig. 4. Synthesis of glycerol carbonate from glycerol and a carbonate source. [6]

1.3.2.1 Phosgene

Transcarbonation using phosgene seems to be a very simple and effective way to produce organic carbonates. However because of the issues related to the handling of this corrosive and highly toxic gas, the use of phosgene is very limited. [5, 6]

1.3.2.2 Ethylene carbonate

Ethylene carbonate is the simplest molecule bearing a 2-oxo-1,3-dioxolane group (ODO group) and can be used as a carbonate source in the transcarbonation reaction with glycerol to form glycerol carbonate in the presence of a basic catalyst. Ethylene carbonate is commercially available and produced by many chemical companies. It has interesting physical properties such as a low toxicity, a low evaporation rate, biodegradability, high solvency, etc. The synthesis of glycerol carbonate is a two step reaction. First ethylene carbonate is formed through the reaction, for instance between ethylene oxide and carbon oxide. Then the glycerol carbonate synthesis takes place through transcarbonation between ethylene carbonate and glycerol. For this reaction, both strong basic homogeneous and heterogeneous catalysts can be successfully used. Although, heterogeneous catalysts are preferred because they can be easily separated and recycled. [5-7]

1.3.2.3 Dimethyl carbonate

Glycerol carbonate can also be prepared starting from glycerol and a dialkyl carbonate such as dimethyl carbonate. Dimethyl carbonate is an environmentally harmless chemical, which can be prepared from methanol and urea. It is widely studied as a carbonate source to prepare glycerol carbonate. A main difference between using ethylene carbonate and dimethyl carbonate is that the reaction equilibrium constant decreases with the temperature when using ethylene carbonate and it increases when dimethyl carbonate is used. Hence, glycerol carbonate can be obtained from ethylene carbonate and glycerol at a temperature as low as 35°C, whereas temperatures higher than 80°C are needed when starting from dimethyl carbonate. However, when using dimethyl carbonate instead of ethylene carbonate, the separation step by distillation is much easier because of the lower boiling point of dimethyl carbonate (90°C) in comparison with the boiling point of ethylene carbonate (261°C).

Thus, from a technical point of view, the key for using one or another carbonate as raw material lies in utilizing a cheap, highly efficient and easily recyclable catalyst. Compared with homogeneous basic catalysts such as NaOH and KOH, heterogeneous catalysts are preferred because they are less corrosive, safer, less expensive and more environmentally friendly. Several heterogeneous alkaline catalysts have been investigated for the synthesis of GC by transesterification of glycerol with dimethyl carbonate. CaO is a good catalyst for this reaction because of its high basicity and its sources, such is calcium carbonate or calcium acetate, are less expensive and less toxic.
Disadvantages of CaO are its vulnerability to deactivate in air and its poor reusability.
Another catalyst, hydrotalcite, has also been investigated. However, it requires a long reaction time or needs an additional solvent environment.
Hydroxyapatite ($Ca_{10}(PO_4)_6(OH)_2$, HAP), in particular KF-modified hydroxyapatite, is recently found as a promising and highly active catalyst for the synthesis of GC from glycerol and dimethyl carbonate. Yields of almost 99 % can be obtained. Although KF is a very toxic substance and its safety should be carefully considered in industrial applications. [7-11]

1.3.3 Transcarbonation of glycerol and urea

An alternative route to produce GC is the transcarbonation of glycerol and urea. Glycerol and urea are both affordable reagents and easily available. Urea is used as alternative source for carbonylation. It represents an activated form of CO_2. Urea is a particularly attractive carbonylating agent because during its glycerolysis, the only significant by-product is ammonia in the gas-phase which can be easily captured and reused to react with CO_2 forming urea according following reactions:

$$2\,NH_3 + CO_2 \rightleftharpoons NH_2COONH_4 \quad (1\text{-}1)$$

$$NH_2COONH_4 \longrightarrow CO(NH_2)_2 + H_2O \quad (1\text{-}2)$$

The formation of urea is a two-step process where the ammonia and carbon dioxide react to form ammonium carbamate, which is then dehydrated to urea. [12, 13]
The glycerolysis of urea operates without a solvent, with high selectivity and yields under very mild conditions (fig. 5).

Normally, the glycerolysis of urea has to be executed under a vacuum condition or a sweeping gas, such as nitrogen, to eliminate the simultaneously formed by-product ammonia in order to shift the chemical equilibrium towards the products. Catalysts bearing Lewis acidic sides seem to provide satisfying results with significant yields. Catalysts active for this reaction are zinc sulfate, magnesium sulfate, γ-zirconium phosphate, cobalt oxide dispersed on zinc oxide, lanthanum oxide, hydrotalcite-like materials and gold based catalysts. Estimations of the chemical equilibrium constants showed that higher temperature and lower pressure are favorable to the reaction of glycerol and urea.

From an ecological point of view, this synthetic route had the advantage of using only biobased reactants. However, this reaction still suffers from several drawbacks.

The formation of ammonia as a by-product, the uses of homogenous and/or uneasily recoverable catalysts and the relatively high reaction temperatures have negative ecological impacts on these synthesis method. [1, 2, 6, 11]

In particular, the transcarbonation of glycerol and urea is the route for producing glycerol carbonate my thesis will be focused on.

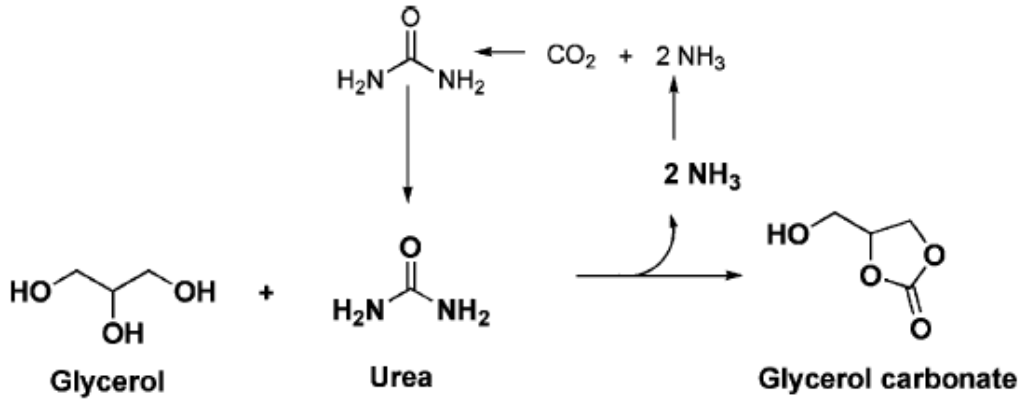

Fig. 5. Reaction setwork for glycerol carbonate synthesis using urea as CO_2 donor. [2]

2 Catalysis

2.1 Definition

According to the definition, a catalyst is a material that affects the reaction speed without consuming itself. They increase the speed of the reaction since they provide an alternative way at which a lower activation energy has to be won over. Herein the overall reaction enthalpy stays indifferent.

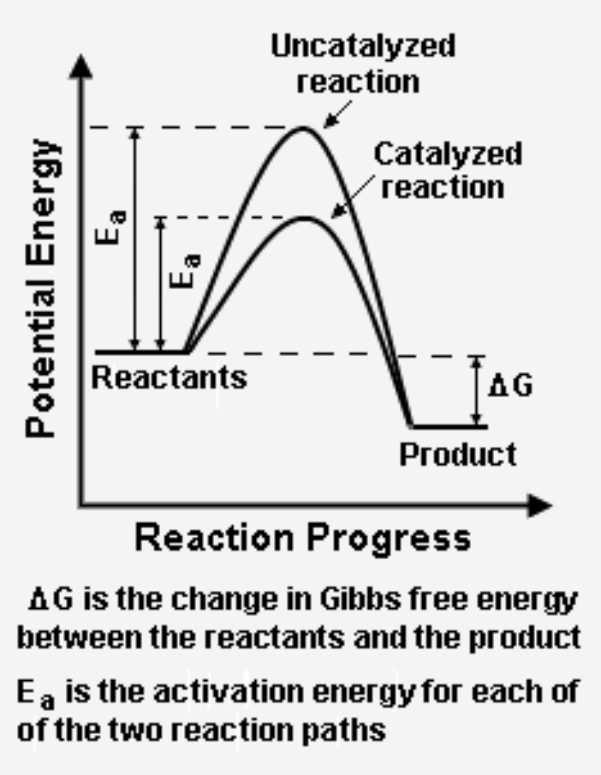

Fig. 6. Influence of the catalyst on the activation energy. [14]

Fig. 6 shows the influence of the catalyst on the activation energy. The addition of a catalyst results in the decrease of the activation energy of the reaction. Therefore, a suitable catalyst is often added in order to speed up the reaction or to allow the reaction to occur at a lower temperature. However, the search for and the synthesis of the right catalyst is challenging and there is no one single formula to prepare the perfect catalyst. [14, 15]

2.2 Different types of catalysis

A catalyst can be integrated in the reaction medium by two methods. First there is the homogeneous catalysis at which the catalyst occurs in the same phase as the reaction medium. On the other hand there is heterogeneous catalysis where catalyst and reaction medium appear in different phases. [16]

2.2.1 Homogeneous catalysis

Because of the similarity of the phases between catalyst and reaction medium, a higher collision frequency can be obtained as a result of the level of dispersion of the catalyst within the reaction medium. This leads to a large connection between the catalyst and the reactants. A disadvantage is that the process can't proceed in a continuous reaction system. For this reason homogeneous catalysts will only be used in batch reactors. A second important disadvantage is that the used catalyst can't be easily recycled because of its strong bonds with the reaction products and because they are in the same phase. Both acid and bases can be utilized as homogeneous catalysts. Also dissolved metal ions are an example of a homogeneous catalyst.
[14, 16, 17]

2.2.2 Heterogeneous catalysis

Here, the catalyst will occur in a different phase than the reaction medium. The design of this type of catalysts usually consist in a support material whereupon the active site (acid/base/metal) is impregnated. The catalysis happens through the adsorption of one or several reagents on the active site where the reaction will take place. A great advantage of this type of catalysis is that an easy separation between catalyst and reactants is possible. Therefore, the reaction can proceed uninterrupted and the method isn't just limited to batch reactions. In comparison with homogeneous catalysis, there are two disadvantages. In the first place, the distribution of the catalyst within the reaction medium will be lower. Secondly, the contact between catalyst and reactants will be decreased since a part of the active element is connected to the support. That is the reason why it is really necessary to select high surface area catalyst supports. In that way, the contact between catalyst and reactants will be high enough, even though they occur in a different state of phase.

Although, due to the immobilization of the active sites, the selectivity of the catalyst can be improved. Generally, heterogeneous catalysts are used more than homogeneous catalysts because their simple recuperation is a main factor for the efficiency of the catalyst and hence, the sustainability of the catalytic process.
[14, 16, 17]

2.3 Catalysts used for the synthesis of glycerol carbonate from glycerol and urea

Although the formation of glycerol carbonate using urea and glycerol can proceed by building up the temperature, different catalysts have been found to upgrade the rate and selectivity of the reaction. In recent years, the transcarbonation of glycerol with urea has been used for the synthesis of glycerol carbonate in both homogeneous and heterogeneous catalytic routes. It is important that the used catalysts show a well-balanced acid-base bi-functionality. This specific property is mainly responsible for the activity and selectivity during the reaction of glycerol and urea. The selectivity of a reaction is the possibility to operate and adjust where it's needed when the reaction can lead to the formation of different unwanted products. Thus, the preference for the desired product can be induced due to a good selectivity. Whereas strong Lewis acid or basic sites often promote polymerization reactions, the weak metal Lewis acid sites activate the carbonyl of the urea and the conjugated Lewis basic sites stimulate the activation of the hydroxyl group of the glycerol (fig. 7). This cooperative mechanism between the Lewis acid and basic sites is highly desirable to favor the selectivity of the reaction. [2, 5]

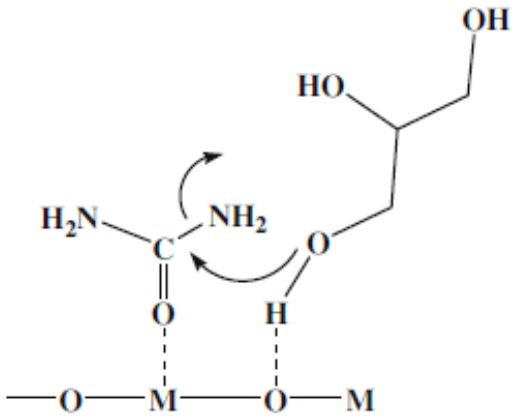

Fig. 7. Acid-base properties. [5]

2.3.1 Homogeneous catalysts

2.3.1.1 Zinc compounds

Metallic salts, organometallic salts and supported metallic compounds are used as homogeneous catalysts in the glycerolysis of urea forming glycerol carbonate. Very good results are obtained using the calcined inorganic salt $ZnSO_4$ as catalyst. Other Zn-containing solid catalysts such as zinc oxide, smectite-like catalysts and hydrotalcite are also used for the synthesis of glycerol carbonate starting from glycerol and urea. This because Zn has Lewis acid sites and those activate the carbonyl group of the urea. It has been observed that a Zn-containing species is dissolved into a liquid phase and the amount of the zinc species dissolved is well correlated with the yield of production. Therefore, the reaction proceeds homogeneously. However, the catalyst can only be partially recovered after the reaction due to the $ZnSO_4$ salt which is soluble in glycerol. In other words, this is a homogeneous catalysis reaction because catalyst and products occurs in the same phase. [5, 18]

2.3.1.2 Magnesium sulfate

Anhydrous $MgSO_4$ is also used as a homogeneous catalyst in the glycerolysis of urea. A preferred amount of this catalyst is 0.001 to 10 wt% based on glycerol.
Table 1 shows a comparison of the performance among several homogeneous catalysts for the synthesis of GC from glycerol and urea at a temperature of 130°C after three hours of reaction time for the first four types of catalysts. For $MgSO_4$ the reaction conditions are at a reaction temperature of 120°C and a six hours reaction time. [5, 18, 19]

Table 1. Comparison of the performance among several homogeneous catalysts. [5, 18]

Catalyst	Conversion (%)	Selectivity (%)
ZnO	61	69
SM(Zn)	65	75
HT(Zn/Al)	82	80
$ZnSO_4$	81	92
$MgSO_4$	65	92

Average results are obtained using zinc oxide and smectite-like catalysts. Better conversion and selectivity values are acquired using hydrotalcites and $MgSO_4$. But the best results are obtained using $ZnSO_4$ as catalyst.

2.3.2 Heterogeneous catalysts

2.3.2.1 γ-zirconium phosphate

Zirconium bis (monohydrogen orthophosphate) n-hydrate or $Zr(HPO_4)_2 \cdot nH_2O$ is of interest because of its ion exchange behavior. Zirconium phosphate is widely used in many applications including catalysis.

The product is usually prepared by mixing phosphoric acid with a soluble zirconium salt and it's gelatinous in nature and of variable composition. The chemical formula of γ-zirconium phosphate is $Zr(HPO_4)_2 \cdot 2H_2O$. A simplified schematic diagram illustrating the essential structural features of crystalline γ-zirconium phosphate (γ-ZrP) is shown in fig. 8. The structure is layered. Each layer can be considered as a two-dimensionally infinite complex molecule, which consists of a plane of roughly coplanar zirconium atoms sandwiched between two sheets of monohydrogen phosphate groups. All zirconium atoms are co-ordinated by six oxygen atoms organized in an octahedral spatial structure. Each monohydrogen phosphate group acts as a three-way bridging ligand, coordinating three different zirconium atoms through three of its oxygen atoms. The fourth non-co-ordination oxygen atom points toward a neighboring layer in the structure.

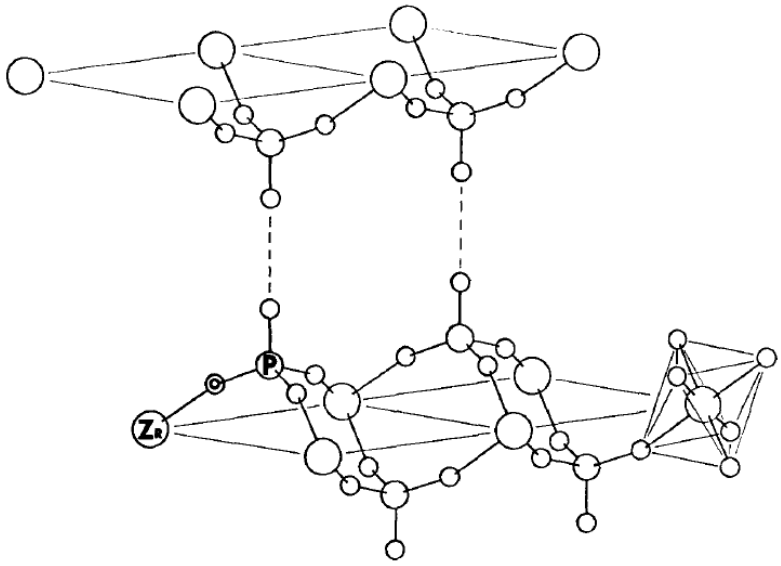

Fig. 8. Schematic illustration of the model structure proposed for γ-ZrP. [20]

The position of the water molecules are unknown, but the water molecules must lie close to the monohydrogen phosphate groups and interact with them through hydrogen bonds. Thus, the interlayer attractions in the proposed γ-ZrP structure are probably hydrogen bonds between the fixed monohydrogen phosphate groups through the intermediate water molecules. The distance between two layers is determined by the phosphate OH-groups and the molecules of water and it is about 12,25 Å. γ-ZrP can be loaded with large organic cations, naked metal ions or metal complexes which occupy interlayer positions and interact through H-bonding with P-O or P-OH groups.

It is known that γ-zirconium phosphate shows a good activity and a high selectivity as catalyst used in the glycerolysis of urea, since it manages to obtain conversions of glycerol of around 80% and a very high selectivity of 100% under mild reaction conditions of 145°C as reaction temperature and a reaction time of three hours. It's an excellent catalytic material and it is easily recoverable and after calcination the catalyst is reusable in sequential cycles of reaction, maintaining the same performance for several cycles. [20-23]

An important technique used for the characterization of this catalyst is temperature-programmed desorption (TPD). This technique determines kinetic and thermodynamic parameters of desorption processes or decomposition reactions, such as the degree and the nature of desorption, the binding energy and the population of the bonding state. A sample is heated with a temperature program and the partial pressures of the desorbed gasses are measured with, for example, mass spectrometry. [20, 24]

2.3.2.2 Cobalt oxide dispersed on zinc oxide

Co_3O_4 nanoparticles dispersed on zinc oxide are highly active in the transformation of renewable materials through transcarbonylation of glycerol with urea. The activity of the nanoparticles is adjusted by their interaction with the ZnO support, which peculiarly depends on the impregnation method. One method is a low-energy dry mixing procedure, resulting in a zinc-cobalt interaction that stabilizes the Co^{2+} sites. Those room-temperature prepared Co_3O_4/ZnO systems show catalytic behavior in the production of glycerol carbonate reaching conversions up to 69% affording nearly a selectivity of 100%. Another method is the conventional impregnation of a ZnO support with an aqueous solution of a cobalt oxide precursor such as $Co(NO_3)_2 \cdot 6H_2O$. With this kind of catalysts, ZnO acts as a heterogeneous catalyst because of the formation of a new crystalline phase, spinel $ZnCo_2O_4$.

This new phase is a stable and inactive. However, the formation of spinel $ZnCo_2O_4$ results in reducing the number of free active sites of Co_3O_4 in the system and therefore, they show a lower catalytic activity.

Co_3O_4/ZnO catalytic systems are found to be completely recoverable and reusable at least three times without any loss in activity and selectivity during the glycerolysis of urea. Besides, the samples containing more Co_3O_4 exhibit a better activity demonstrating that a good dispersion of the Co_3O_4 catalytically active sites in the interface of the system plays an important role during reaction. Furthermore, the catalytic activity depends on the specific preparation procedure and treatment temperature. For example cobalt oxide loading in Co_3O_4/ZnO increases the activity for the series prepared by dry nanodispersion at room temperature, but it performs a moderate increase for series calcined at 500°C.
[3, 25]

2.3.2.3 Lanthanum oxide

Lanthanum oxide is a rare earth oxide and it is used in many applications in environmental chemistry and exhibits interesting versatility in catalytic reactions, especially in base catalyzed reactions.

An important factor in defining the reaction mechanism is the basic character of materials such as rare earth oxides. The basic character of rare earth oxides depends on its structural or textural properties, which in turn relies on its synthesis and pretreatment conditions. Therefore many research devoted exclusively to less conventional preparation routes to create rare earth oxides with specific properties was done.

Lanthanum oxides show a good catalytic performance in the synthesis of glycerol carbonate from urea and glycerol with a conversion of glycercol of nearly 70% and a selectivity of 98%. The catalyst can be reused without significant loss in catalytic activity. Advantages such as the simple synthesis method, the high catalytic performance, the facile separation due to its heterogeneous character, and a good recyclability make this type of catalyst a candidate for application in industrial manufacture of glycerol carbonate.
[26, 27]

2.3.2.4 Mixed magnesium and aluminium oxides derived from hydrotalcites

Layered double hydroxides (LDHs), also known as hydrotalcite-like materials, are a class of two-dimensional nanostructured anionic clays whose structure is based on brucite ($Mg(OH)_2$)-like layers.

The idealized layered structure of hydrotalcite-like materials is shown in fig. 9. Their general formula is $[M^{II}_{1-x}M^{III}_{x}(OH)_2]^{x+}[A^{n-}]_{x/n}\cdot nH_2O$, in which M^{II} and M^{III} stand for divalent (M = Mg, Fe, Co, Cu, Ni or Zn) and trivalent (M = Al, Cr, Ga, Mn or Fe) cations. A is a charge-balancing anion and the value of x is equal to the molar ratio and is generally in the range 0,2 - 0,33:

$$x = \frac{M^{II}}{M^{II}+M^{III}} \tag{2-1}$$

Hydrotalcites are usually prepared by co-precipitation from metal salts in an alkaline medium at constant pH, followed by a controlled hydrothermal treatment in order to convert the layered double hydroxides into mixed oxides with high specific surface areas, homogeneous dispersion of metal cations and strong Lewis basic sites.

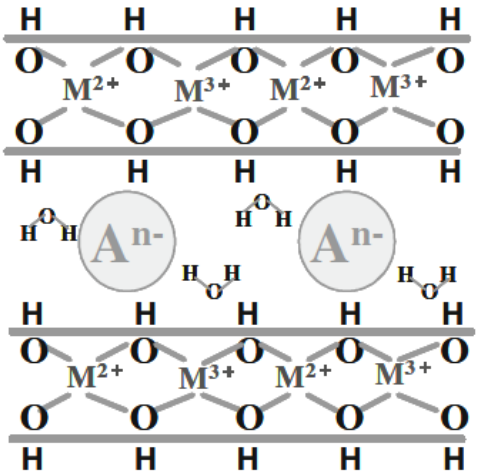

Fig. 9. The idealized structural illustration of hydrotalcite-like materials. [28]

The presence of the anionic species such as carbonate and hydroxide, is the result of the charge compensation of the brucite layer which is positively charged. Due to their unique properties such as the cation- and anion-exchangeability of this brucite layer and interlayer, their tunable surface basicity and the “memory effect” of the layered structure, hydrotalcite-like compounds have been demonstrated to be effective solid base catalysts.

The most popular hydrotalcite-like compounds are composed of magnesium-aluminium combination. Mg-Al hydrotalcite ($Mg_6Al_2(OH)_{16}CO_3 \cdot nH_2O$) is commonly used as an active solid-base catalyst for several reactions such as aldol condensation, olefin epoxidation, alkylation, hydrogenation and transesterification.

Sometimes metals like zinc, nickel or gallium are added in the preparation of hydrotalcite-like compounds, but the promotional effects of the added metal elements on the preparation of LDHs is closely related to the catalytic performances of homogeneous metal salts for the synthesis of glycerol carbonate from glycerol and urea. This is investigated by doing the same reaction with the related metal halides, such as $NiCl_2$, as homogeneous catalysts. Herefrom, it is found that the catalytic performance was not that high and comparable with that of metal impregnated LDHs. Furthermore it is found that the addition of zinc to Mg-Al hydrotalcite is more helpful than the addition of nickel or gallium for the synthesis of GC by carbonylation of glycerol with urea under solvent-free conditions, since recycling investigations point out that Mg-Zn-Al hydrotalcite catalyst maintains high stability during the reaction. Nevertheless, this reaction must be performed at a high temperature (>120°C) and a low pressure (30 - 50 mbar) to shift the equilibrium towards the formation of GC.

The calcination of hydrotalcite catalysts using the “memory effect”, which allows the reconstitution of the original hydrotalcite structure, leads to the possession of a more open structure, resulting in a higher surface area, and improved basic properties. The “memory effect” is caused by the reversible dehydration-rehydration behavior of LDHs. More specifically, hydroxyl or water molecules can re-enter into the interlayers of dehydrated or calcined LDHs because of the flexible intercalation ability in the interlayer space, which results in the recovery of the layered structure. Moreover, the basicity can be fine-tuned by the simple adjustment of the final calcination temperature. High calcination temperatures (500°C - 600°C) give catalysts with a high basicity: three kinds of basic sites, including weak OH^- sites, medium Mg/M-O pair sites and strong O^{2-} sites, ascribe high activity performances.

Two important techniques to characterize this type of materials are X-ray diffraction (XRD) and Fourier-transform infrared spectroscopy (FT-IR). Those methods are used to analyze the crystal structure of the material. [4, 28-33]

2.3.2.5 Gold-based catalysts

Heterogeneous catalysts based on gallium or zinc supported on oxides are used for the reaction of urea and glycerol forming glycerol carbonate. But supported gold catalysts display the highest activity. [2]

Gold has attracted a huge amount of interest due to its activity as both a homogeneous and heterogeneous catalyst. In particular, gold is able to selectively oxidize glycerol to glyceric acid in aqueous solution. Moreover it is a good catalyst for solvent-free selective oxidation of alcohols. When gold is supported on an appropriate oxide, in preference magnesium oxide, it can also behave as a Lewis acid catalyst. Due to their capability of acting as a Lewis acid, gold nanoparticles show high activities towards the oxidation of glycerol. These observations lead to the consideration of using gold for the glycerolysis of urea. [2, 34]

Gold nanoparticles supported on metal oxide surfaces with controllable shape can be prepared by the adsorption or deposition-precipitation methods. They can be easily handled and they are practically air-stable. [35]

In this thesis, this type of catalyst will be used for the glycerolysis of urea forming glycerol carbonate. Next chapter gives more information about this catalysts. Synthesis methods of magnesium oxide, deposition methods to impregnate magnesium oxide with gold and different factors that influence the catalytic behavior of this kind of catalysts will all be discussed in the third chapter.

3 Gold supported on magnesium oxide

3.1 Introduction

Gold catalysts have attracted huge interest because of their unique catalytic performance and, in particular, their exceptional selectivity in many reactions. [36] Generally, the catalytic behaviour of gold-supported catalysts depends on several factors:

- the size of the gold nanoparticles;
- the oxidation state of the gold nanoparticles;
- the gold-support interactions;
- the properties of the support.

3.1.1 Size of gold nanoparticles

It is known that the size of gold nanoparticles significantly influences their catalytic behaviour in many reactions. As a matter of fact, it has been found that the best performances are exhibited by smaller gold nanoparticles due to an increase of the catalytic activity. This phenomenon can be explained by taking into account that, when the particle size decreases, the number of low coordinated atoms that are acknowledged to be the active sites of the support, increases. Thus, the smaller the particle size, the better the activity properties, the higher the conversions of the reactants.
By modifying the concentration of the gold precursor, the aging time and the calcination conditions used at the final stages of the preparation of the catalyst, gold-supported catalyst with different particle sizes can be synthesized. More specifically, the increase of the gold precursor concentration leads to a decrease in particle size of gold. Moreover, extending the aging time significantly increases the size of the gold nanoparticles, presumably due to the Ostwald ripening, which is caused by the sintering of the smaller gold nanoparticles with the larger particles. [36-38]

3.1.2 Oxidation state of gold nanoparticles

The oxidation state of the gold active site is an unresolved issue in some reactions catalyzed with supported gold-based catalysts. Nevertheless the many studies on the nature of the active site, contradicting articles keep appearing declaring different oxidation states for the active gold species.

The electronic structure of the active species in the gold nanoclusters are represented as neutral [39], cationic [40] or anionic [41]. However, in the case of for example Au/Fe_2O_3, with gold in its oxidized form, Au(I) [42] or $Au^{\delta+}$ [43], are both claimed to play the dominant role in the catalytic field, for example with the catalytic oxidation of carbon monoxide. It is reported that the most active supported gold catalysts are prepared by calcination in air at 300°C, where, generally, gold precursors are transformed into metallic particles (neutral). [44]

In this thesis, the aim is to obtain fixed metallic gold nanoparticles through the calcination of the resulting Au/MgO catalyst at 300°C.

3.1.3 Gold-support interactions

3.1.3.1 Influence of the support on gold particles

It is documented that the difference in binding energy of gold on the 4f level in comparison with bulk gold varies with its support. For example fig. 10 shows that the increase of the binding energy with Au/SiO_2 (1,6 eV) is greater and starts at a larger size, than with Au/TiO_2 (0,8 eV).

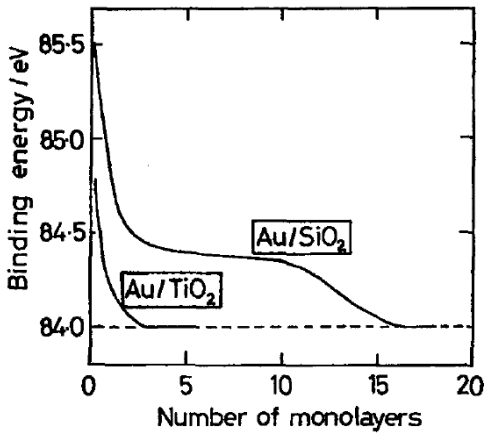

Fig. 10. Dependence of binding energy of the 4f electrons on gold coverage (number of monolayers) for the Au/TiO_2 and Au/SiO_2 systems. [45]

Other work mentions that the sequence beginning from high to low binding energy is the following:

$$Au/ZrO_2 > Au/TiO_2 > Au/Al_2O_3 \quad (3\text{-}1)$$

However, no correlation with the activity for the reaction is found. [45]
Binding energies are not only element specific, but they contain chemical information as well because the energy levels of core electrons depend slightly on the chemical state of the atom. Generally, the binding energy increases with increasing oxidation state. [46]
There is one thing worth mentioning in which the support may influence the state of the gold. Ceria and zirconia appear to stabilize ionic states of gold. By a process such as:

$$Au^0 + Ce^{4+} \longrightarrow Au^+ + Ce^{3+} \quad (3\text{-}2)$$

the charge of gold is increased by one. This can be explained by the consuming of gold atoms at the outer edge of the gold particles. This phenomenon is probably the reason why gold atoms dissolve into other supports having reducible cations, such as titania and ferric oxide. Basic oxides (La_2O_3, MgO) decrease the effective ionic charge of gold. [45, 47]

3.1.3.2 Influence of gold particles on the support

Gold influences the properties of the support. For example, the reduction of reducible supports (TiO_2, CeO_2, Fe_2O_3) by hydrogen is catalyzed by gold. This is caused by hydrogen overflow from the metal or by changes induced in the electronic properties of the support. For example, gold modifies the band gap of titania and ceria and it generates a shift in the $Ce^{4+} \leftarrow O^{2-}$ charge-transfer band in the UV. Moreover, with Au/Fe_2O_3, the reduction of the support takes place during the oxidation of carbon monoxide. This results in a phase transformation of the support. [45, 47]

3.1.4 Magnesium oxide as support

Principally, the role of the support on the catalytic activity of gold catalysts is to stabilize the small gold particles during the preparation and further thermal treatments. Furthermore, metal oxides functioning as supports show a very high efficiency, caused not only by their high surface area, but also by their high concentration of low coordinated sites. Additionally, solid strong bases, such as MgO, are extremely desirable for developing environmentally friendly processes to catalyse reactions under mild conditions and to minimize the production of contaminants. [48-50]

Gold loaded on a commercial magnesium oxide support shows a high activity in low temperature carbon oxide oxidation. [51] This is an important reaction mechanism in industry since it provides the removal of CO in the reforming process used to produce hydrogen. But due to CO poisoning, the catalyst is rapidly being deactivated. [52] However, Margitfalvi et al. increased the activity of this catalyst for CO oxidation, by modification with ascorbic acid in a relatively narrow concentration range. This is due to the change of the ionic/metallic gold ratio when ascorbic acid is added and also the suppression of carbonate formation. [51]

Another reaction where gold nanoparticles supported on magnesium oxide are used as heterogeneous catalysts, is the aerobic oxidation of alcohols resulting in different carbonyl compounds which are widely employed in various fields of chemical industry. Normally, this reaction occurs with the present of a base to advance the abstraction of hydrogen from the substrate and to capture free carboxylic acid formed at the reaction, which could poison the catalyst. But with the use of a Au/MgO catalyst, aerobic oxidation reactions, such as the esterification of benzyl alcohol, take place in the absence of a base or any other additive. [53]

It is reported that MgO exhibits a quite interesting reactivity regarding to the supported-gold during the glycerolysis of urea. A great conversion (80%) and a high selectivity towards glycerol carbonate (70%) is observed with gold catalysts supported on MgO when they are calcined at 400°C. So from a practical point of view, the choice of the support is directly connected with the reaction that should be catalysed by gold. [34]

3.2 Preparation of gold-supported catalysts

It is well known that the catalytic performance of catalysts is certainly dependent on their preparation methods. In this manuscript, only preparation methods using gold chloride precursors will be presented and discussed. Nonetheless, it is important to mention that there are other methods using chloride-free gold precursors, such as: impregnation in the aqueous phase, deposition of gold-phosphine or other organogold complexes, deposition of colloidal gold onto supports, chemical vapour deposition, cation exchange and adsorption and the deposition of dendrimer-stabilised gold particles. [45]

3.2.1 Impregnation

This method is one of the first used for binding particles on a certain support. With the impregnation method the pores of the support are filled with a solution of the gold precursor. Here, the metal dispersion depends critically on the conditions of drying. In literature, three different impregnation methods are mentioned: wet impregnation, direct impregnation and solid-state impregnation. [45, 54-58]

3.2.1.1 Wet impregnation

An aqueous solution of the metal precursor is added to the pure support. Then, the solution is exposed to a reducing agent, such as sodium borohydride or hydrogen. After the removal of the solvent by evaporation or filtration, the solid is subjected to a high temperature treatment with the aim of activating the surface. The advantage of this method is that a high loading can be acquired. On the other hand, the method leads to bigger, and consequently less catalytic active nanoparticles.

3.2.1.2 Direct impregnation

Another possibility is the direct impregnation of nanoparticles. With this method, metal nanoparticles are prepared separately, before adding them to the support. Direct impregnation is a good method to deposit a metal onto a support. The ion exchange process is effective and results in avoiding the problem of fill-up of the porous structure. A large amount of metal can be impregnated while the porous structure stays intact.

3.2.1.3 Solid-state impregnation

Compared with solution-based methods, solid-state impregnation has hardly received any attention. However, this method involves many advantages. With the solid-state impregnation method, the support is prepared separately. Subsequently, by means of mechanical mixing using a mortar and a pestle, an amount of metal precursor salt is mixed intensely with the support. The resulting powder is brought into a muffle furnace for calcination. The salts are decomposed by the thermal treatment and the oxides remain in the solid. This preparation method is very energy efficient and time-saving. Moreover, it does not produce product residues and requires no purification or recycling.

3.2.2 Coprecipitation

In an alkaline medium, some metals form hydroxides or hydrated oxides, which are poorly soluble in water. Thus, by means of adjusting the pH is it possible to precipitate the metal hydroxides. Coprecipitation is a method based on this principle. It is a single step mechanism where metal salts (functioning as support and as co-catalyst) are dissolved in an aqueous solution of $HAuCl_4$. Then, a base, such as ammonia or sodium hydroxide, is added. After that, the coprecipitate is washed and dried. Finally the material is calcined. With this method, a high gold dispersion can be obtained with particle sizes smaller than 10 nm. [45]

3.2.3 Deposition-precipitation (heterogeneous DP)

Deposition-precipitation (DP) implies a process where the metal hydroxide or hydrated oxide is deposited onto the surface of the support as a result of moderately increasing the pH of the solution in which the support is suspended. The method is widely used to prepare gold-supported catalysts with small particle sizes (< 5 nm). The process is as follows. The gold precursor is precipitated in a suspension of the support. The surface of the support behaves as a nucleation place, thus favoring the attachment of all the gold species. The pH of the suspension is raised by adding a weak base or a base that, only under certain conditions, releases hydroxyl ions. This is an essential property because a local excess of hydroxyl ions in the solution is undesirable. Bases used for this method are sodium hydroxide and sodium carbonate. After filtration and washing with water to remove as much of the sodium and chlorine as possible, the product is dried and often calcined at a higher temperature.

Different parameters of the DP method such as the pH, the type of precursor, the type of precipitating agent, the solvent and the use of other bases, including for example ammonia, can influence the loading and the dispersion of the metal on the support. The main advantages of the DP method are:

- The particles are smaller and they have a narrow particle size distribution;
- A higher load factor is obtained in comparison with for example anion adsorption;
- The method is reproducible;
- The dispersed nanoparticles will not easily agglomerate due to their strong interactions with the support. [45, 59, 60]

3.2.4 Deposition-precipitation with urea (homogeneous DP)

One of the most suitable methods to obtain nanosized gold supported on a metal oxide is the homogeneous DP using an excess of urea ($CO(NH_2)_2$) as precipitating agent. The purpose of this method is to transform the gold precursor into an insoluble form that is generated slowly in the solution. Here, urea acts as a delay base since there is no reaction when it is dissolved in the aqueous metal salt solution at room temperature. Slow hydrolysis (the release of hydroxide ions) only starts when the solution is heated above 60°C according to following reaction:

$$CO(NH_2)_2 + 3H_2O \longrightarrow CO_2 + 2NH_4^+ + 2OH^- \quad (3\text{-}3)$$

At that moment, there is a gradual and homogeneous release of hydroxyl ions throughout the solution, which results in a slow increase of the pH. However, strong mixing is needed to prevent sintering of the gold particles. The control of the pH control is fundamental for this procedure. This can be explained by means of fig. 11. At the beginning (room temperature), the pH of the solution that contains $HAuCl_4 \cdot 3H_2O$ (gold precursor) and urea is around 2,5. This value resembles the complex of $[AuCl_4]$-, which forms $[AuCl_3(OH)]^-$ as a result of hydrolyzation. By increasing gradually the pH through the slow addition of the support, different gold complexes are developed: $[AuCl_2(OH)_2]^-$, $[AuCl(OH)_3]^-$ and finally $[Au(OH)_4]^-$, at a pH above 7,5. During the stirring and heating process, a pH decrease takes place as a result of the replacement of the hydroxyl groups from the surface of the support into gold-hydroxyl groups.

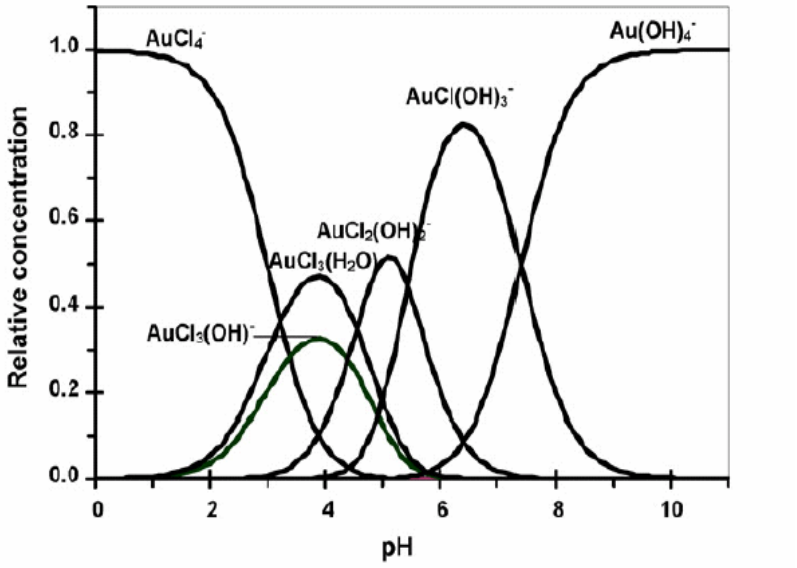

Fig. 11. Distribution of gold species coming from the hydrolysis of $AuCl_4^-$ anions as a function of the pH of the solution. [48]

Finally, the pH will be around 8, so the solution will consist of the complexes $[AuCl(OH)_3]^-$ and $[Au(OH)_4]^-$. After the deposition of gold, the excess of chloride species have to be eliminated because they can cause the growth of the gold particles during the calcination step. The washing with concentrated ammonium hydroxide has been reported as an efficient way to eliminate the remaining Cl^- species.

Besides the pH of the gold solution, another very important aspect to be considered is the isoelectric point of the support. Solid oxide particles are often electrically charged in aqueous suspensions. Charged particles occur when there is a lack of balance between the densities of absorbed H^+, OH^- and ionised surface OH groups. The isoelectric point is the pH at which the oxide surface has a net zero charge. Below the isoelectric point, the support surface area is positively charged and it will interact with the negatively charged complexes. Above the isoelectric point, the charge of surface of the support reverses and turns negative. Consequently, the surface will interact with positively charged ions. The isoelectric point reported for the magnesium oxide is at a pH of ~12. So, the control of the pH is really important during this DP method. Otherwise, when the pH is higher than that of the isoelectric point of magnesium oxide, the surface of the support will show repulsion with the negatively charged gold complexes.

This procedure leads to small gold nanoparticles, but it occurs with a longer preparation time (at least four hours instead of a one hour preparation by the common DP method). It has also the great advantage that all the gold in solution is deposited onto the support. Moreover, with this method, it is easy to prepare a set of samples with the same loading of gold, but different particle sizes, just by systematically varying the preparation time. [45, 48, 61, 62]
In this thesis, this method is used to impregnate magnesium oxide supports with gold since it seems to be the most efficient way to obtain Au/MgO catalysts with gold nanoparticles well dispersed on the support.

3.2.5 Anion adsorption

When the pH of the solution is lower than the isoelectric point of the support, anionic gold precursors, such as $HAuCl_4$, can be adsorbed onto the OH groups of the surface of the support. However, this method seems to be inefficient since the loading of gold does not reach the target value. That is why anion adsorption is barely used as method for the deposition of gold. [45]

3.3 Synthesis of porous magnesium oxide

3.3.1 Introduction

Porous materials show many interesting properties such as a high specific surface area and a large pore volume thanks to the presence of pores. They are capable to interact with molecules, atoms and ions, not only at their external surface, but also inside the pores. Due to all these advantages, those materials can be used for applications such as adsorption and catalysis.
According to the International Union of Pure and Applied Chemistry (IUPAC), three types of porous materials can be distinguished depending on the size of their pores: microporous materials with a pore size smaller than 2 nm, mesoporous materials which own pores with pore sizes between 2 nm and 50 nm and macroporous materials which have pores with sizes of larger than 50 nm. [63-65]

3.3.2 Surfactants

Surfactants are tensioactive components characterized by the presence of both a hydrophilic and a hydrophobic part in their structures. Those compounds serve as a template during the condensation reactions of the synthesis of a mesoporous material. They have influence on the crystal structure and morphology of the final material. Surfactants can be divided in three large groups:

- ionic surfactants;
- non-ionic surfactants;
- amphoteric surfactants.

The ionic surfactants are subdivided in anionic and cationic surfactants. Thus, molecules are respectively negatively and positively charged as opposed to non-ionic surfactants, which are not charged. Amphoteric surfactants can be positively, as well as negatively, charged.

3.3.2.1 Ionic surfactants

A great advantage of ionic surfactants is that they create more interaction with the metal precursor due to their charge. Although, the use of ionic surfactants leads to a decrease in stability of the mesoporous material and to obtaining thinner pore walls. Two examples of cationic surfactants are cetyltrimethylammonium bromide (CTAB) and cetylpyridinium bromide (CPB). They are utilized for the formation of negatively charged metal precursors. Anionic surfactants such as sodium dodecyl sulfate (SDS), are used for the synthesis of positively charged precursors. They possess a lot of good qualities: they are biodegradable, cheap and environmentally friendly, they are strong emulsifiers and they deliver outstanding mesoporous structures. [66, 67]

3.3.2.2 Non-ionic surfactants

Most non-ionic surfactants are made out of chains of polyethelene oxide (PEO) which perform as hydrophilic groups. Because of their interesting properties such as the low cost price, the low toxicity and the biodegradability, they are often used in many sectors of the industry.

The most important classes within the non-ionic surfactants are the oligomeric alkyl polyethylene oxides, the oligomeric alkyl fenolethylene oxides, the sorbitan esters and the amphipatic polyblock copolymers, containing Pluronics such as P123 and F127, which are two essential surfactants used in the synthesis of mesoporous materials. The different features of the surfactant can be helpful to select a suitable surfactant for a specific application. The hydrophilic/hydrophobic ratio, the critical micelle concentration (CMC) and critical micelle temperature (CMT) are significant parameters where to many attention is drawn. The balance between the hydrophilic and the hydrophobic part is also relevant. Furthermore, it's important that the temperature where the surfactant precipitates in hot water is known. This temperature is called the cloud point. [68]

3.3.2.3 Amphoteric surfactants

Amphoteric surfactants are able to both receive protons and remise protons. This is dependent on the acidity of the solution in which the surfactant is dissolved. Hence, the surfactant functions as a ampholyte. Those surfactants are derivatives of amino acids and their general structural formula is R-NH-CH_2COOH. Consequently, this kind of surfactants occur as zwitterions, where R-$^{+}NH_2$-CH_2COO^{-} is the formation of the zwitterion. An example is dimethyldodecylamine oxide (DDAO). Amphoteric surfactants are great emulsifiers. However, they are expensive and therefore, they are not utilized frequently. [69]

3.3.3 Synthesis routes for porous magnesium oxide

3.3.3.1 Soft templating

Soft templating, or the endotemplate method, is mostly used for the synthesis of mesoporous silica materials. With this method, an organic molecule or a block copolymer is utilized as surfactant. Commonly used non-ionic surfactants for the preparation of mesoporous materials are commercial available Pluronic P123 ($PEO_{20}PPO_{70}PEO_{20}$) and F127 ($PEO_{106}PPO_{70}PEO_{106}$). The characters 'P' and 'F' stands for the physical forms of paste and flake. Fig. 12 represents the principle of the soft templating mechanism. When a surfactant and a precursor, for example $Mg(NO_3)_2{\cdot}6H_2O$, are dissolved in a polar solvent, the surfactant will aggregate in micelles. Dependent of the used surfactant, the temperature, the solvent and the presence of counter ions in the reaction medium, micelles can take different shapes.

Those shapes can be spherical, lamellar, tube-like or reversed micelles (with the heads one the inside and the tails on the outside). After the formation of the micelles, the metal precursor is added. It will condensate around the micelles of the surfactant. As a result of polycondensation reactions a spontaneously organized structure of the precursor occurs. This phenomenon is known as self-assembly. Eventually, the template consisting of micelles is removed by an extraction method or by calcination. Calcination is a process where the material is heated until a temperature lower than its melting temperature in order to obtain a phase transition of the material. The final product is a mesoporous material in which the shape and size are derived from the template and synthesis conditions. [70, 71]

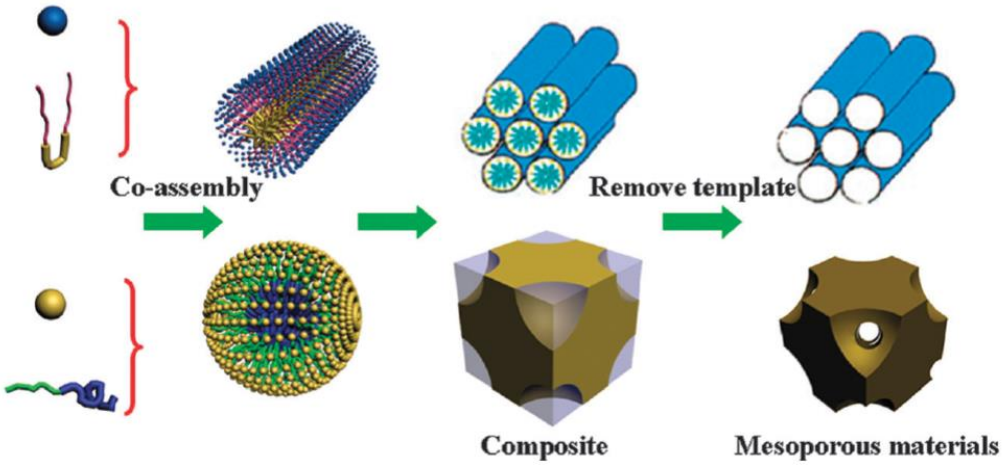

Fig. 12. Schematic principle of the soft templating process. [71]

3.3.3.2 Hard templating

Many mesoporous materials cannot be acquired by the soft templating method. Therefore, another method, hard templating, is evolved. With hard templating, also known as the exotemplate method or nanocasting, mesoporous silica or carbon are used as readily complete and available templates instead of the assistance of a surfactant.

Those materials are very suitable for this synthesis method due to their ordered structure and uniform pore size. The process of nanocasting consists out of four important stages. Fig. 13 shows the different steps of the mechanism. First the mesoporous template is prepared. Then the metal precursor is deposited in the empty spaces of the template. Usually, this is a repetitive process. Thereafter, the precursor is transformed into the desirable product by means of a heat treatment.

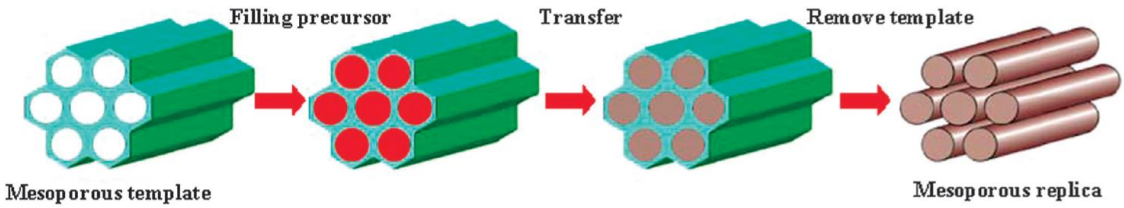

Fig. 13. Scheme of the hard templating method. [71]

Finally, the template is removed and a negative image of the porous system of the template appears. Some advantages inherent to mesoporous materials obtained by hard templating are:

- The mesostructure can be easily modified by the use of another template;
- Crystalline materials can be obtained through a high temperature treatment while they still are protected by the strong template;
- This synthesis route averts the necessity to manage the condensation process and for this reason the method is useful to make a wide range of materials.
- The collapse of the pores as a result of the formation forces is avoided.
  [50, 70-72]

3.3.3.3 Evaporation-Induced Self-Assembly and the hydrothermal method

With the Evaporation-Induced Self-Assembly (EISA) method the phenomenon self-assembly is caused by the evaporation of the solvent. A homogeneous solution consisting of a surfactant, usually CTAB (cationic) or P123 (non-ionic), a soluble metal alkoxide or metal salt, an alcohol, typically ethanol, water and often an acid, usually HCl, are mixed intensely. The surfactant is added with a concentration lower than the CMC.
The next step is casting the solution on a substrate by spray, spin or dip coating and evaporation of the volatile compounds (especially the alcohol, water and the acid) takes place. As a result of the evaporation, the concentration of the surfactant increases until a value higher than that of the CMC which leads to the self-assembly of the micelles. Fig. 14 describes the subsequent stages after evaporation. Around the micelles of the surfactant, which serves now as a template, different reactions such as condensation, polymerization, precipitation and gelation occur.

Finally, the template is eliminated in order to obtain a porous structure and to condense the inorganic network. Normally, calcination in the temperature range of 400 to 550°C is performed. In this range, the temperature will be high enough to remove most of the surfactant, but it is also low enough to avoid the collapse of the pores. The final product is dependent on three essential factors: the ratio of the surfactant to the metal oxide precursor, the nature of the precursor, and the relative humidity. [73]

The difference between the EISA method and the hydrothermal method is that with the hydrothermal method, only water is used as solvent. In this thesis, the hydrothermal method is utilized to synthesize mesoporous magnesium oxide.

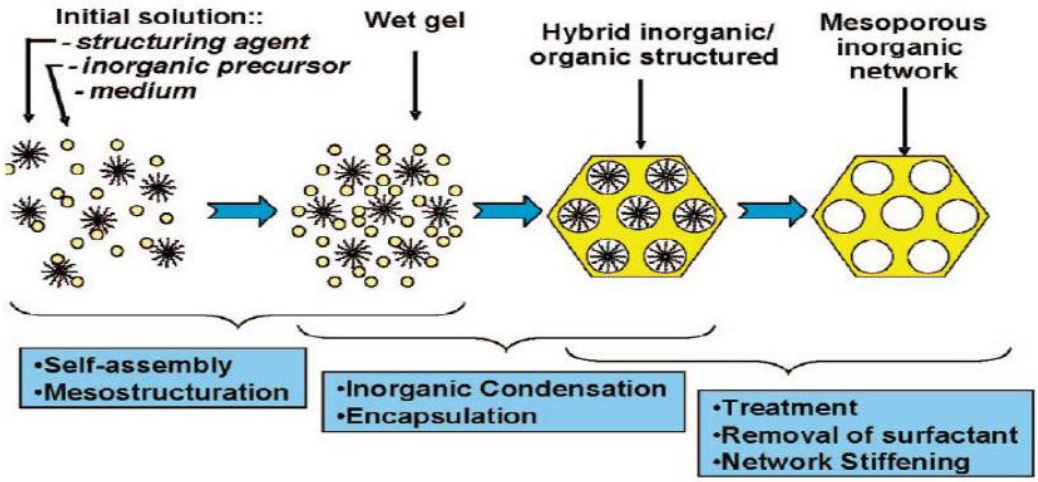

Fig. 14. Scheme of the various steps involved in the EISA process. [73]

3.3.3.4 Combustion method

The combustion method is a technique where a magnesium salt as oxidizer and a fuel, for example glycine, are mixed in water. Then the mixture is heated in order to evaporate the water until a wet powder remains. After that, the powder is introduced into a muffle furnace which is kept at a certain temperature. First, the powder is dehydrated and then an oxidation takes place between the magnesium salt and the fuel. In this way, gases are formed. This results in the formation of a voluminous and porous network of a nanocrystalline material. Initially, the powder is black colored due to the presence of carbon. To become a non-carbonaceous product, the powder is held in the muffle furnace for another 30 minutes for further oxidation. This method allows the production of contamination free magnesium oxide powder in large quantities and in a short time. [74]

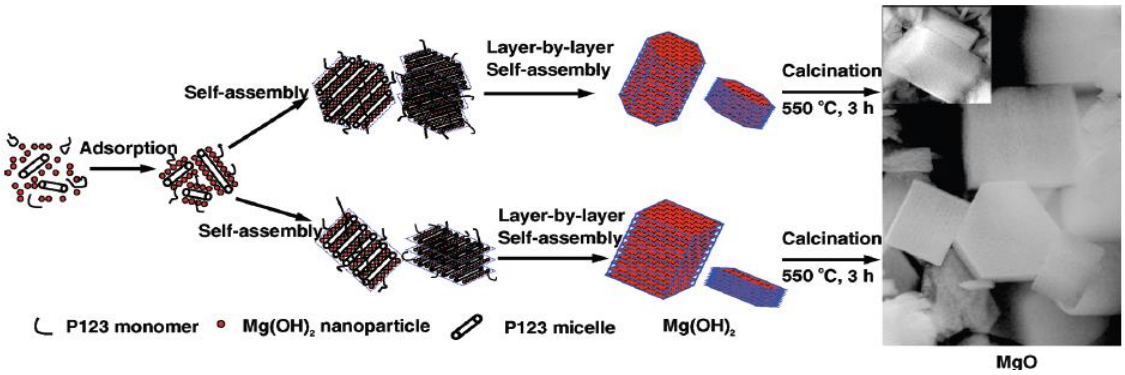

Fig. 15. Schematic illustration of the formation of $Mg(OH)_2$ and the corresponding mesoporous MgO. [77]

3.3.4 Importance of the morphology of the support

It is agreed that metal oxide supports prepared by different routes have different surface morphologies (such as spheres, sheets, flower-like, rod-like and plate shapes) and properties, thus the catalytic activity, the selectivity and stability features may differ, causing different interactions of the basic places with glycerol during the overall reaction: the glycerolysis of urea. To obtain supports with different morphologies, the surfactant/precursor molar ratio can be adjusted, or frankly another surfactant can be applied. The comparison can also be made with supports made without a surfactant. [49, 75, 76]

In this thesis, magnesium oxide supports with different morphologies are synthesized by a hydrothermal method using the surfactants Pluronic P123 (non-ionic) and CTAB (cationic) and also without surfactant in order to compare the morphologies of the resulting powders. Furthermore, parameters such as synthesis time and synthesis temperature are varied in order to get information whether or not they influence the surface area of the support. Fig. 15 shows a possible formation mechanism of $Mg(OH)_2$ and porous MgO.

CTAB has a few advantages in comparison with the non-ionic surfactant P123. At first, the CMT value of CTAB is better than that of P123, which means that CTAB solutions can be made at room temperature with quite large amounts of surfactant dissolving in an aqueous phase. In addition, the CMC value of CTAB is lower than that of P123. Moreover, the cloud-point is a major issue with non-ionic surfactants. Therefore, a careful adjustment of the temperature is necessary to dissolve P123. CTAB can be utilized in both acidic and basic conditions. However; the challenge for the use of this material is the toxicity and the relatively higher cost compared to the surfactant P123. [73]

4 Characterization and analysis techniques

4.1 Characterization of the catalyst

4.1.1 X-Ray Diffraction (XRD)

X-ray diffraction is a useful characterization technique used to determine the crystal structure and the crystal domain size of solids. XRD is based on the principle of diffraction. [78-80]

4.1.1.1 Bragg's law

An X-ray is an electromagnetic radiation with a high content of energy and a short wavelength. The size of the wavelength is in relation with the distance between two atoms. Incoming X-rays can be scattered due to the atoms lying on their path. This results in a phenomenon called interference between the scattered waves. This interference can be both constructive and destructive.

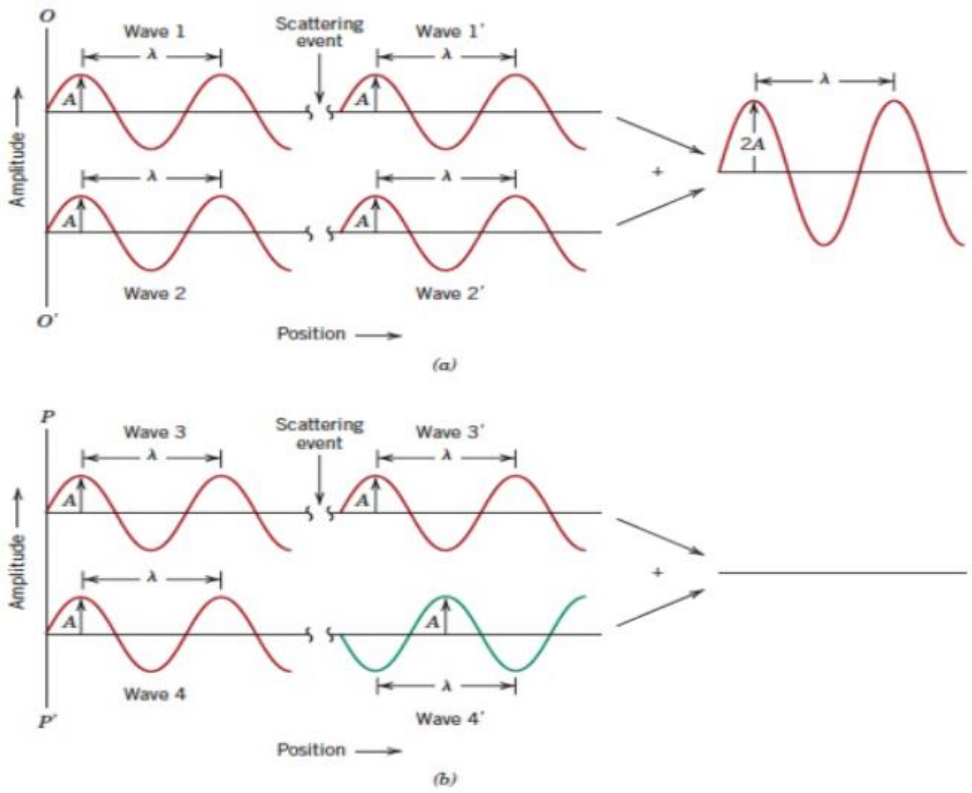

Fig. 16. Constructive (a) and destructive (b) interference. [78]

If the interference is constructive, the waves are in phase. Therefore, the measured wave will have an amplitude which is the summation of the scattered waves. This principle is called diffraction. The waves are in phase when the distance between two atoms is in proportion with the wavelength of the incoming beam. This is described in fig. 16.
This concept can be explained according to Bragg's law. As condition it is considered that the material exhibits any crystallinity. If that isn't the case, the sample has an amorphous structure and a destructive interference will occur between the scattered waves. To clarify Bragg's law, an example with two parallel plains is used. Following figure shows the common arrangement (fig. 17).

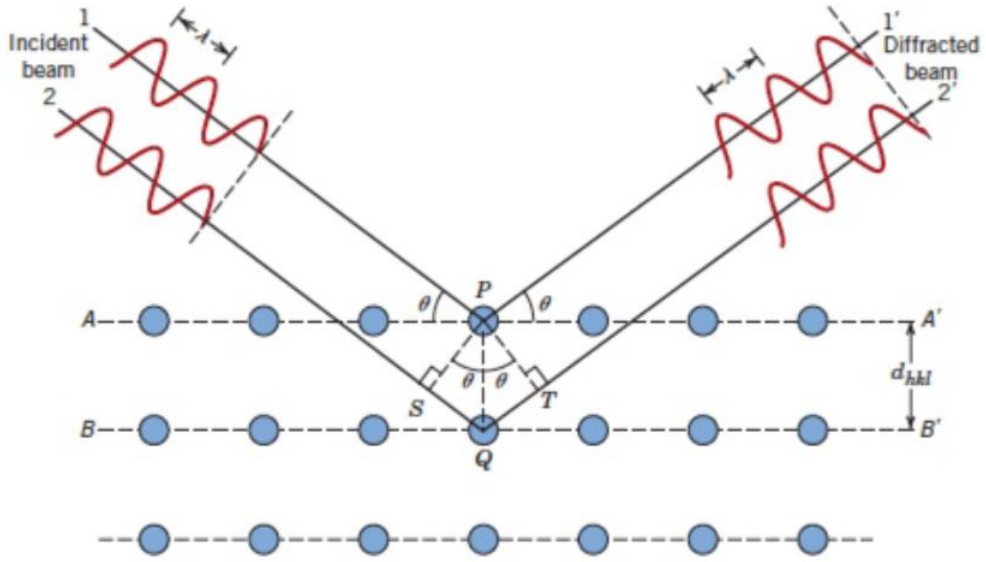

Fig. 17. Diffraction of X-rays. [78]

Bragg's law implies that in order to obtain a constructive interference, the phase difference has to be equal with an integral number multiplied with the wavelength:

$$n\lambda = 2\, d_{hkl} \sin\theta \qquad (4\text{-}1)$$

Here, n is an integral number and d_{hkl} is the distance between two planes.

4.1.1.2 Device

Below, the setup of an XRD is showed (fig. 18). The source consists of a beam of X-rays built from a tungsten cathode that is heated. Accelerated electrons arise, which run up against the anode due to a connected voltage difference. Several materials, according to the desired wavelength, can be used for the manufacturing of the anode. In this thesis, copper will be used as anodic material. Due to the collision between the accelerated electrons, primary X-rays arise which leave the source along a thin beryllium frame.

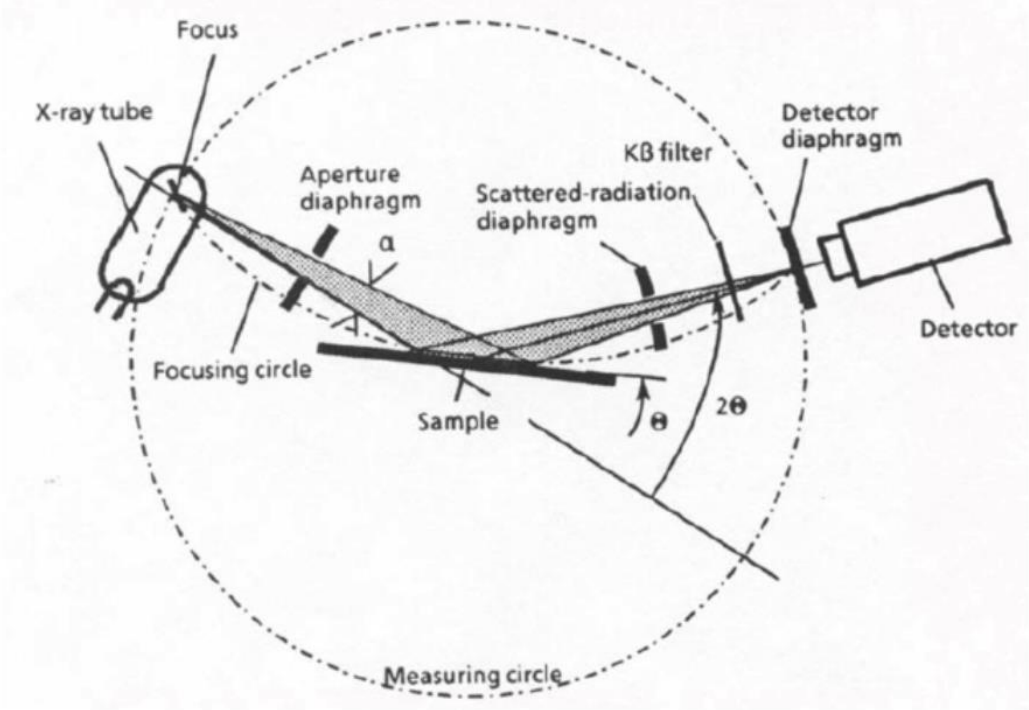

Fig. 18. Setup of the XRD device. [79]

Before measurement, the sample is crushed and therefore, it consists out of tiny and fine crystals, which are oriented in a random way. To acquire a representative view of the structure of the sample, an adequate amount of material has to be used. This way, enough particles will be available for diffraction in order to examine whether or not possible structures are present.

The sample is radiated with monochromatic X-rays. Afterwards, the scattered radiation is captured on the detector, which is equipped with a diffraction measurer. This device is able to define the angle whereat diffraction occurs. The signal is detected by means of a proportional counter. In front of this detector, a monochromator is often placed in order to allow beams with a specific wavelength.

In this thesis, XRD is practiced to obtain some information about the structure (brucite/periclase) and the crystallinity of the magnesium oxide supports. XRD measurements are carried out by using an ARL^{TM} X'TRA Powder Diffractometer from Thermo Scientific. The diffraction patterns are recorded at an interval of 5-70 2θ° with a step size of 0,02° and a measuring time of one second per step. So the duration of each measurement is approximately 32 minutes.

4.1.1.3 Interpretation of the data

The intensity of the signal is plotted in function of the angle of diffraction. This can be correlated with the crystal structure of the atoms.
The Scherrer equation gives information about the crystal domain size of the solid. This parameter can be correlated with the particle size in nanosized materials. The Scherrer equation is presented as follow:

$$r = \frac{K\,\lambda}{\beta \cos\theta} \tag{4-2}$$

r is the mean size of the nanoparticle. K is a dimensionless factor, depending on the shape of the crystal. This factor varies from 0.89 for a spherical particle, to 0.94 for a cubic one. If the shape is unknown, 0.9 is usually established. β is the latitude of the peak at half intensity. θ is the angle of diffraction.

4.1.2 Scanning Electron Microscopy (SEM)

Scanning electron microscopy is a technique to examine the surface morphology of a sample using a primary beam of electrons for the production of X-rays, to analyze the elastic scattering of electrons and also for the production of secondary electrons. Since the optical microscope is only able to enlarge something one thousand times, the electron microscope is used in this thesis in order to characterize the micro and nanometric properties of the synthesized catalysts.
The electrons will be accelerated until they possess high energies between 2 and 40 keV. This is called the accelerating voltage. Those electrons are defined as the primary beam of electrons. This beam will be emitted on a point of the surface. This is repeated many times. In this way, an overall picture of the surface is obtained. This is the reason why the method is called "scanning" electron microscopy.

The first signal is acquired due to the secondary electrons. They give information about the first 5 nm on the outside of the sample. They originate as a result of the invasion of the primar electron beam on the surface. This beam can't penetrate deeply into the surface, a drop shaped zone with a depth of 1-3 µm is excited (fig. 19), and for this reason they can't scatter. Hence, the surface where the secondary electrons originate, is small. Those secondary electrons have a low content of energy which amounts up to 50 eV. Here, an inelastic collision takes place.

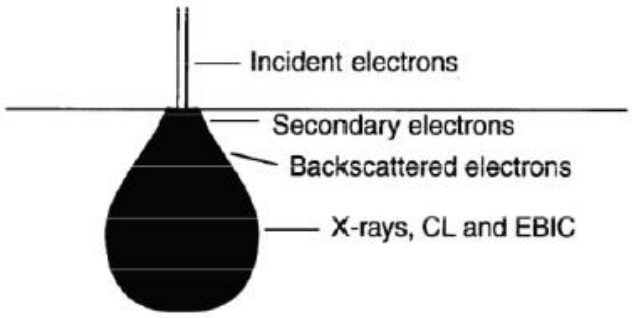

Fig. 19. Interaction of the electrons with the sample. [81]

The second signal occurs due to the backscattered electrons. Those electrons are formed when the primary beam of electrons invades close enough to the core of the atom. That way the primary beam is scattered at a bigger angle. A complete reflection is possible. The backscattered electrons are less numerous than the secondary electrons, but collisions happen in an elastic way. By consequence they possess a higher energy content. The X-rays originate due to the interaction between the primary electron beam and the electrons. This happens through knocking away an electron from the inner shell of an atom. Hereby, an electron from a higher shell will fall back to the vacant position. The release of the created energy can occur through two different ways. The first manner is by means of electromagnetic radiant energy (X-radiation) and the second way is through the loss of kinetic energy due to Auger electrons. The X-rays are characteristic for the present atoms. Therefore, XRD is often connected with SEM. It is a collaboration between two methodologies where the surface of the sample is scanned. This is performed by the dividing of the surface in small fragments whereupon a primary electron beam is emitted. This measurements provide both qualitative information, through the characteristic X-radiation, as quantitative information, through the intensity of this radiation.

Following figure (fig. 20) shows the emplacement of SEM. Just as with a common light microscope, the radiation will be focused over different lenses. That way, the electrons are sent in on the sample. Here, it's important that the sample is conductive. Otherwise, a charge build-up appears. As a result of this increase, the final image can be deformed. This can be prevented through coating of the sample with a layer of gold. [79, 81-84]

In this thesis SEM is used to analyze the morphology of the magnesium oxide nanoparticles. Because different morphologies for each MgO support gives different stability properties and other catalytic activities of the catalyst when they are impregnated with gold. The measurements were accomplished by a FEI Quanta 200 FEG-SEM apparatus.

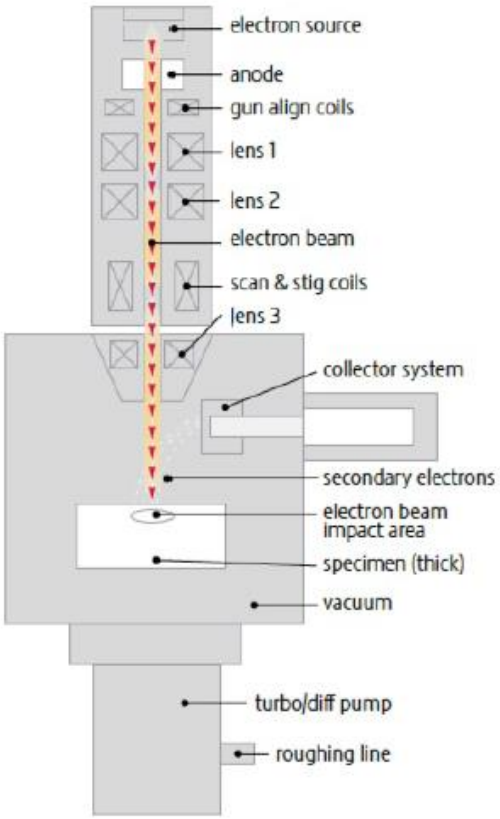

Fig. 20. Emplacement of a SEM device. [84]

4.1.3 Transmission Electron Microscopy (TEM)

Just as with SEM, electrons are used as source with TEM. [84, 85]

4.1.3.1 Device

The architecture of TEM is presented in fig. 21. An electron gun is employed as source. The speed of the electrons can be adjusted. This is realized by increasing the acceleration voltage, which amounts about 200 keV. Then, the electrons are led through lenses. Those lenses do not consist out of glass, but they are electromagnetic. As a result of this property, the lenses vary in proportion as the current through the lenses vary. Thus, the focus of the microscope happens automatically, unlike with the light microscope, where the focus happens mechanical. The beam eventually will be fired through the sample. Therefore, the preparation of the sample is very important since it has to be thin enough to let the beam of electrons through.

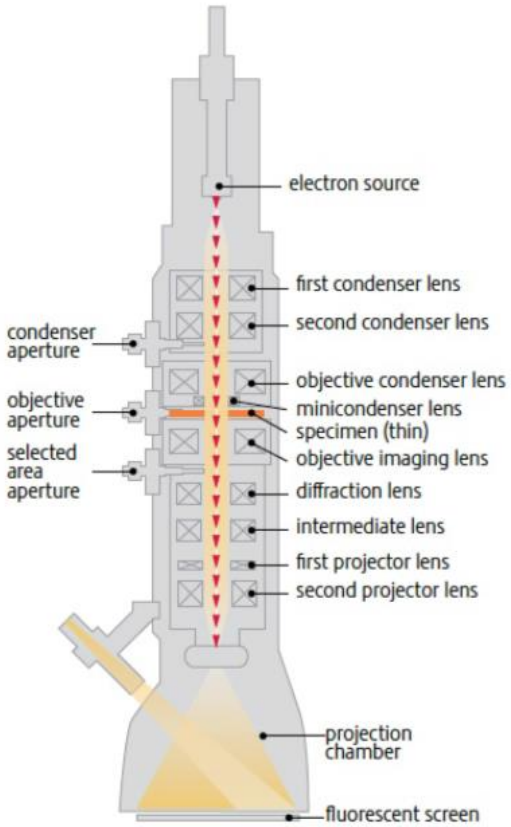

Fig. 21. Architecture of a TEM device. [84]

By means of a fluorescent screen or with a more sophisticated charge-coupled device (CCD) camera, an image is formed. Interpretation of the image is not obvious due to the diversity of interaction phenomena. When the machine is programmed in the normal mode, a difference in dispersion of the beam of electrons gives rise to a difference in intensity. This difference in dispersion can have a double origin: on the one hand a difference in thickness of the sample, on the other hand a difference in composition. In the diffraction mode, it is possible to visualize diffraction patterns of crystalline materials.
In this thesis, TEM is used in the normal mode to analyze the dispersion and the size of the gold nanoparticles which are deposited on magnesium oxide. The TEM measurements are performed with a Cs-corrected JEOL JEM 2200 FS microscope, operating at 200 kV.

4.1.3.2 Preparation of the sample

Since the electrons transmitted through the sample are analyzed, the pathway has to be as thin as possible. Aggregation (the presence of big particles of the material) of the sample is repellent, therefore the sample is dispersed in a solvent, like ethanol. To disperse the solid completely, the suspension is transferred into an ultrasound bath for five minutes until the dispersion is homogeneous. Next is to place one drop of the mixture ethanol-sample onto a 300-mesh holey carbon copper grid that is utilized to hold the sample on site during TEM analysis.

4.1.4 Nitrogen adsorption (N_2-adsorption)

To determine the specific surface area, the pore volume and the pore distribution of a substance, a nitrogen adsorption technique is employed. BET method (Brunauer, Emmett and Teller) was used in order to analyze the surface area of the materials. This method is mostly used for describing multilayer adsorption. The variation of the adsorbed volume particles as a function of the pressure is shown for a certain temperature. Following formula describes the BET isotherm:

$$\frac{V}{V_{mon}} = \frac{cz}{(1-z)[1-(1-c)z]} \tag{4-3}$$

V_{mon} is the volume which matches with monolayer adsorption, z is the proportion of pressure p on p* (the vapor pressure above a layer adsorbate which is more than one molecule thick and looks like the pure bulk liquid) and c is a constant dependent on the desorption and evaporation enthalpy:

$$c = e^{(\Delta_{des}H^\circ - \Delta_{vap}H^\circ)/RT} \quad (4\text{-}4)$$

Different BET isotherms can be divided in five types (fig. 22):

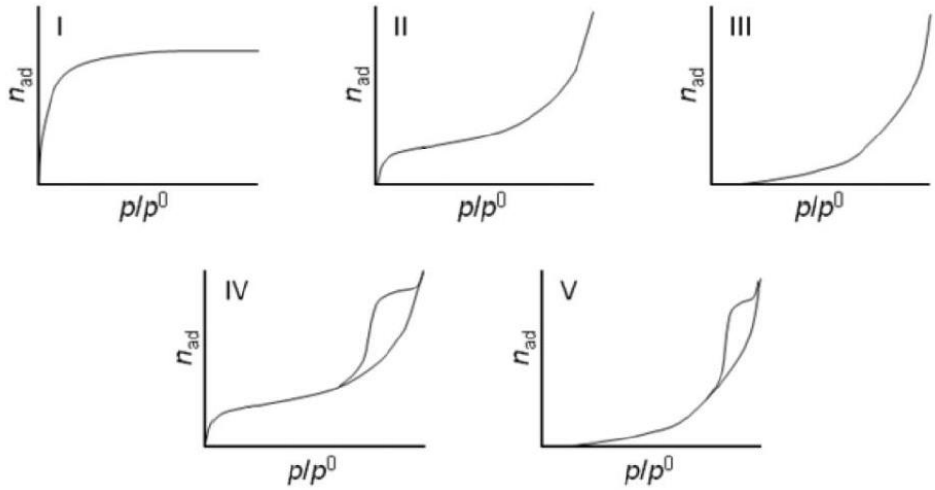

Fig. 22. Types of BET isotherms. [15]

Type I isotherm occurs when the adsorption is limited to monolayer adsorption and is described by the so called Langmuir isotherm. Materials with this type of isotherm have microporous pores. Isotherms of type II take place when the material isn't porous or macroporous. Here, multilayer adsorption occurs. When the multilayer adsorption performs before the monolayer adsorption is complete, a type III isotherm takes place. Type IV and V are similar to previous types, but they occur when mesoporous materials are analyzed. At high relative pressures, the adsorption in mesopores leads to multilayer formation until, at a high pressure dependent on Kelvin-type rules (the larger the mesopore, the higher the pressure), a big leap can be observed due to capillary condensation. This is a phenomenon where layers of adsorbed molecules pile up until they condensate a thin layer of gas (capillar) which is still present in what is left of the pore. This results in a sudden increase of the volume adsorbed nitrogen gas. As mesopores are filled adsorption continues on the low external surface. The gradient of the leap is determined by the pore distribution.

The steeper the graph, the more uniform the pore size. Most oxides such as carriers and most catalysts belong to this class of solids. Also something typical for this kind of isotherms is the hysteresis loop caused by the filling and emptying of the mesopores. Desorption takes place at a lower relative pressure due to de difference in condensation and desorption enthalpy. Calculation of the internal surface happens in the relative pressure area between 0.05 and 0.35. A monolayer of nitrogen molecules is adsorbed at these pressures.

By rewriting the BET equation and expand it in function of the relative pressure, V_{mon} can be determined. Thereafter the specific surface area can be calculated:

$$S\left[\frac{m^2}{g}\right] = \frac{m_{mon}}{a} \cdot N_A \cdot A \tag{4-5}$$

A is the surface that is taken by one adsorbed molecule. For nitrogen A amounts $0.162 \cdot 10^{-18}$ m². N_A is Avogadro's number and a is the mass of the adsorbent. [15, 86]

The nitrogen adsorption technique is used to calculate the BET surface area of the MgO supports and to determine the BET isotherm, which indicates the type of porosity of the samples. Here, a Tristar 3000 and a Tristar 3020 is used. Prior to measurement, each sample is degasified in vacuum at room temperature overnight, or at 120°C for three hours. This is necessary because any presence of water in the sample would slack up the measurement significantly.

4.1.5 X-Ray Fluorescence (XRF)

X-ray fluorescence is a technique where a solid or a liquid sample is radiated with primary X-rays. Electrons on the K-, L- and M- shell are excited because of the adsorption. Macroscopically, the transitions occur at the same time. When the electrons fall back to a lower energy state, secondary X-rays are emitted. This is called the fluorescence of the atom. Those X-rays are diffused in many directions with the same intensity. Fig. 23 describes the principle of an XRF. The measurement of the X-rays is fulfilled in an angle of 90°. In this way, rays coming from the source can't end up on the detector. According to Planck's law:

$$\Delta E = \frac{hc}{\lambda} \tag{4-6}$$

the wavelength of the X-rays is a qualitative criterion. h is Planck's constant ($6{,}626 \cdot 10^{-34}$ Js). c is the velocity of light and has a value of 299 792 458 $m \cdot s^{-1}$ and λ is the wavelength in meters. The intensity is in accordance with the law of Lambert-Beer, a quantitative criterion:

$$A = \log \frac{I_0}{I} = K \cdot c \cdot l \tag{4-7}$$

K is the absorbance constant, c is the concentration of the element to be analyzed. l is the path length of the flame. [79, 87]

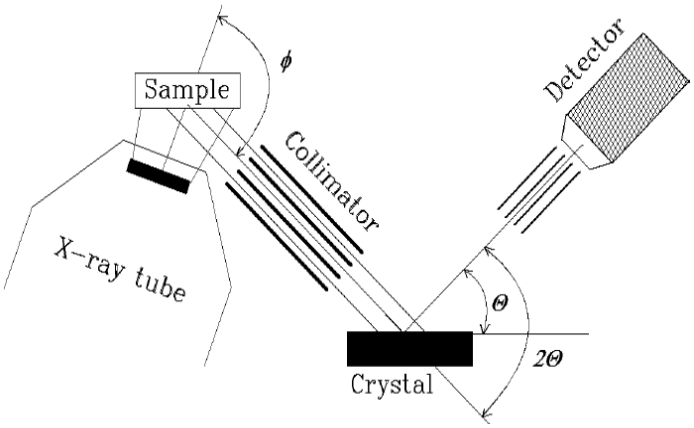

Fig. 23. Setup of an XRF appliance. [87]

In this thesis, XRF is employed to figure out the loading of gold on the magnesium oxide support. XRF measurements are carried out by using the Rigaku NeX CG. The X-rays are emitted by an X-ray tube made from Cu.

4.1.6 Ultraviolet-Visible Spectroscopy (UV-VIS)

The electromagnetic spectrum includes different forms of radiation such as cosmic, γ-rays, X-rays, ultraviolet light, visible radiation, infrared (IR), microwaves, and radio. Ultraviolet light is shorter than visible light and had a wavelength between 10 and 400 nm. Visible light lies in the wavelength range of 400-700 nm.

A spectrophotometer is used to measure the transmittance or absorbance of a sample as a function of the wavelength of electromagnetic radiation. The main elements of the spectrophotometer are (fig. 24):

- a source of electromagnetic radiation;
- a dispersion device that selects the wavelength whereat the measurement takes place;
- a sample area;
- a detector to measure the intensity.

When a material absorbs light, outer-shell electrons are excited from their ground state to a higher energy level. Because only a minuscule amount of absorbing molecules is required, it is practical to have the sample in solution. However, powders can also be measured. Electromagnetic radiation is transmitted through the sample which is held in a small square cell (usually 1 x 1 cm). Over a period of circa 30 seconds, radiation of the entire ultraviolet/visible range is focused on the sample. Photocells detect the radiation transmitted and the absorption is detected by the spectrometer by comparing the variation of the intensities of the radiation passing through the sample and the reference cell. [88]

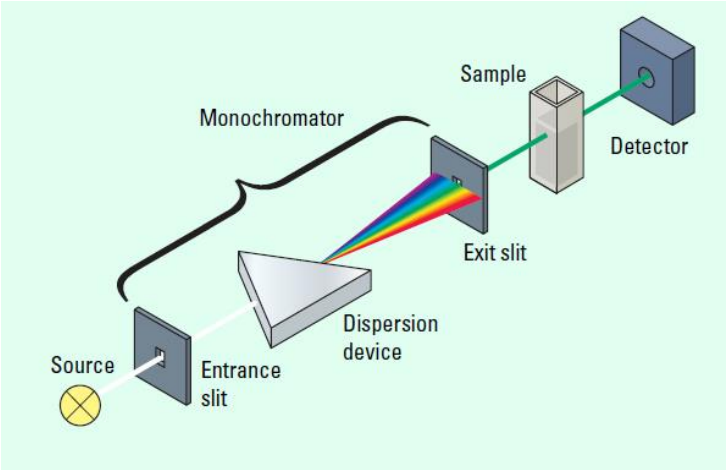

Fig. 24. Schematic picture of a conventional spectrophotometer. [88]

In this thesis, UV-VIS spectrometry is used to have an additional indication of the size of the gold nanoparticles according to the intensity of the plasmon resonance peak coming from the metallic gold nanoparticles. Such peak appears between 500 and 600 nm and is characteristic of the electronic cloud resonance that occurs around the metallic gold nanoparticles. The bigger the gold particle, the larger the plasmon, and the more intense the peak. An augment in the intensity of the plasmon resonance peak is normally accompanied by a red-shift in its position. To do the measurements a Cary 500 Varian UV-VIS/NIR spectrophotometer is used. Light from a wavelength range of 250-800 nm is focused onto the sample.

4.1.7 Diffuse Reflectance Infrared Fourier Transform Spectroscopy (DRIFTS)

[89, 90]

4.1.7.1 Theory

There are two different types of reflected light: specular and diffuse. A common example of specular reflection is light reflected from mirrors. Specular reflectance takes place at any interface between two materials with different refractive indices. Specularly reflected light is characterized by the rule that the angle of reflection is equal to the angle of incidence. An example of diffusely reflecting surfaces are the matte surfaces, which are characteristic for certain types of powders. This kind of reflected radiation is the light reflected from a diffusely reflecting sample for which the angle of reflection does not equal the angle of incidence (fig. 25).

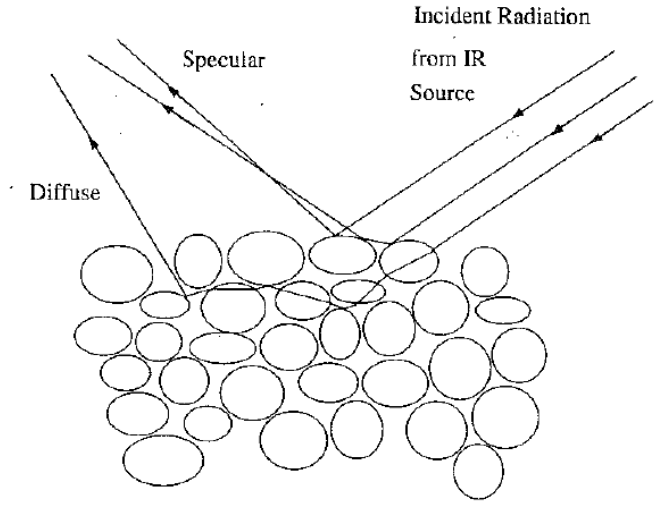

Fig. 25. Schematic diagram of the DRIFT interaction: the difference between specular and diffuse reflected light. [89]

4.1.7.2 Kubelka-Munk expression

With this kind of investigations, the Kubelka-Munk expression is useful for relating the observed reflectance spectrum to the concentration of the analyte. This is the most commonly used expression and has two parameters:

$$f(R_\infty) = \frac{(1-R_\infty)^2}{2R_\infty} = \frac{k}{s} \qquad (4\text{-}8)$$

R_∞ is the absolute reflectance of an infinitely thick sample, $f(R_\infty)$ represents the value of the Kubelka-Munk function, k is the absorption coefficient:

$$k' = \frac{k}{4\pi\upsilon} \tag{4-9}$$

where k' is the absorption index en υ is the frequency of the radiation (per centimeter). The character 's' of the Kubelka-Munk expression stands for the scattering coefficient defined for purely scattering samples by:

$$I = I_0\, e^{-sx} \tag{4-10}$$

4.1.7.3 Device

Diffuse reflectance infrared Fourier transform spectroscopy is a quantitative technique that collects and analyses infrared radiation. With this application the chemical structure and the composition of fine particles and powders, but also of polymer fibers and films, can be obtained. This infrared sampling method involves minimal sample preparation in terms of time and sample manipulation. The sample only has to be mixed with a proper diluent, often KBr. When the infrared beam hits the sample, it can be reflected or it can be transmitted through the particle. The energy that is transferred through the particle can in turn reflect off the next particle or can be transmitted through the next particle. The infrared beam reflected off the surface of the particles is usually perished. The alternation between transmission and reflectance can occur many times, resulting in the prolongation of the path length. Finally, the scattered infrared energy is gathered by a spherical mirror that is focused onto the detector. The observed infrared light is partially absorbed by the particles of the sample, delivering the sample information.
In this thesis, DRIFT is used to observe if the template of the magnesium oxide support is genuinely removed through a Soxhlet extraction. DRIFT measurements are taken by the Nicolet 6700 FT-IR Spectrometer purchased from Thermo Scientific.

4.2 Evaluation of the overall reaction

4.2.1 Gas Chromatography (GC)

Gas chromatography is used to divide several components and to determine the different components of an unknown solution. The emplacement is shown in following figure (fig. 26). The sample is injected in the injection column (No. 3). The injection room is pre-heated in order to evaporate the sample directly after it is injected into the column. The sample expands because it ends up in the gas phase. That way only a part of the evaporated sample is carried through the column. This can be adjusted by the split ratio. The split ratio is the ratio of the injected volume on the actual amount of sample that is carried through the column. The split ratio will also prevent the saturation of the signal in the detector. The sample is carried over the column by means of an inert carrier gas (No. 1). As carrier gas, N_2, H_2, Ar or He are often used. The choice is determined by the cost (for example, He is a quite expensive gas) and by the kind of detector that is used. By a control valve (No. 2), the pressure and the flow of the gas can be adjusted. The column in which the sample is injected, is surrounded with an oven. In the separation column (No. 4), the segregation occurs by a gas/liquid equilibrium. Inasmuch this equilibrium with equilibrium constant K is depending on the temperature, a temperature profile is used in gas chromatography in order to keep the analysis time as short as possible. The temperature profile is depending on the components which have to be determined. By adapting the parameters of the gas chromatograph, a well separation will be obtained. No. 5 is the actual detector. In this thesis a thermal conductivity detector (TCD detector) is used. This detector will perceive a difference in conductivity between the carrier gas (reference) and the sample. That difference will provide a signal which is converted by the recorder (No. 6). [79]

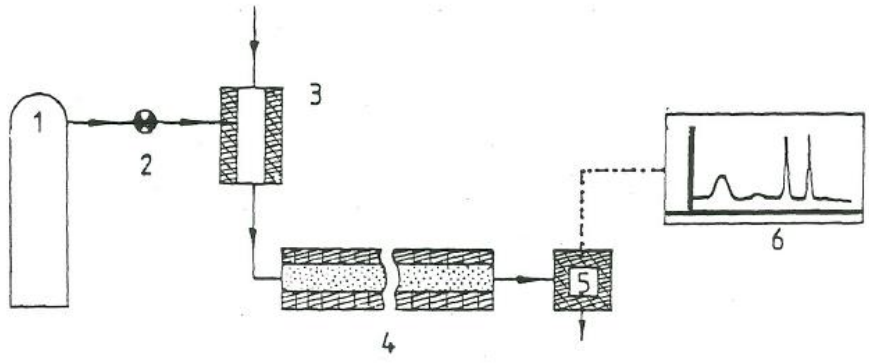

Fig. 26. Configuration of the gas chromatograph. [79]

GC is used to determine the progress of the glycerolysis of urea. The conversion of glycerol and the yield glycerol carbonate are investigated. Therefrom, the selectivity of the catalyst can be calculated. In this thesis, the type of gas chromatograph is a Hewlett Packard 5890 series II. The column which is utilized is a Biorad Superox II polar column with a dimension of 30 m x 0,32 mm x 0,50 µm.

4.2.2 Gas Chromatography and Mass Spectrometry (GC-MS)

By using linked detection systems, the detection of different components takes places by means of mass spectrometry. In this way, the separation as well as the detection can occur at the same time. When the components leave the column of the gas chromatograph, they enter the mass spectrometer where they are immediately radiated with an electron beam (electron ionization). As a result of the collision with the molecules, an electron is knocked away and a positive ion arises. When the internal energy of the positive ion is high enough, fragmentation occurs. The ion dissociates in a secondary ion and a neutral particle. If the secondary ion possesses still enough internal energy, it will continue to fragment. The ionization and fragmentation take place as follows [79]:

- Ionization

$$ABC + e^- \longrightarrow ABC^+ + 2e^- \quad (4\text{-}11)$$

- Fragmentation

$$ABC^+ \longrightarrow AB + C^+ \quad (4\text{-}12)$$
$$ABC^+ \longrightarrow A^+ + BC \quad (4\text{-}13)$$
$$ABC^+ \longrightarrow AB^+ + C \quad (4\text{-}14)$$
$$ABC^+ \longrightarrow AC^+ + B \quad (4\text{-}15)$$
$$etc.$$

In this thesis, GC-MS is used to obtain information about the possible by-products that can be formed during the glycerolysis of urea. The measurements are performed by using a Hewlett Packard 5890 Series II gas chromatograph, provided by a XTI-5 column (apolar) and MS400 detector (electronic ionization).

4.2.3 Titrimetry

The goal of titrimetry is to determine a specific component in an unknown solution. The volumetric determination of an amount of solute is obtained by a titration. Considering the nature of the reaction which occurs, different types of titrations can be distinguished:

- neutralization titrations;
- redox titrations;
- precipitation titrations;
- complexation titrations.

During the titration the concentration of the reagent varies continuously. The titration curve usually consists of a graphic with the negative logarithm of the reagent concentration as a function of the titrated volume standard solution. The end point of the titration, the equivalence point, is characterized with a sudden leap, associated with a clear change of color by cause of the added indicator. The calculation of the concentration of the specific component is derived from the titrated volume standard solution. Those values are expressed in molar or normal concentrations, which show the amount of solute per liter solution. When the equivalence point is reached, equivalent amounts of reagent and component have reacted. Therefore, following equation counts:

$$V \cdot N = V' \cdot N' \tag{4-16}$$

V and V' are the volumes of the reacted components. N and N' are the concentrations of the components (eq/l). Usually, by executing a titration of an unknown solution with known volume V, N' and V' of the standard solution can be determined. Then, the concentration of the unknown component can be easily calculated.
This technique is used in order to determine the amount of ammonia that is formed during the reaction. The produced ammonia is collected in a HCl acid trap to neutralize. Then this solution will be titrated back with NaOH. [91]

PART II

Experimental work

5 Catalyst preparation

The aim of this thesis is to obtain magnesium oxide supports with different morphologies through surfactant modification and variable synthesis conditions. Hence, by depositing gold on those supports, the acquisition of catalysts with different gold-support interactions is expected. These type of addition could have an influence on the activity and stability properties of the synthesized catalysts. Then, the catalytic activity of the most promising materials (in terms of surface area and morphology) is evaluated in the reaction of glycerolysis of urea for producing glycerol carbonate. Glycerol conversion, yield to glycerol carbonate and selectivity of the process are used as evaluation parameters. The reactivity of the magnesium oxide support by itself is also an important parameter, since its morphology and surface basic properties can play a role during the reaction of glycerol and urea.

5.1 Synthesis of the magnesium oxide support

5.1.1 Hydrothermal synthesis of magnesium hydroxide

With a hydrothermal dissolution-recrystallization soft templating method different magnesium hydroxide ($Mg(OH)_2$) support materials are prepared. As surfactant CTAB (≥98%) or pluronic P123 are used, which serve as a template. The utilized magnesium precursor is magnesium nitrate hexahydrate ($Mg(NO_3)_2{\cdot}6H_2O$, ≥98%). All materials are purchased from Sigma Aldrich. The following procedure describes the process for the synthesis of magnesium hydroxide. [77]

5.1.1.1 Calculations

$$Final\ desirable\ product\colon 3\ g\ MgO\ support\ \left(Mw = 40{,}31\ \frac{g}{mole}\right)$$

$$Obtained\ from\colon Mg(NO_3)_2 \cdot 6H_2O\ \left(Mw = 256{,}41\ \frac{g}{mole}\right)$$

$$\frac{surfactant}{Mg}\ molar\ ratio = 0{,}03$$

$$\frac{3\ g}{40{,}31\ \frac{g}{mole}} = 0{,}07442\ mole\ MgO\ \longrightarrow 0{,}07442\ mole\ Mg\ and\ 0{,}07442\ mole\ O$$

$$Mw\ CTAB = 364{,}45\ \frac{g}{mole}$$

$$Average\ Mw\ P123 = \sim 5800\ \frac{g}{mole}$$

$$\frac{surfactant}{Mg} = 0{,}03\ \longrightarrow mole\ surfactant = 0{,}07442\ mole * 0{,}03 = 0{,}002233\ mole$$

$$weight\ CTAB = 0{,}002233\ mole * 364{,}45\ \frac{g}{mole} = 0{,}8137\ g$$

$$weight\ P123 = 0{,}002233\ mole * 5800\ \frac{g}{mole} = 12{,}9514\ g$$

$$weight\ Mg(NO_3)_2 \cdot 6H_2O = 0{,}07442\ mole * 256{,}41\ \frac{g}{mole} = 19{,}0876\ g$$

5.1.1.2 Synthesis procedure

First the surfactant is dissolved in 50 ml distilled water. When using P123 as surfactant, the solution needs to be heated to a temperature of 60°C, otherwise the surfactant will not dissolve. Then, $Mg(NO_3)_2 \cdot 6H_2O$ is added to the solution. The surfactant/magnesium molar ratio is equal to 0,03. After that, an aqueous ammonia solution (25%) is added drop wise at room temperature to the liquid mixture until the final pH is approximately 10 in order to fix the pH and create a buffer. Afterwards, the solution is transferred into a 50 ml Teflon-lined stainless steel autoclave for hydrothermal treatment at the selected temperature of 120°C or 240°C and a synthesis time of 12 or 24 hours. After the hydrothermal treatment, the obtained solid is filtered out and washed three times with distilled water and ethanol for the removal of a great part of the template. The obtained material is dried in the oven at 80°C overnight. White $Mg(OH)_2$ powder is acquired. Fig. 27 shows the different synthesis parameters that have been evaluated. In total, twelve samples were obtained.

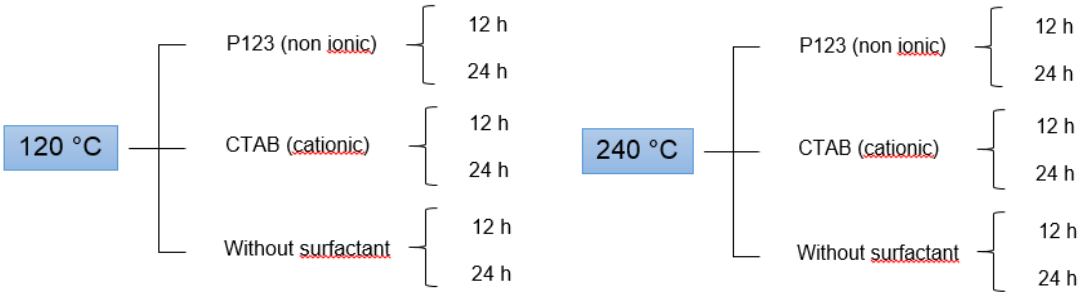

Fig. 27. Different circumstances for the synthesis of $Mg(OH)_2$.

5.1.2 Transformation $Mg(OH)_2$ to MgO through a calcination step

For the conversion of $Mg(OH)_2$ to MgO, the powder is calcined by using a very slow calcination program at 500°C for three hours, represented in fig. 28. [93]

This kind of calcination program is applied in order to avoid the collapse of the porous structure generated during the templated-assisted systhesis method, and to keep the feature morpholgy of the samples. During the first step of the calcination program (room temperature to 300°C) the brucite $Mg(OH)_2$ sample is dehydrated. After that, the temperature increment is reduced to be 30°C every hour until 360°C, which is the phase transition point from the brucite structure of $Mg(OH)_2$ to periclase MgO. The temperature is then kept at this point for another 5 hours. During the last step of the program, the temperature is increased again until 500°C and held there for 3 hours in order to fix and stabilize the periclase MgO samples.

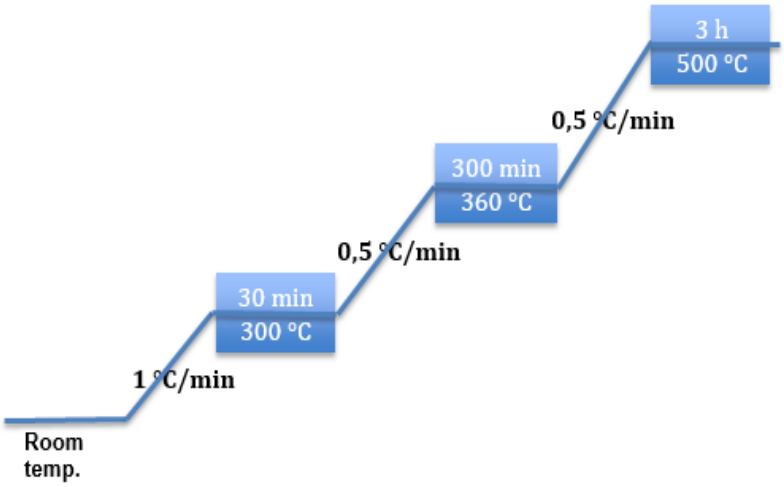

Fig. 28. Slow calcination program for the transformation of $Mg(OH)_2$ to MgO.

5.1.3 Results and discussion

For every “batch” of supports, three different solutions are made based on the hydrothermal dissolution-recrystallization method. One with CTAB (C) as surfactant, another with P123 (P) and a last one without surfactant (W). Hence, we have four parameters (synthesis time, synthesis temperature, surfactant and whether or not calcined) of which we examine the effects on the MgO support.

The obtained $Mg(OH)_2$/MgO-powders prepared are named considering the used surfactant - synthesis temperature - synthesis time - dry/calcination temperature, as follows:

- C - 120°C - 12 hours - 80°C
- P - 120°C - 12 hours - 80°C
- W - 120°C - 12 hours - 80°C
- C - 120°C - 24 hours - 500°C
- P - 120°C - 24 hours - 500°C
- W - 120°C - 24 hours - 500°C
- C - 120°C - 12 hours - 500°C
- P - 120°C - 12 hours - 500°C
- W - 120°C - 12 hours - 500°C
- C - 240°C - 12 hours - 80°C
- P - 240°C - 12 hours - 80°C
- W - 240°C - 12 hours - 80°C
- C - 120°C - 24 hours - 80°C
- P - 120°C - 24 hours - 80°C
- W - 120°C - 24 hours - 80°C
- C - 240°C - 12 hours - 500°C
- P - 240°C - 12 hours - 500°C
- W - 240°C - 12 hours - 500°C

5.1.3.1 Nitrogen adsorption

The textural properties of the synthesized magnesium oxide supports were analyzed from their respective nitrogen adsorption-desorption isotherms. Table 2 summarizes the BET surface area, pore volume and pore size values calculated for those materials.

After calcination, the increment of the BET surface area occurs. This is due to the combustion of the template necessary to create a porous structure. High surface areas are obtained when the template made out of the surfactant is as much as possible burned away and when the calcination program is adjusted to avoid pore collapse during this high temperature treatment.

By means of the BET surface area, the two best MgO supports are selected (framed in green). The one made with the surfactant P123, with a synthesis temperature of 120°C and a synthesis time of 12 hours. The other is made with the surfactant CTAB at a synthesis temperature of 120°C for 24 hours.

Table 2. BET surface area of the synthesized MgO supports.

Sample	BET surface area (m^2/g)	Total pore volume (cm^3/g)	Average pore diameter (A)
		Single point desorption	**Desorption**
C-120-12-80	21	0,04	78
P-120-12-80	15	0,05	146
W-120-12-80	16	0,03	81
C-120-12-500	97	0,23	97
P-120-12-500	163	0,31	76
W-120-12-500	136	0,22	64
C-120-24-500	168	0,22	53
P-120-24-500	148	0,28	76
W-120-24-500	146	0,22	61
C-240-12-500	116	0,19	65
P-240-12-500	109	0,24	87
W-240-12-500	109	0,18	66

It can be concluded that a synthesis temperature of 240°C is too high, since the BET surface area decreases.

The highlighted samples are the ones we will work further with for additional research.

5.1.3.1.1 Nitrogen adsorption-desorption isotherms

In order to gain information concerning the type of porosity, the isotherms of the most important MgO materials are plotted and discussed. The isotherms of the materials synthesized with the same surfactant but under different conditions are compared. The shape of the isotherm provides information about the solid porous texture. The isotherms are all type IV isotherms, which means that the samples are all mesoporous, i.e. they have pores with pore sizes between 2 and 50 nm. [15, 86]

- Influence of the synthesis time

The isotherms on fig. 29, top figure, are the MgO samples made with the surfactant CTAB. Their only difference is the synthesis time. The blue curve (synthesis time of 12 hours) is located lower than the red curve (synthesis time of 24 hours). This indicates that the adsorption starts at a higher pressure, resulting in a lower BET surface area.
The isotherms on the bottom figure are from the MgO samples made with the surfactant P123. They show the same characteristics but here, the blue curve (synthesis time of 12 hours) is lying above the red curve, implying that a synthesis time of 12 hours for the sample made with P123 results in samples with a higher BET surface area.

- Influence of the calcination temperature

Wang et al. synthesized MgO powders by a P123-assisted hydrothermal synthesis method. However they used a synthesis time of 72 hours and a synthesis temperature of 240°C. The samples were calcined at 550°C and had a surface area of 297 m^2/g. [77]
Thus, with the aim of increasing the BET surface area, the most promising supports made with CTAB and P123 are calcined again at 550°C during 10 hours. Nevertheless, a higher BET surface area could not be obtained, instead the surface area drops after the recalcination at 550°C (table 3).

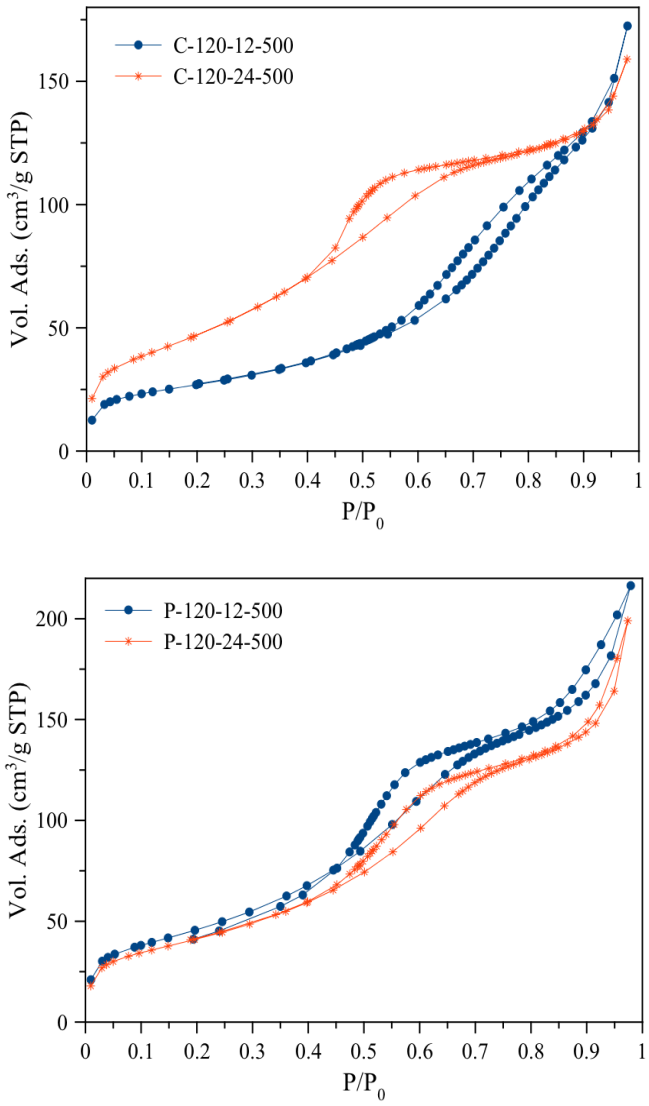

Fig. 29. BET isotherms of the two most promising MgO supports and their counterparts concerning the influence of the synthesis time.

Table 3. BET surface area of the two most promising supports in reference to commercial MgO calcined at 500°C and at 550°C.

	BET surface area (m²/g)	
MgO Sample	**Calcined at 500°C**	**Calcined at 550°C**
Commercial MgO	127	65
P - 120°C - 12 hours	163	89
C - 120°C - 24 hours	168	74

This is also illustrated in following N_2-adsorption-desorption isotherms (fig. 30). Samples synthesized both with CTAB and P123 calcined at 550°C deliver isotherms lying lower than the isotherms of the MgO powders calcined at 500°C, which indicates a decrease in surface area.

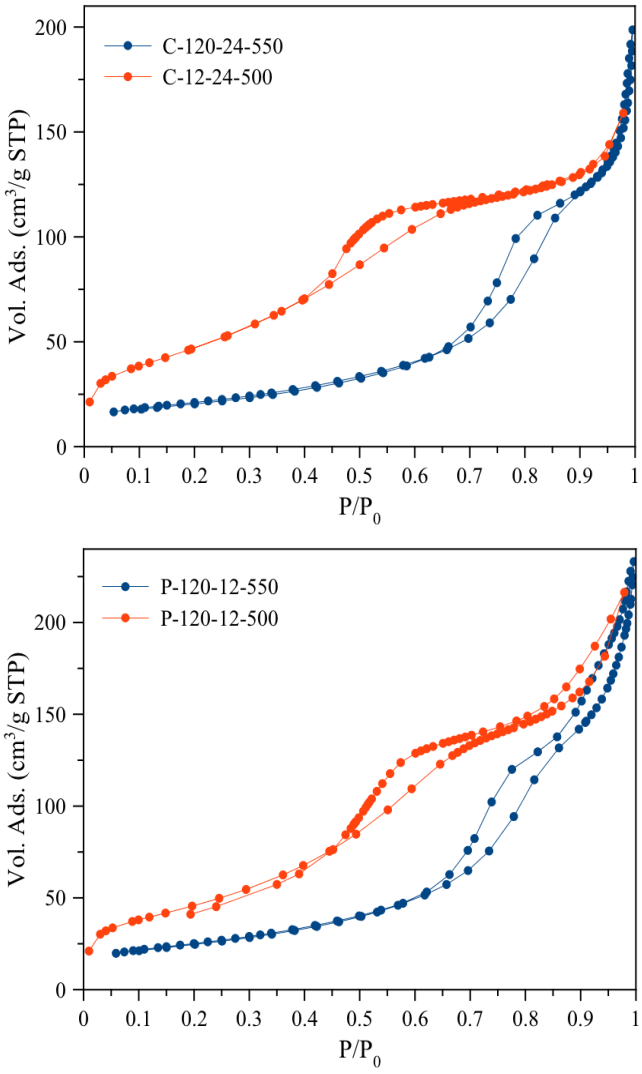

Fig. 30. BET isotherms of the two most promising MgO supports and their counterparts concerning the calcination temperature.

5.1.3.1.2 BJH pore size distributions

In order to obtain some information about the size of the pores, the different BJH pore size distributions (Barrer, Joiyner and Halenda) are plotted in following figures. The BJH method is the most widely used by commercial instruments to perform calculation on mesopores. [86] A comparison of the isotherms is made up again concerning the influence of the synthesis time and the calcination temperature.

- Influence of the synthesis time

Out of the image below (fig. 31, top figure), there can be concluded that the sample with a synthesis time of 24 hours has pore sizes between 30 - 50 Å, equal to 3 - 5 nm. The blue curve shows a totally different pore size distribution. The pores are not that uniform and pore sizes in a bigger range of 30 - 100 nm occur. In other words, the sample consists not only out of mesopores, but macropores are also present.

Concerning the pore size distributions in fig. 31, bottom figure, the difference is not that significant. With both synthesis times of 12 and 24 hours, the pores of the obtained MgO samples are more or less uniform and the pore size of both materials falls within the range of 30 - 50 Å. Thus, the effect of the synthesis time of the samples prepared with the surfactant P123 is not considerable concerning the size of the pores.

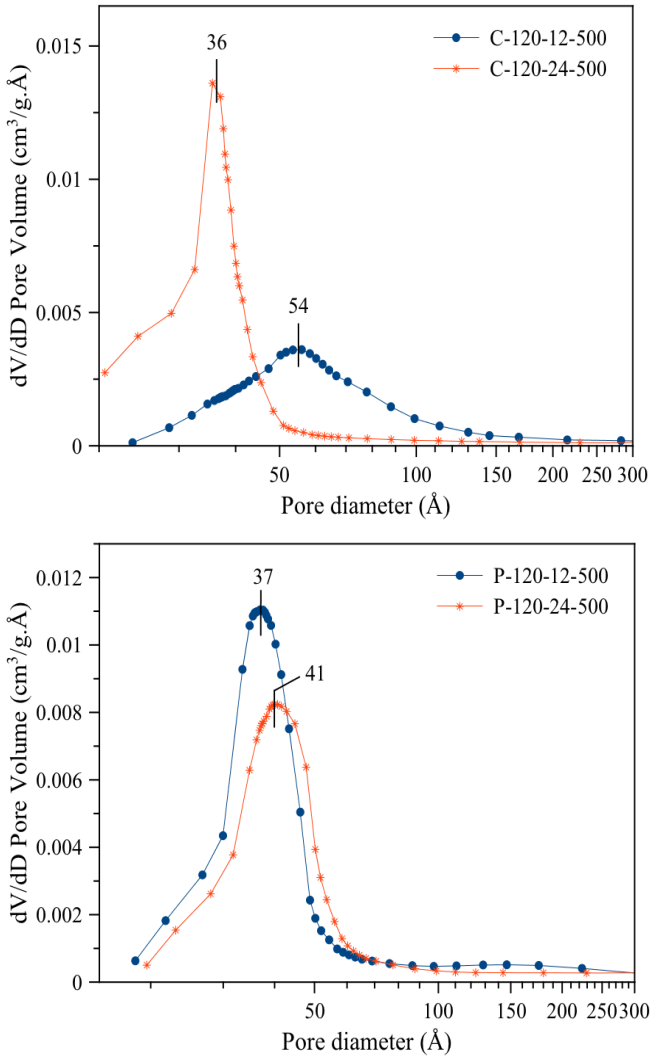

Fig. 31. BJH pore size distributions of the two most promising MgO supports and their counterparts concerning the influence of the synthesis time.

- Influence of the calcination temperature

Calcination at a higher temperature of 550°C results for both materials in an increase of the pore size (fig. 32). Those materials have pores between 50 and 100 Å which indicates the presence of macropores.

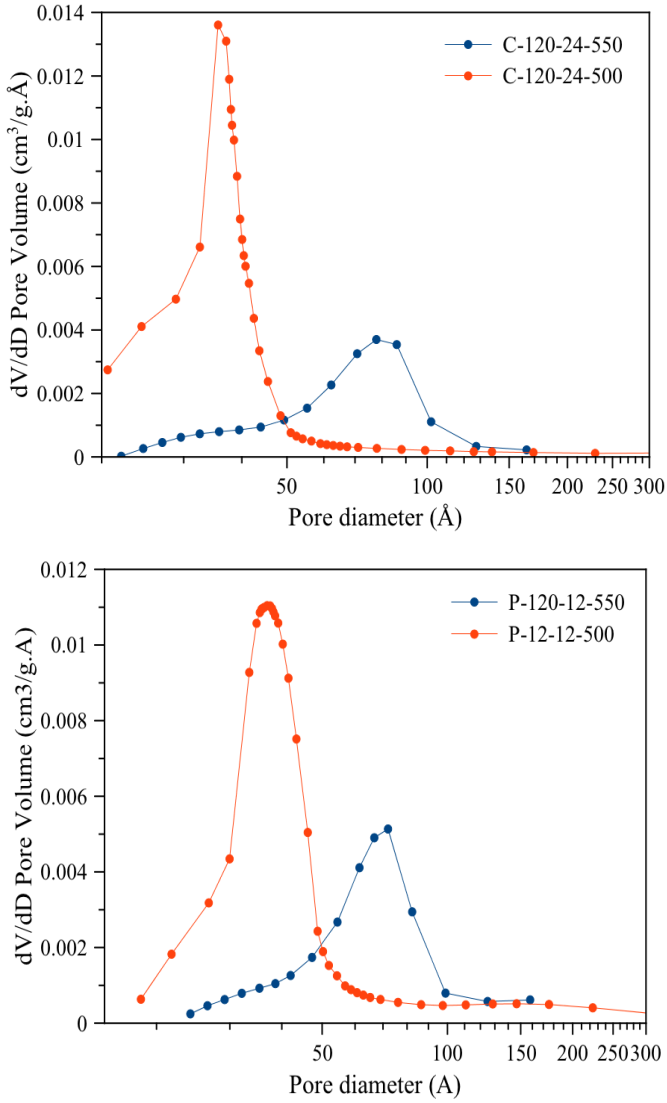

Fig. 32. BJH pore size distributions of the two most promising MgO supports and their counterparts concerning the calcination temperature.

Hence, for further research, more mesoporous MgO will be prepared. Considering previous results, for the sample prepared with CTAB, the synthesis time will be held at 24 hours and for the sample made with P123 the synthesis time remains 12 hours. Further, the calcination temperature of 550°C leads to a decrease in BET surface area and the presence of macropores. Therefore, additional synthesized MgO samples will be calcined at 500°C instead of 550°C.

5.1.3.2 X-ray diffraction

To obtain some information about the structure and the crystallinity of the supports, the samples are analyzed by XRD. Fig. 33 shows two kinds of XRD diffractograms. The patterns of the figure on top are those of the uncalcined $Mg(OH)_2$ samples. According to the literature, the XRD patterns observed for the uncalcined $Mg(OH)_2$ samples are characteristics of the brucite-type structure. The figure on the bottom illustrates the XRD patterns of calcined MgO materials. As reported by the literature, those samples possess the periclase crystal structure. [77, 92]

Thus, the different synthesis conditions used for the preparation of these materials (nature of the surfactant, temperature and time reaction) does not affect their final crystal structure.

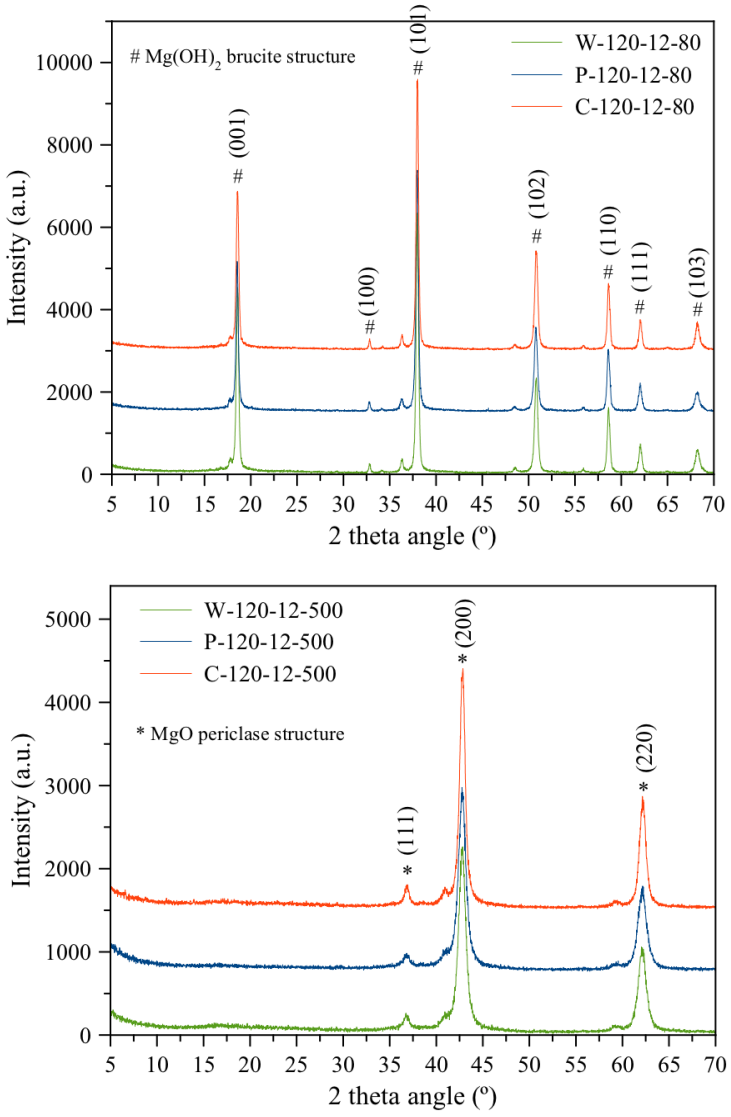

Fig. 33. XRD diffractograms of the uncalcined $Mg(OH)_2$ samples (top) which have the brucite structure and their calcined MgO counterparts (bottom) which possess the periclase crystal structure.

5.1.3.3 Scanning electron microscopy

The technique of scanning electron microscopy is applied in order to analyze the morphological properties of the two most promising supports (the ones with the highest BET surface) made with CTAB and P123, before and after calcination. For this research, it is of great relevance to be able to obtain different morphologies in order to know what is the effect of the morphology on the reactivity, catalytic activity and stability properties of the gold-supported catalysts. It is also from great interest that after calcination, the morphology does not change, in contrast to the crystal structure of the materials.

Fig. 34 shows the SEM pictures of the uncalcined $Mg(OH)_2$ material prepared with the surfactant CTAB at 120°C for 24 hours.

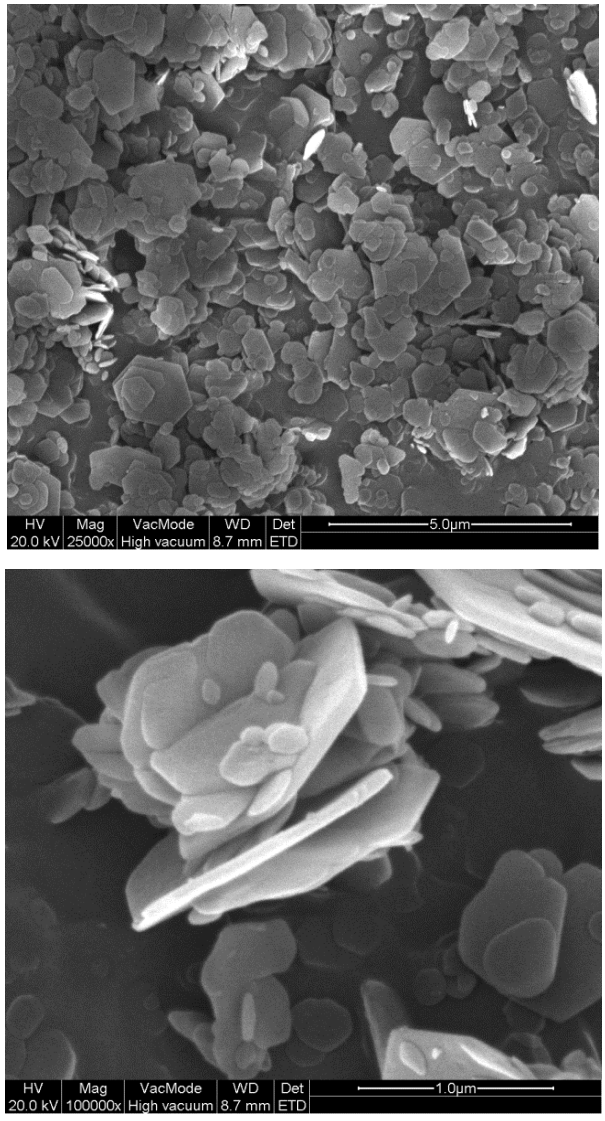

Fig. 34. SEM images of the uncalcined $Mg(OH)_2$ material synthesized with the surfactant CTAB at 120°C for 24 hours.

Those pictures visualize clearly the hexagonal formed nanosheets of the $Mg(OH)_2$ material. They are monodispersed and very divided throughout the whole surface. They have a size of around 1 micrometer or smaller. Similar morphological properties have been reported in the literature by using CTAB as a surfactant or by using a template-free hydrothermal synthesis method. [77, 93, 94]

Fig. 35 shows the images of the calcined MgO sample made with CTAB. Basically, the morphology does not differ from that of the uncalcined sample. The nanosheets are still hexagonal formed. They are monodispersed and also spread throughout the entire surface.

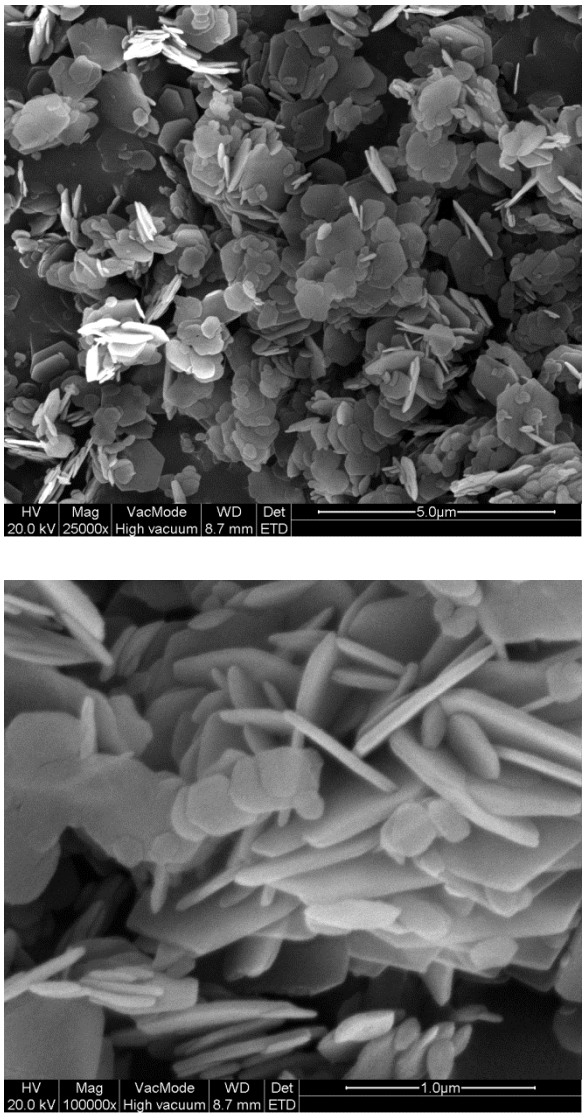

Fig. 35. SEM images of the calcined MgO material synthesized with the surfactant CTAB at 120°C for 24 hours.

Fig. 36 represent the morphology of the uncalcined samples made with the surfactant P123 at a synthesis temperature of 120°C and a synthesis time of 12 hours. The morphology completely differs from that of the calcined and uncalcined samples synthesized with CTAB. Here, The sample made with P123 shows agglomeration of the nanosheets.

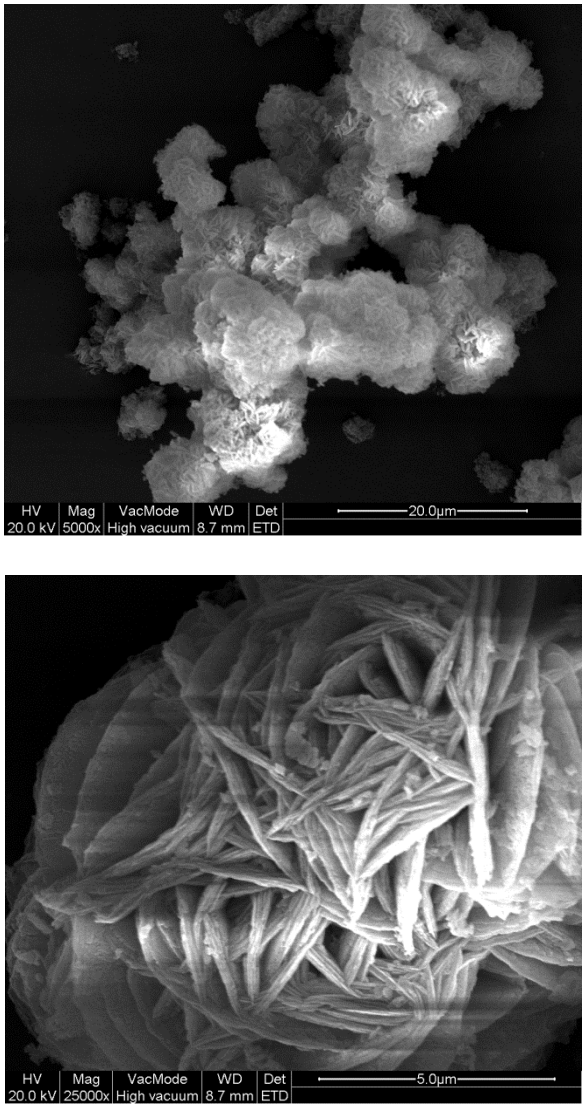

Fig. 36. SEM images of the uncalcined $Mg(OH)_2$ material synthesized with the surfactant P123 at 120°C for 12 hours.

The same morphology occurs with the calcined sample produced with the surfactant P123 (fig. 37). Agglomeration of the nanosheets takes place. The agglomerated parts are divided throughout the whole structure and they have a flower-like appearance.

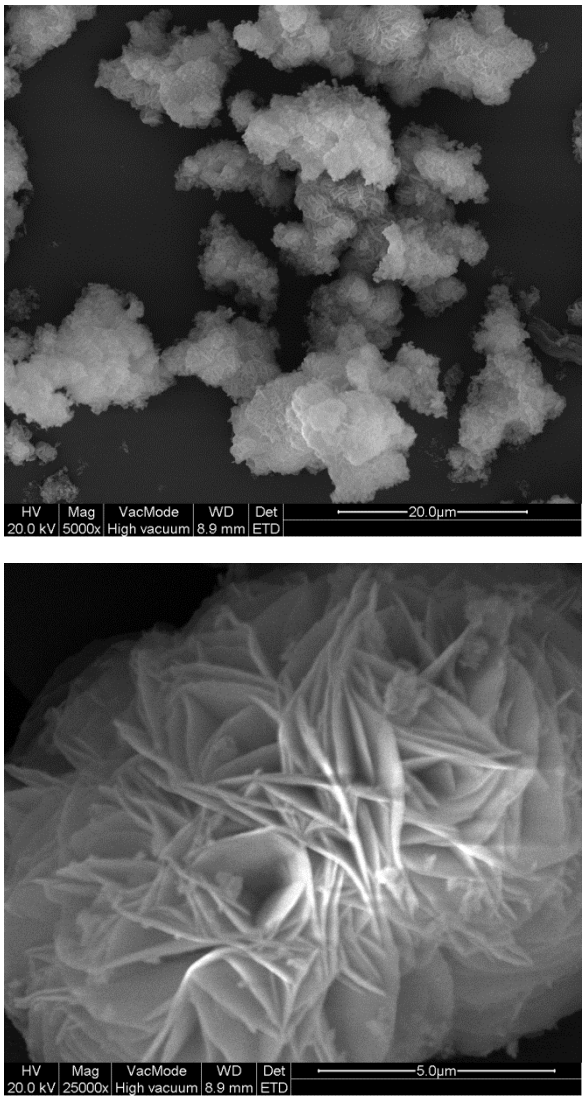

Fig. 37. SEM images of the calcined MgO material synthesized with the surfactant P123 at 120°C for 12 hours.

5.2 Integration of the Soxhlet extraction after hydrothermal synthesis

5.2.1 Goal and set up

In order to try to increase the surface area of the two most promising supports, those materials are synthesized again by the same hydrothermal synthesis method of the very beginning at exactly the same synthesis conditions:

- P - 120°C - 12 hours - 80°C
- C - 120°C - 24 hours - 80°C

Then, the removal of the surfactant by a Soxhlet extraction is carried out instead of a calcination. For both samples, acetone is used as solvent and the procedure went overnight (18 hours). By doing this additional treatment, a more efficient elimination of the surfactant is expected and afterwards, the support could be treated at lower temperatures to avoid the collapse of the porous structure. Fig. 38 shows the set up of the Soxhlet extraction procedure.

Fig. 38. Set up of the Soxhlet extraction.

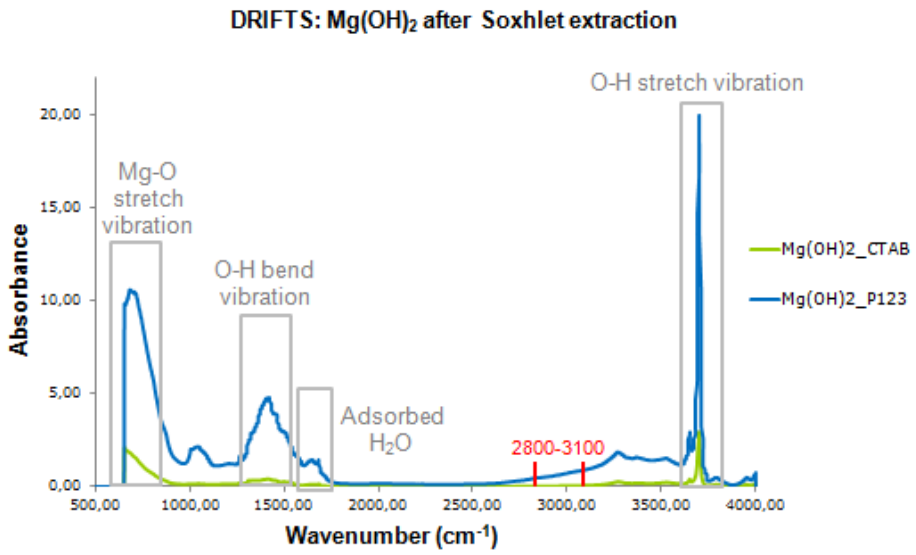

Fig. 39. DRIFT spectra of the two most promising $Mg(OH)_2$ supports after Soxhlet extraction before calcination.

5.2.2 Results and discussion before calcination

5.2.2.1 Diffuse reflectance infrared Fourier transform spectroscopy

Fig. 39 represents the spectrum of the uncalcined $Mg(OH)_2$ samples prepared with CTAB and P123 after the Soxhlet extraction. This DRIFTS measurement shows that practically most of the surfactant is washed away because there are no significant peaks in the interval 2800-3100 cm^{-1} where the peaks of the surfactant are supposed to arise. [93]
The peak around 3650 cm^{-1} is present because of the OH-stretch vibrations. The weak band observed in the spectrum around 1680 cm^{-1} represents the bending modes of the adsorbed water molecules. The peak at approximately 1400 cm^{-1} is due to the OH-bend vibrations. The stretching vibrations of the Mg-O bands are observed at approximately 700 cm^{-1}.

5.2.2.2 Nitrogen adsorption

5.2.2.2.1 BET surface area

Table 4. BET surface area of the two most promising supports after Soxhlet extraction and before calcination.

$Mg(OH)_2$ sample	**BET surface area (m^2/g)**
C - 120°C - 24 hours	19
P - 120°C - 12 hours	31

The BET surface area of the samples treated with a Soxhlet extraction and before calcination is very low. It is possible that it is related to the fact that before calcination, $Mg(OH)_2$ is formed. $Mg(OH)_2$ has the brucite crystal structure and this is a layered structure. The structural layers are very close to each other, which makes the accessibility to the structure very difficult for the nitrogen molecule. Thus, calcination after the treatment with Soxhlet is still needed to transform the layered brucite structure into the porous periclase structure of MgO.

5.2.2.3 X-ray diffraction

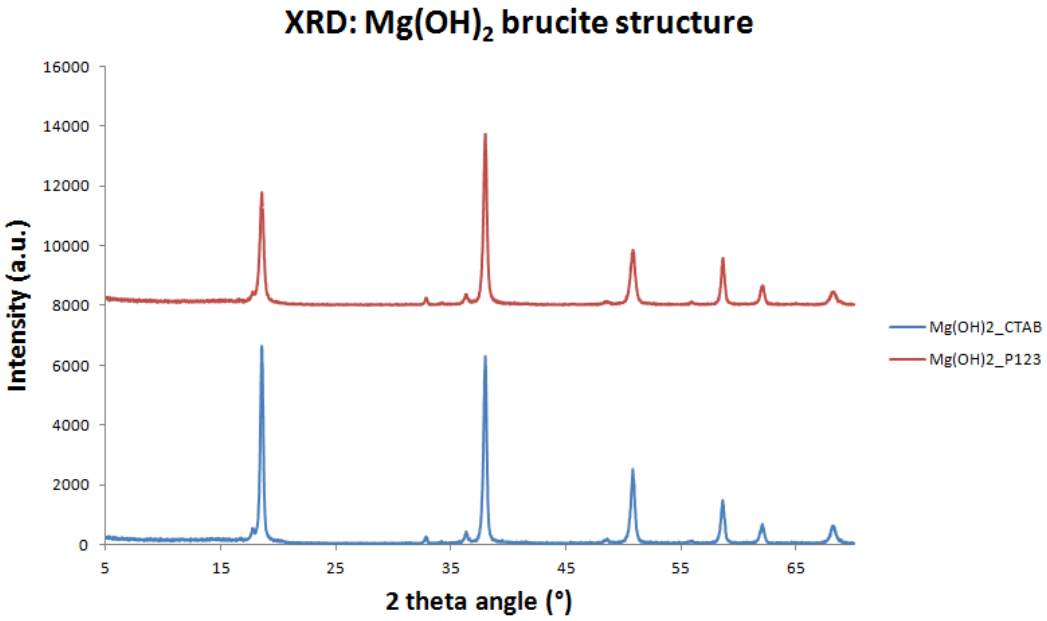

Fig. 40. XRD diffractograms of the most promising $Mg(OH)_2$ supports after Soxhlet extraction and before calcination.

The diffractograms of the Soxhlet treated sample (fig. 40) are characterized by the brucite-type structure of the magnesium hydroxide. [77, 92]
This means that after the Soxhlet extraction procedure, the structure of the magnesium hydroxide materials does not change.

5.2.3 Results and discussion after calcination

5.2.3.1 Nitrogen adsorption

5.2.3.1.1 BET surface area

Table 5. BET surface area of the two most promising supports after Soxhlet extraction and calcination (500 ºC/3 hours).

MgO sample	BET surface area (m^2/g)
C - 120°C - 24 hours	185
P - 120°C - 12 hours	187

The BET surface area of the samples treated with a Soxhlet extraction after calcination is about 20 m^2/g higher than the first samples prepared in the beginning of this chapter (5.1.1). Thus, the removal of the surfactant through a Soxhlet extraction and a calcination procedure after that, delivers mesoporous MgO supports with high BET surface areas. This method will be maintained further in this thesis to synthesize more MgO support materials as actual supports for the catalytic reaction.

5.2.3.1.2 Nitrogen adsorption-desorption isotherms

The isotherms of the supports treated with a Soxhlet extraction, before and after calcination are plotted in fig. 41 and fig. 42 (blue color for uncalcined samples and red color for calcined ones). The uncalcined samples are characterized by type III isotherms. This type of isotherms occurs when the analysed material is macroporous or non-porous. In this case, the layered structure of the $Mg(OH)_2$ brucite phase inhibits the accessibility of the nitrogen into the porous structure. In the case of the calcined samples, both isotherms are type IV isotherms. This means that the obtained MgO supports are mesoporous. [15, 86]

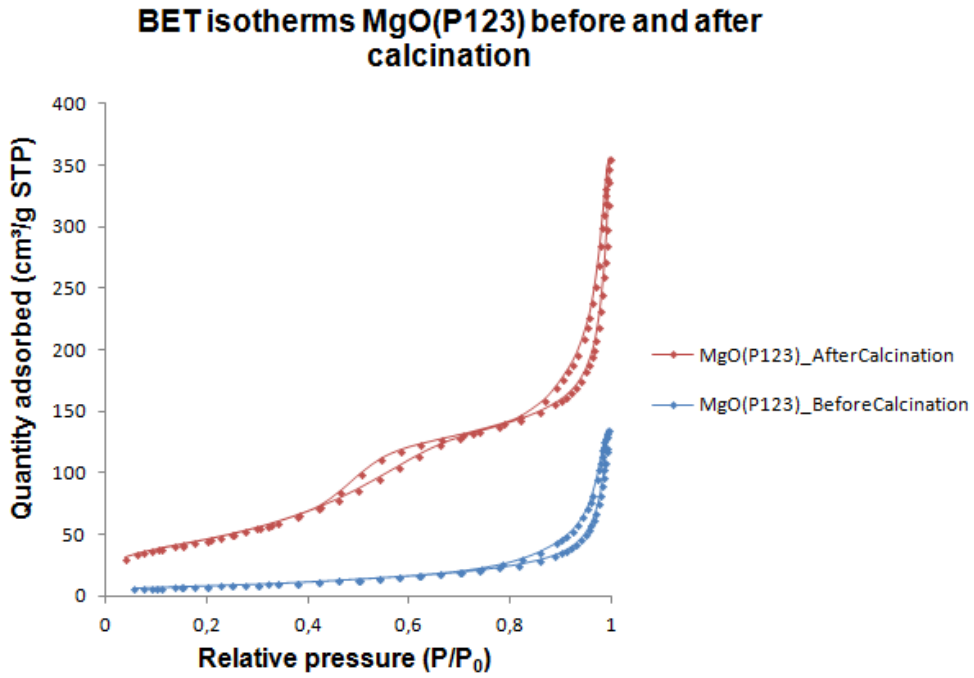

Fig. 41. BET isotherms of the MgO support made with P123 after a Soxhlet extraction treatment before (blue curve) and after (red curve) calcination.

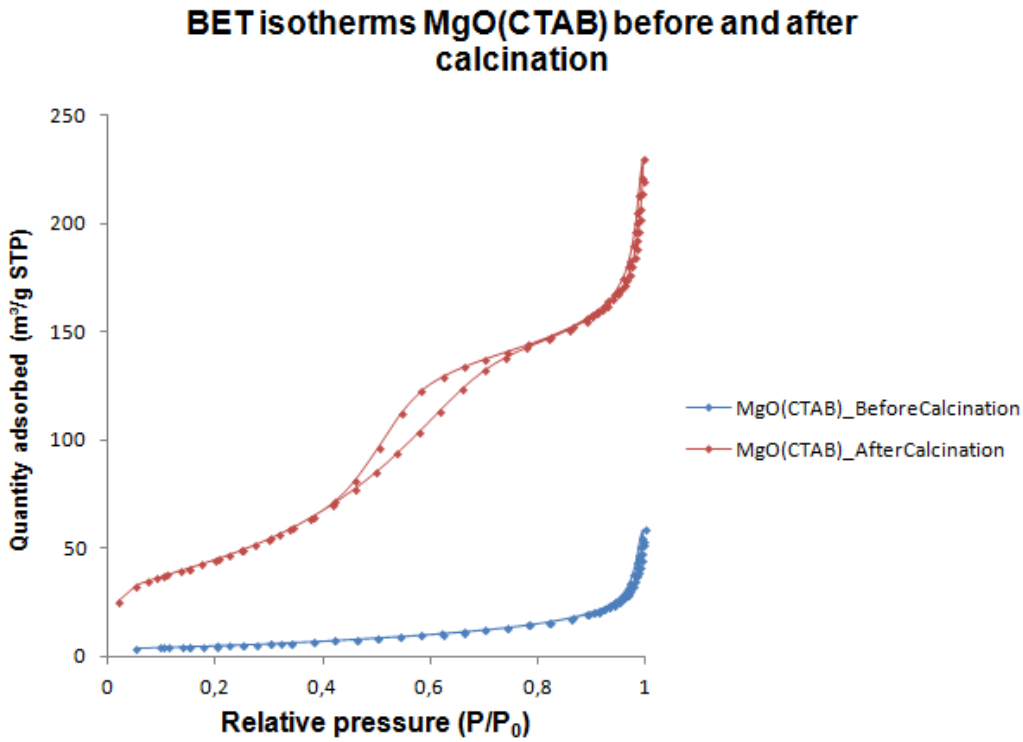

Fig. 42. BET isotherms of the MgO support made with CTAB after a Soxhlet extraction treatment before (blue curve) and after (red curve) calcination.

5.2.3.2 X-ray diffraction

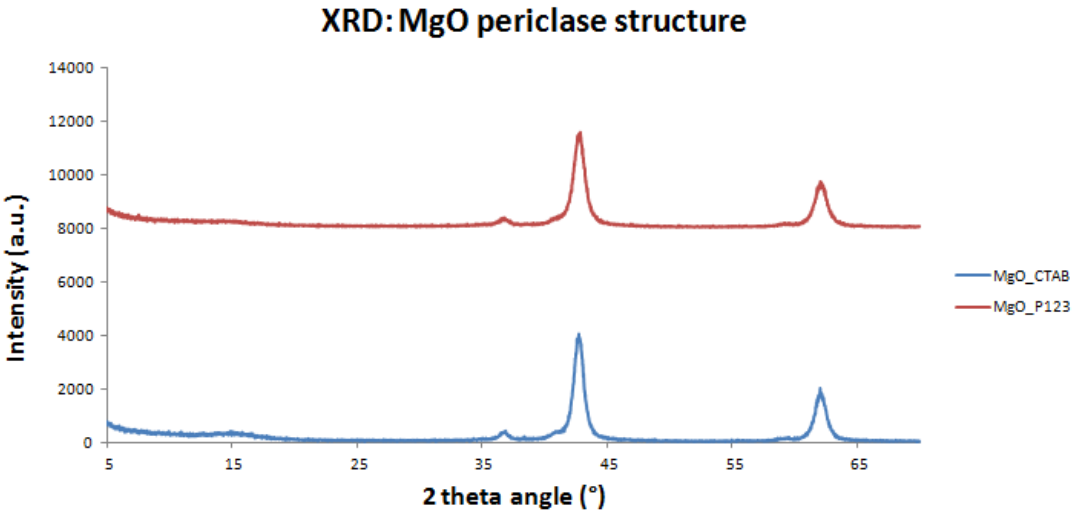

Fig. 43. XRD diffractograms of the most promising MgO supports after Soxhlet extraction and after calcination.

According to the literature, the reflectance peaks in fig. 42 can be correlated to those of the periclase phase of MgO. [77, 92]

5.3 Deposition of gold on commercial magnesium oxide

5.3.1 Deposition of gold by method A and method B

First gold is deposited on commercial MgO in order to use this catalyst as a reference material and also to gain experience on the gold deposition procedure. The gold deposition is performed by a deposition-precipitation method using urea as precipitation agent. In this thesis, this procedure is used due to the fact that very small gold nanoparticles can be acquired. [62]

To impregnate two grams of the commercial MgO support with 1% of gold, two different deposition-precipitation methods using urea are executed.

5.3.1.1 Calculations

$$Deposition\ of\ 1\ wt\%\ Au\ on\ 2\ g\ MgO\ \longrightarrow\ 0{,}02\ g\ Au$$

$$Mw\ HAuCl_4 = 339{,}79\ \frac{g}{mole}$$

$$Mw\ Au = 196{,}97\ \frac{g}{mole}$$

$$weight\ HAuCl_4 =\ 0{,}02\ g\ Au * \frac{1\ mole\ Au}{196{,}97\ \frac{g}{mole}\ Au} * \frac{1\ mole\ HAuCl_4}{1\ mole\ Au} * \frac{339{,}79\ \frac{g}{mole}}{1\ mole\ HAuCl_4}$$

$$= 0{,}0345\ g$$

$$[HAuCl_4] =\ 1{,}6 * 10^{-3}\ M$$

$$mole\ HAuCl_4 = \frac{0{,}0345\ g}{339{,}79\ \frac{g}{mole}} = 1{,}0153 * 10^{-4}\ mole$$

$$1{,}6 * 10^{-3}\ mole\ \longrightarrow 1\ l$$

$$1{,}0153 * 10^{-4}\ mole\ \longrightarrow\ 0{,}0634\ l\ \approx 65\ ml$$

$$[urea] =\ 0{,}42\ M$$

$$mole\ urea = 0{,}42\ \frac{mole}{l} * 0{,}065\ l = 0{,}0273\ mole$$

$$weight\ urea = 0{,}0273\ mole * 60{,}06\ \frac{g}{mole} = 1{,}6396\ g$$

5.3.1.2 Synthesis procedure

With method A, 0,0345 grams of the gold precursor, i.e. chloroauric acid ($HAuCl_4$), and 1,6396 grams of urea is dissolved in 65 ml of distilled water. Then the pH of the solution is measured and it has to be around 2,5. After that, the MgO support is slowly added to the solution. In this way, the pH of the suspension is increased very carefully and hydroxyl ions are produced homogeneously throughout the solution. Strong mixing is required to prevent agglomeration of the gold nanoparticles. Subsequently, the pH of the solution is checked again and it has to amount approximately 10. Then the solution is heated up until 80°C for four hours. After that period of time, the final pH is measured.

There is a decrease in pH during stirring and heating process because the hydroxyl groups from the surface of MgO are replaced by gold-hydroxyl groups. To replace the remaining chloride groups into hydroxyl groups, 25 ml of ammonium hydroxide (25%) is added and the mixture is stirred for another 10 minutes. Like that, the growth of the size of the gold nanoparticles can be avoided. Then the sample is filtered and washed three to four times with distilled water. The obtained powder is dried in the oven at a temperature of 100°C overnight. Finally, the dry sample is pulverized and placed in the furnace for a calcination treatment at 300°C during three hours.

With method B completely the same procedure steps are followed. The only difference is that after dissolving chloroauric acid and the urea precipitation agent in distilled water, the mixture is first warmed up till 80°C and afterwards the commercial MgO support is slowly added. The picture below (fig. 44) shows the difference in intensity of the color of the Au/MgO catalysts. The purple color (due to the gold nanoparticles) on the right vial (method A) is a little bit more intense than that of the vial on the left (method B). This probably means that the deposition with method A went better than with method B.

Fig. 44. Image which shows the difference in intensity between gold deposited on commercial MgO with method A and with method B.

5.3.2 Preliminary tests to determine which method is the best

5.3.2.1 Ultraviolet-visible spectroscopy

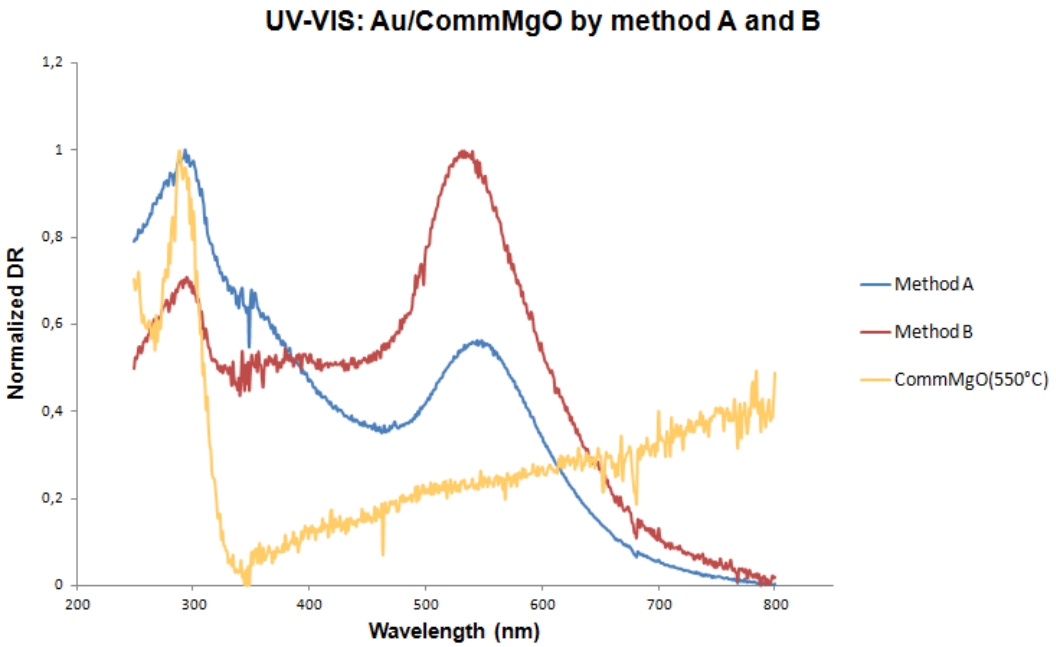

Fig. 45. UV-VIS spectra of the Au/MgO catalyst prepared with method A and with method B and of commercial MgO calcined at 550°C.

The UV-VIS results in fig. 45 display the spectra of gold deposited on commercial magnesium oxide by method A and also by method B. It also shows the spectrum of commercial MgO calcined at 550°C in order to make a comparison with the deposited samples. Around 300 nm the peaks caused by the oxygen to magnesium charge transfer occur. [74] In the case of the gold-catalysts, a broad and intense absorption band appears between 500 and 600 nm due to the absorption of the electronic cloud which occurs around metallic gold particles. [51] This phenomenon is called the surface plasmon resonance. [47, 53] The bigger the gold particle, the larger the plasmon, the more intense the peak. The spectra show that the peak of the sample prepared with method A is less intense, so there can be concluded that de gold catalyst made with this method possesses smaller gold nanoparticles. That is already one reason why method A is used in this thesis to do the deposition of gold on the actual MgO supports.

The wavelength can also be linked with the particle size. The higher the wavelength, the bigger the particle size. However, this applies only when the gold nanoparticles are in a suspension. In the case of the samples analyzed in this thesis, the gold nanoparticles are supported, being difficult to correlate the position of the absorption band with the particle size.

5.3.2.2 Transmission electron microscopy

From fig. 46 it can be derived that the dispersion of the gold nanoparticles is better with method A (top image). With method B (bottom image) the nanoparticles occur in groups and are not homogeneously dispersed. So with method B, the deposition of gold does not appear in a well dispersed way and that is a first reason why method A will be used for the deposition of the actual MgO carriers.

On the other hand, it seems that the morphology of MgO is changed during the deposition of gold with method B. With method A the morphology stays more or less the same (hexagonal formed nanosheets), but with method B the morpholgy of MgO is fiberlike. This could be the result of the faster hydrolysis of the MgO support due to adding the support after heating up the mixture. Presumably, this leads to the rehydration of more MgO to $Mg(OH)_2$. Hence the structure becomes fiberlike.

Finally, the scale of the token images tells something about the particle size of the gold nanoparticles. With method B the particle size of gold is bigger (50-100 nm) than with method A (5-10 nm). This observation is also concluded in the previous preliminary test of UV-VIS measurement. For the catalytic reaction, small gold particles are desired. That is a third reason why method B will not be used for the deposition of gold on the MgO support materials.

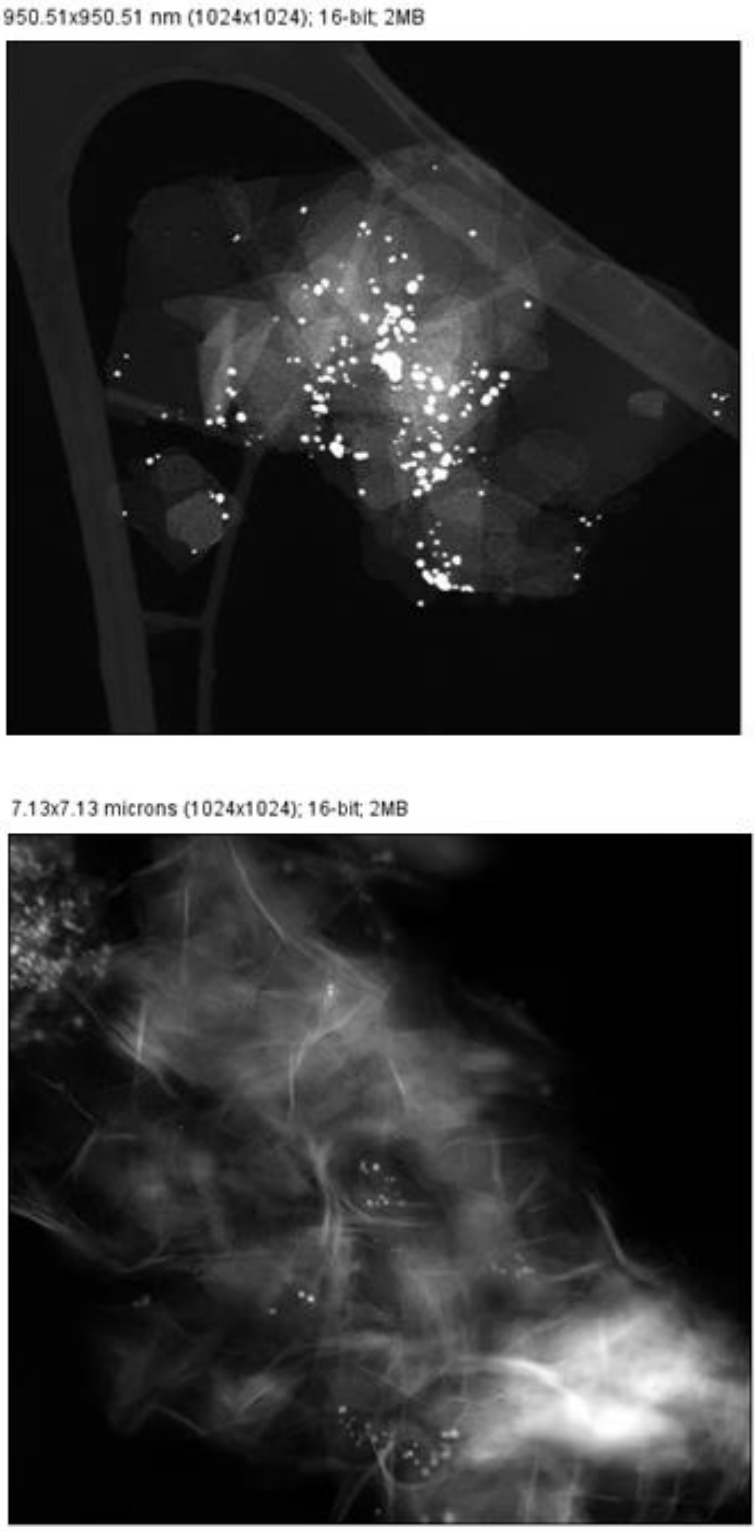

Fig. 46. Preliminary TEM images of gold deposited on commercial MgO by method A (top) and by method B (bottom).

5.3.2.3 X-ray fluorescence

5.3.2.3.1 Sample preparation

In a mortar 0,0200 g of the gold catalyst, 0,0020 g of PbO and 0,1000 g of silica (commercial SiO treated with HNO_3 to remove all of the present metals) are homogenized with a pestle. PbO is used as internal standard and silica as filling material.

5.3.2.3.2 Measurement

For the measurement a calibration curve with PbO as internal standard is utilized (annex 1).
By the following calculation the theoretical value of the number of mmole gold deposited on one gram catalyst is determined.

$$1\%\ Au \longrightarrow 1\ g\ catalyst \longrightarrow 0{,}01\ g\ Au$$

$$\frac{mmole\ Au}{g\ catalyst} = 0{,}01\ g\ Au * \frac{1\ mole\ Au}{196{,}97\ g\ Au} * \frac{1\ mmole}{1 * 10^{-3}\ mole} = 0{,}0508\ \frac{mmole\ Au}{g\ catalyst}$$

$$Method\ A \longrightarrow 0{,}0442\ \frac{mmole\ Au}{g\ catalyst}$$

$$Method\ B \longrightarrow 0{,}0284\ \frac{mmole\ Au}{g\ catalyst}$$

$$Loading\ of\ gold\ with\ method\ A \longrightarrow \frac{0{,}0442}{0{,}0508} = 0{,}87\%$$

$$Loading\ of\ gold\ with\ method\ B \longrightarrow \frac{0{,}0284}{0{,}0508} = 0{,}56\%$$

The experimental values of the loading of gold on the commercial MgO support are less than 1% (target loading). But with method A, a loading of gold of nearly 1% is obtained. Thus, method A will definitely be used for the deposition of gold in the actual MgO carriers.

5.3.3 Effect of the gold deposition on the MgO support (commercial MgO)

5.3.3.1 X-ray diffraction

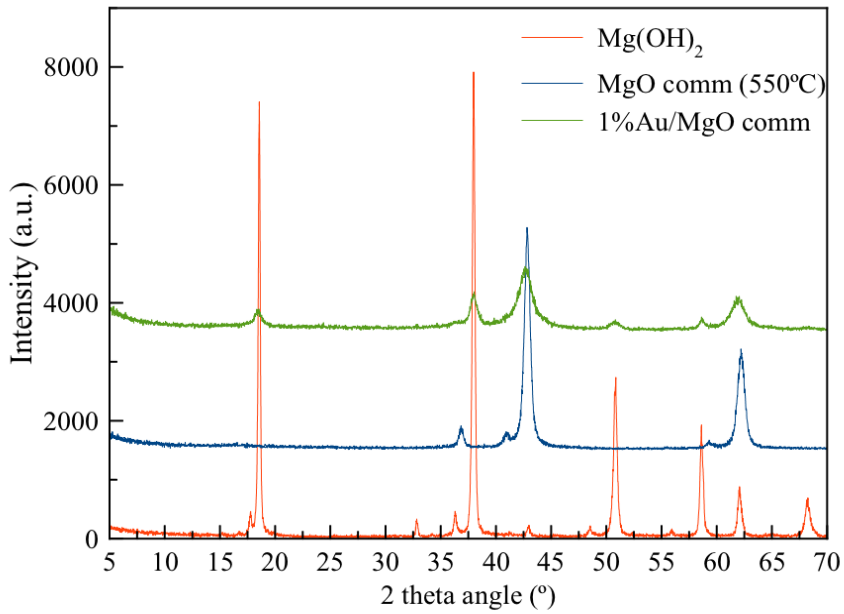

Fig. 47. XRD diffractograms of gold deposited on commercial MgO in comparison with commercial MgO (550°C) and $Mg(OH)_2$.

The XRD diffractograms presented in fig. 47 show the patterns of brucite commercial $Mg(OH)_2$ (red), periclase MgO from the commercial $Mg(OH)_2$ calcined at 550°C (blue) and 1% of gold deposited on the obtained commercial MgO (green). It is observed that the green pattern of the Au/commMgO catalyst matches with the red curve of brucite $Mg(OH)_2$ as well as the blue curve of periclase MgO. According to literature, this can be explained through the partial rehydration of the support during the deposition process. [38, 62] It is also noted that no peaks related with the reflections of the metallic gold (which usually occur at 38° or 44°) nanoparticles are detected in the XRD pattern. [62] This could be explained by the relatively small size of the gold nanoparticles, which is already demonstrated with TEM. Or in this case the overlapping of the peaks from the periclase structure is also possible.

5.3.3.2 Nitrogen adsorption

5.3.3.2.1 BET surface area

Table 6. BET surface area of commercial MgO before and after deposition of gold with method A.

	BET surface area (m^2/g)	
	Before gold deposition	**After gold deposition**
Commercial MgO	127	64

5.3.3.2.2 Nitrogen adsorption-desorption isotherms

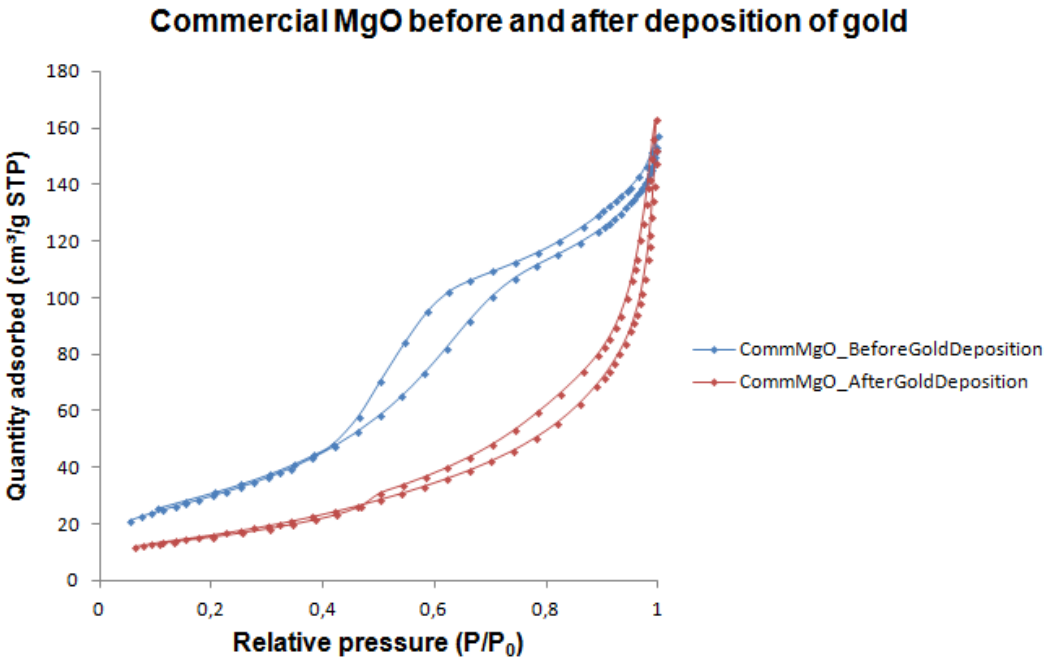

Fig. 48. BET isotherms of commercial MgO before (blue curve) and after (red curve) the deposition of gold.

The deposition of gold influences the crystal structure of the support material as well as the BET surface area of the material. Fig. 48 represents the isotherms of commercial MgO before and after the deposition of gold with method A. The blue curve (before deposition of gold) is a type IV isotherm. The red isotherm (after deposition of gold) represents a type III isotherm. [15, 86]

Thus, the impregnation of gold onto the surface of MgO influences the crystal structure, as well as the porosity, a lot. The BET surface area decreases after deposition of gold until only half of it is left. This phenomenon can also be explained by the partial rehydration of the periclase structure of MgO to the brucite phase of $Mg(OH)_2$. This results in a more layered crystal structure of the support material causing a change in the porosity (hysteresis loop is clearly different) and a low BET surface area.

5.4 Synthesis of the selected MgO supports for the reaction: glycerolysis of urea

In order to have enough MgO support to do the deposition of gold and the catalytic reaction, the synthesis of the two most promising MgO supports is executed again by the same hydrothermal soft templating method used in the beginning of this chapter (5.1). The Soxhlet extraction with acetone is integrated in the procedure and the calcination program (500°C) is also kept the same:

- P - 120°C - 12 hours - 500°C
- C - 120°C - 24 hours - 500°C

Unfortunately, after doing the synthesis of each sample (MgO prepared with P123 and MgO made with CTAB) twice, a surface area as high as that of the initial samples synthesized (with a Soxhlet treatment included), could not be obtained anymore. Thus, there can be concluded that the synthesis method is not that reliable nor reproducible or that something went wrong with the calcination. Due to a lack of time, the synthesis of the MgO supports could not be performed once again. So, for the reaction, gold supported catalysts are made with the initial MgO supports (good surface area) and also with the lower surface area samples in order to see what is the catalytic influence of this parameter.
Thus, from now on the results will be splitted up in two parts: those from the low surface area (LSA, repeated synthesis) supports and their gold catalysts and results from the high surface area (HSA, initial synthesis) supports and their gold catalysts.

5.4.1 Results and discussion

5.4.1.1 X-ray diffraction

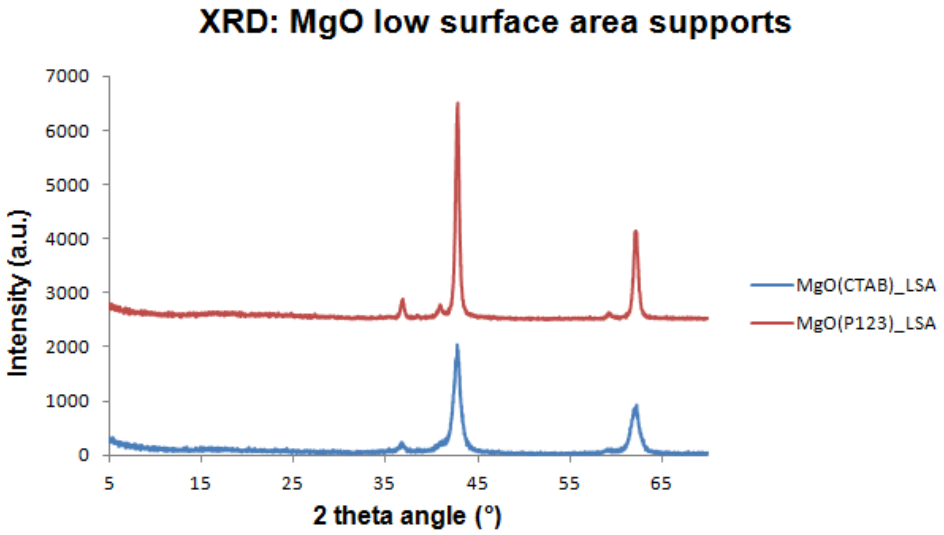

Fig. 49. XRD patterns of the selected low surface area supports made with CTAB and P123 after calcination.

According to literature, the XRD diffractograms in fig. 49 represent the periclase phase of the low surface area supports synthesized with CTAB (blue pattern) and P123 (red pattern) after calcination. [72, 92]

It can also be observed that the reflections of MgO(CTAB) sample are broader and less intense than those of MgO(P123). This means that the MgO material made with CTAB is less crystalline and that the sample has a smaller grain size. [95]

5.4.1.2 Nitrogen adsorption

5.4.1.2.1 BET surface area

Table 7. BET surface area of the low surface area MgO supports.

Low surface area support	BET surface area (m^2/g)
MgO(CTAB)	50
MgO(P123)	109

5.4.1.2.2 Nitrogen adsorption-desorption isotherms

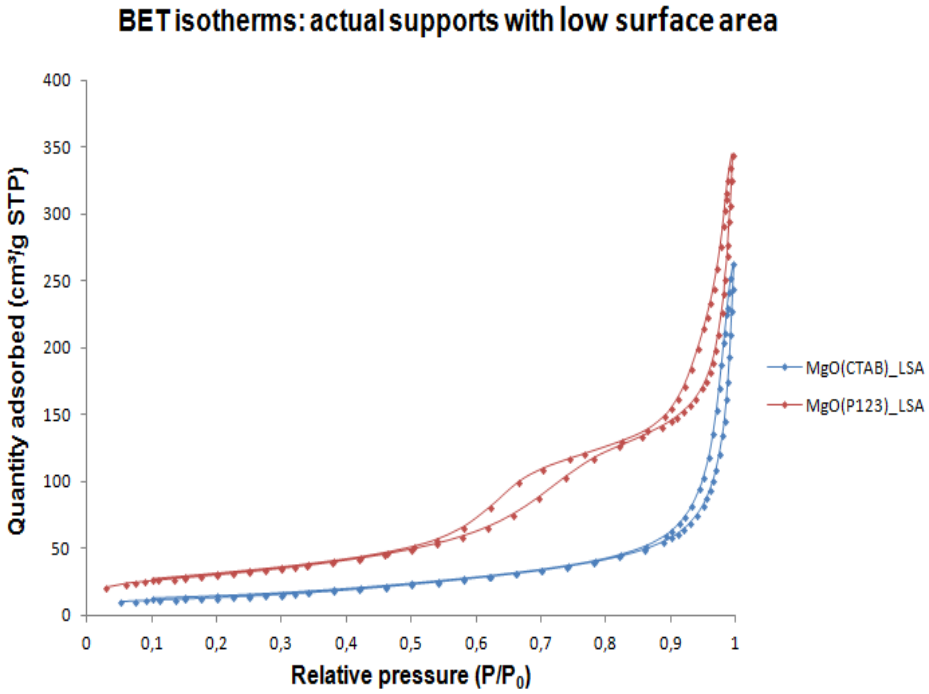

Fig. 50. BET isotherms of the low surface area MgO supports made with CTAB (blue isotherm) and P123 (red isotherm) after calcination.

In fig. 50, the isotherm of the “low surface” MgO support prepared with P123 is a type IV isotherm, which indicates the mesoporosity of the material. However, the isotherm of the low surface area support made with CTAB is a type III isotherm, which points out that the material is not porous. [15, 86]

5.4.2 General overview of the different low and high surface area supports and the respective gold-supported catalysts

Table 8. General overview of the supports and catalysts used for the catalytic reaction.

Low surface area supports	**BET surface area (m^2/g)**	**Low surface area catalysts**	**BET surface area (m^2/g)**
CommMgO	127	Au/CommMgO	64
MgO(CTAB)	50	Au/MgO(CTAB)	115
MgO(P123)	109	Au/MgO(P123)	186

High surface area supports	**BET surface area (m^2/g)**	**High surface area catalysts**	**BET surface area (m^2/g)**
MgO(CTAB)	185	Au/MgO(CTAB)	232
MgO(P123)	187	Au/MgO(P123)	140

Table 8 represents the BET surface area of the selected supports and the respective catalysts utilized for the catalytic reaction. Concerning the BET surface area of the supports and catalysts, a certain trend is noticed. In the case of the synthesized MgO supports, the surface area is increased after gold deposition (only with the high surface area MgO(P123) support the surface area decreases after deposition). This is in contrast to the commercial magnesium oxide support, where the surface area reduces after gold deposition. All of the magnesium oxide supports have the periclase crystal structure conforming to the XRD diffractograms. The XRD patterns of the respective catalysts all show that the samples possess the periclase as well as the brucite structure due to the partial rehydration of the MgO support into $Mg(OH)_2$ during the gold deposition.

6 Catalytic reaction: the glycerolysis of urea

6.1 Calibration of the gas chromatograph for glycerol and glycerol carbonate

6.1.1 Calibration method

In this thesis the method of the response factor (RF) is used to calculate the final concentration of the component which is analyzed. Diethyleneglycolmonomethylether (DEGME) is used as internal standard. Following calculations are applied to obtain the value for the response factor.

$$\frac{A_{component}}{A_{internal\ standard}} = RF * \frac{C_{component}}{C_{internal\ standard}}$$

$$C_{component} = \frac{A_{component} * C_{internal\ standard}}{A_{internal\ standard} * RF}$$

When the horizontal axis of the calibration curve is equal to the concentration (C) of the component divided by the concentration of the internal standard and the vertical axis is equal to the area (A) of the component divided by the area of the internal standard, then the response factor is the slope of the calibration curve.

At least five calibration solutions are made containing glycerol or glycerol carbonate, DEGME and methanol as solvent, all using volumetric flasks of 100 ml. The methanol (99,8%) is purchased from Romil Pure Chemistry. Glycerol (≥99,5%) is purchased from Sigma-Aldrich and the used glycerol carbonate (90%) for obtaining the calibration curve is acquired from abcr GmbH & Co. KG. Table 9 shows the utilized concentrations.

However, glycerol is very viscous so it is not possible to work on volume basis. To make the calibration solutions, all the products have to be weighed in order to work in a consistent way. Then, the experimental masses have to be calculated back into the experimental concentrations.

Table 9. Concentrations of the components of the five different calibration solutions.

Solution	Concentration DEGME (mg/ml)	Concentration glycerol or glycerol carbonate (mg/ml)	Theoretical weight (mg) for 100 ml
1	5,0	1,0	100
2	5,0	2,0	200
3	5,0	3,0	300
4	5,0	4,0	400
5	5,0	5,0	500

Calculation of the theoretical weight of glycerol or glycerol carbonate for 100 ml solution for example for a concentration of 1,0 mg/ml:

$$1{,}0\ \frac{mg}{ml} * 100\ ml = 100\ mg = 0{,}100\ g$$

Calculation of the actual concentration for example for 1 mg/ml glycerol by means of the theoretical weighed mass of glycerol:

$$\frac{0{,}1144\ g\ * \frac{1000\ mg}{g}}{100\ ml} = \ 1{,}144\ \frac{mg}{ml}$$

Each time it is the same calculation to determine the actual concentrations of glycerol and glycerol carbonate and the 5 mg/ml DEGME in every solution. The calibration curves are presented in annex 2 and annex 3.

6.1.2 Preparing stock solution

After reaction, 50 ml of the stock solution is added to the reaction mixture in order to dilute the mixture and to make it less viscous. Like that, an easier separation of the catalyst and the reaction mixture will occur.

The stock solution contains methanol and DEGME with a concentration of 200 mg DEGME per ml methanol and it serves as an external standard. An experimental mass of 100,00 g DEGME is diluted in 500 ml methanol.

6.2 Reaction set up

6.2.1 Glycerolysis of urea under bubbling nitrogen

Fig. 51 shows the reaction set up for the glycerolysis of urea under bubbling nitrogen conditions. A three-neck flask is connected onto a reflux condenser and placed in a heating mantle. The heating mantle, regulated by a PID controller, is positioned on a magnetic stirrer.

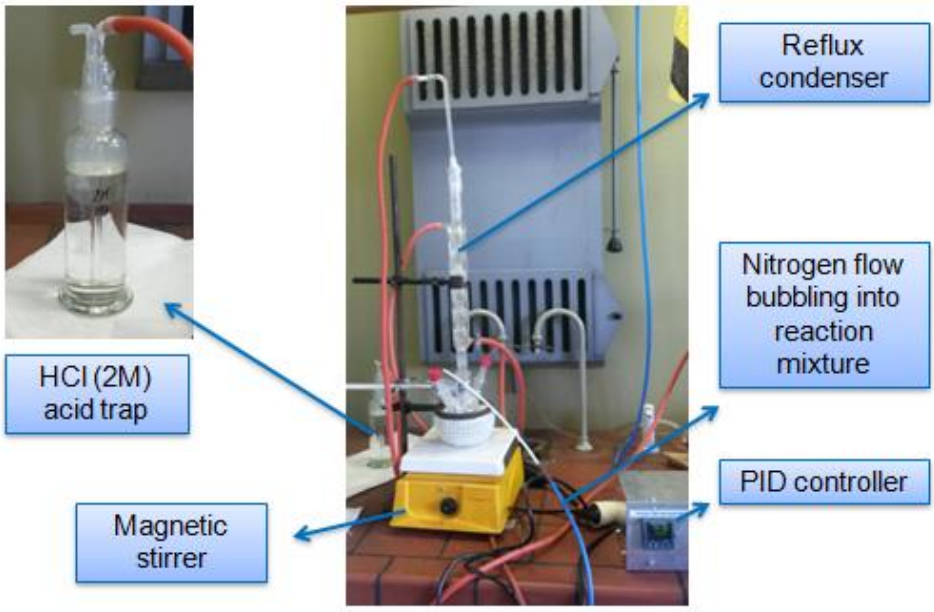

Fig. 51. Reaction set up for the glycerolysis of urea under bubbling nitrogen conditions.

On one side of the three-neck flask, the temperature is measured. The other side is used for the tube with flowing nitrogen. Nitrogen is bubbling into the reaction mixture and is supposed to sweep the formed ammonia away during reaction. The ammonia has to be removed to move the equilibrium of the reaction towards glycerol carbonate and avoid as much as possible the generation of some side products. The ammonia is captured in an acid trap containing HCl (2M) in order to determine the concentration of the formed ammonia by using of a back titration technique.

6.2.2 Glycerolysis of urea under vacuum

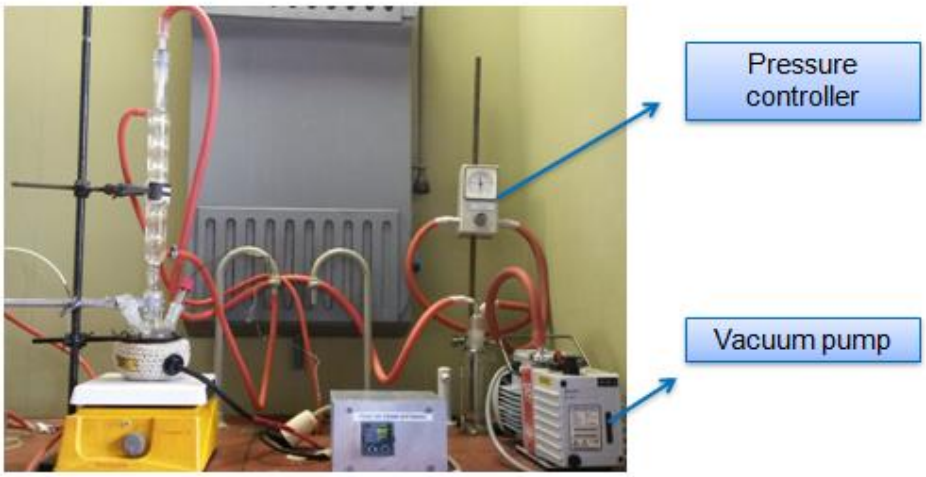

Fig. 52. Reaction set up for the glycerolysis of urea under vacuum conditions.

The set up for the catalytic reaction under vacuum (fig. 52) is practically the same as the previous set up for the reaction with bubbling nitrogen (fig. 51). The only difference is that the nitrogen is replaced by a vacuum pump. Thus, the produced ammonia is pulled away by the vacuum conditions.

6.3 Reaction procedure

6.3.1 Glycerolysis of urea under bubbling nitrogen

6.3.1.1 Reaction mixture and catalyst treatment

10 g of glycerol is poured into a three-neck flask. Then, the tube for the nitrogen flow is put in the flask. The tube has to be in the solution to make sure the nitrogen is bubbling through the reaction mixture. The nitrogen flow is endured at 60-70 ml/min. Afterwards, glycerol is stirred and heated up until a temperature of 140°C. The temperature is held there for 30 minutes. This pre-heating step is necessary to remove the water that could be present in the glycerol. After that, urea and the gold catalyst (5 wt% respect to the glycerol) are added. The glycerol/urea molar ratio is 1. Subsequently, 250 ml of HCl 2M is poured in the acid trap. From now on, a reaction time of four hours can be timed. After the duration of four hours, the reaction is stopped and the system has to be cooled down until room temperature.

The nitrogen flow is left in the reaction mixture till it is cooled down. After cooling down, 50 ml of the stock solution is added to the reaction mixture. The solution is stirred for 5 minutes and then put in the centrifuge at a velocity of 3000 rpm for 15 minutes. Afterwards the catalyst is removed from the reaction mixture and washed two times with acetone and dried for two hours in the furnace at 100°C. The reaction mixture is diluted again for gas chromatography. The calculation of the dilution is as follows:

$$C_1 * V_1 = C_2 * V_2$$

$$V_1 = \frac{C_2 * V_2}{C_1}$$

$$V_1 = \frac{5\ \frac{mg}{ml} * 50\ ml}{200\ \frac{mg}{ml}} = 1{,}25\ ml = 1250\ \mu l$$

Thus, with a micropipette 1250 µl is added in a volumetric flask of 50 ml. Then, the flask is filled with methanol until the calibration line. The mixture is homogenized (this means creating a vortex for at least 10 seconds) and after that, a couple of drops are put in a gas chromatograph vial for analysis.

6.3.1.2 Determination of the concentration of the produced ammonia

The concentration of the formed ammonia is determined by a back titration with sodium hydroxide (NaOH).

First, the exact concentration of NaOH is calculated by means of a titration with a standard solution of oxalic acid ($(COOH)_2 \cdot 2H_2O$). 20 ml of a 0,5 M oxalic acid solution is pipetted into an erlenmeyer. Three drops of phenolphthalein are added. The mixture is titrated with a 2 M NaOH solution until the color of the solution changes from colorless to pink (intense). After that, a second titration of HCl with NaOH, of which the actual concentration is known, is executed in order to determine the exact concentration of HCl. 20 ml of HCl is pipetted in an erlenmeyer and three drops of phenolphthalein are added. The solution is titrated with NaOH. The color of the solution changes from colorless to pink (intense). After 4 hours of reaction time, the HCl (with a known concentration) from the acid trap is titrated back with NaOH to calculate the concentration of the formed ammonia. Again, three drops of phenolphthalein are added. The color of the titrated solution changes from colorless to very light pink (almost transparent).

6.3.1.2.1 Calculations

- Preparation of 1 l HCl (37%) 2 M

$$1{,}19\ \frac{kg}{l} * 0{,}37 = 0{,}4403\ \frac{kg\ HCl}{l\ solution} = 440{,}3\ \frac{g}{l}$$

$$Mw\ HCl = 36{,}46\ \frac{g}{mole}$$

$$\frac{440{,}3\ \frac{g}{l}}{36{,}46\ \frac{g}{mole}} = 12{,}08\ \frac{mole}{l} = 12{,}08\ M$$

$$C_1 * V_1 = C_2 * V_2$$

$$V_1 = \frac{1{,}000\ l * 2\ \frac{mol}{l}}{12{,}08\ \frac{mol}{l}} = 0{,}1656\ l = 165{,}6\ ml$$

165,6 ml of HCl (37%) is diluted with distilled water in a volumetric flask of 1 l until the calibration line and homogenized.

- Preparation of 500 ml NaOH 2 M

$$Weight\ NaOH = C_{NaOH} * Mw_{NaOH} * V_{NaOH}$$

$$Weight\ NaOH = 2\ \frac{mole}{l} * 40{,}00\ \frac{g}{mole} * 0{,}5000\ l = 40{,}0000\ g$$

40,0000 g NaOH is dissolved in a volumetric flask of 500 ml with distilled water and homogenized.

- Preparation of 250 ml $(COOH)_2 \cdot 2H_2O$ 0,5 M

$$Weight\ (COOH)_2 \cdot 2H_2O = C_{(COOH)_2 \cdot 2H_2O} * Mw_{(COOH)_2 \cdot 2H_2O} * V_{(COOH)_2 \cdot 2H_2O}$$

$$Weight\ (COOH)_2 \cdot 2H_2O = 0{,}5\ \frac{mole}{l} * 126{,}07\ \frac{g}{mole} * 0{,}2500\ l = 15{,}7588\ g$$

15,7588 g of oxalic acid is dissolved in a volumetric flask of 250 ml with distilled water and homogenized.

- Calculation of the actual NaOH concentration

$$C_{NaOH} * V_{NaOH} * a_{NaOH} = C_{(COOH)_2 \cdot 2H_2O} * V_{(COOH)_2 \cdot 2H_2O} * a_{(COOH)_2 \cdot 2H_2O}$$

$$C_{NaOH} = \frac{0{,}020\ l * 0{,}5\ M * 2}{V_{NaOH} * 1}$$

- Calculation of the actual HCl concentration $[HCl]_0$

$$C_{NaOH} * V_{NaOH} * a_{NaOH} = C_{HCl} * V_{HCl} * a_{HCl}$$

$$C_{HCl} = \frac{C_{NaOH} * V_{NaOH} * 1}{0{,}020\ l * 1} = [HCl]_0$$

- Calculation of the HCl concentration after reaction $[HCl]_1$ and determination of the concentration of the formed ammonia $[NH_3]$

$$C_{NaOH} * V_{NaOH} * a_{NaOH} = C_{HCl} * V_{HCl} * a_{HCl}$$

$$C_{HCl} = \frac{C_{NaOH} * V_{NaOH} * 1}{0{,}020\ l * 1} = [HCl]_1$$

$$[NH_3] = [HCl]_0 - [HCl]_1$$

6.3.1.2.2 Complications inherent to this method

Unfortunately, this method for the determination of the concentration of the formed ammonia is not that reliable since a great part of the ammonia formed, leaks out from the reaction system. Therefore, the concentration of the produced NH_3 calculated by means of a back titration is much lower than expected and it does not conform with amount of produced glycerol carbonate.

6.3.2 Glycerolysis of urea under vacuum conditions

The procedure for this catalytic reaction under vacuum conditions is basically the same. The only difference between the bubbling nitrogen and with a vacuum pump is already described in the reaction set up.

The tube with the nitrogen flow and the acid trap are withdrawn. Instead, a vacuum pump is installed to extract the produced ammonia away from the reaction mixture. The pressure of the pump is adjusted until a value of 500 mbar.

6.3.3 Glycerolysis of urea under bubbling nitrogen: implementation

6.3.3.1 Calculations by means of peak area obtained via gas chromatography

In this thesis, the calculations for the determination of the conversion of glycerol, yield of glycerol carbonate and selectivity towards glycerol carbonate are made for the catalytic reaction with the commercial MgO support. However, the calculation procedure is exactly the same for each reaction.

$$Weight\ glycerol = 10{,}0356\ g$$

$$Initial\ concentration\ of\ glycerol = \left(\frac{10{,}0356\ g * 1000\ \frac{mg}{g}}{50\ ml}\right) * \frac{1{,}25\ ml}{50\ ml} = 5{,}0178\ \frac{mg}{ml}$$

$$= C_{glycerol,i}$$

$$A_{glycerol} = 3701{,}8$$

$$A_{internal\ standard} = 12198{,}7$$

$$A_{glycerol\ carbonate} = 2405{,}5$$

$$End\ concentration\ of\ glycerol = \frac{A_{glycerol} * C_{internal\ standard}}{A_{internal\ standard} * RF_{glycerol}} = \frac{3701{,}8 * 5\ \frac{mg}{ml}}{12198{,}7 * 0{,}6238}$$

$$= 2{,}4323\ \frac{mg}{ml} = C_{gly,e}$$

$$End\ concentration\ of\ glycerol\ carbonate = \frac{A_{glycerol\ carbonate} * C_{internal\ standard}}{A_{internal\ standard} * RF_{glycerol\ carbonate}}$$

$$= \frac{2405{,}5 * 5\ \frac{mg}{ml}}{12198{,}7 * 0{,}6058} = 1{,}6276\ \frac{mg}{ml} = C_{glycerol\ carbonate,e}$$

$$Conversion\ of\ glycerol = \left(\frac{C_{gly,i} - C_{gly,e}}{C_{gly,i}}\right) * 100\% = 51{,}53\%$$

$$Molecular\ weight\ ratio\ between\ glycerol\ and\ glycerol\ carbonate = \frac{92{,}09\ \frac{g}{mole}}{118{,}09\ \frac{g}{mole}}$$

$$= 0{,}78$$

$$Yield\ of\ glycerol\ carbonate = \left(\frac{Moles_{glycerol\ carbonate,e}}{Moles_{gly,i}}\right) * 100\% * 0{,}78 = 25{,}30\%$$

$$Selectivity\ towards\ glycerol\ carbonate = \left(\frac{Yield\ of\ glycerol\ carbonate}{Conversion\ of\ glycerol}\right) * 100\%$$

$$= 49{,}10\%$$

6.3.3.2 Results

6.3.3.2.1 Conversion, yield and selectivity

First, the commercial MgO support and the gold supported on commercial MgO catalyst are tested during the glycerolysis of urea. Fig. 53 shows that for both the support and the catalyst of commercial MgO the percentages concerning conversion of glycerol, yield of glycerol carbonate and selectivity towards glycerol carbonate are very similar. However, this is impossible according to literature. [34]

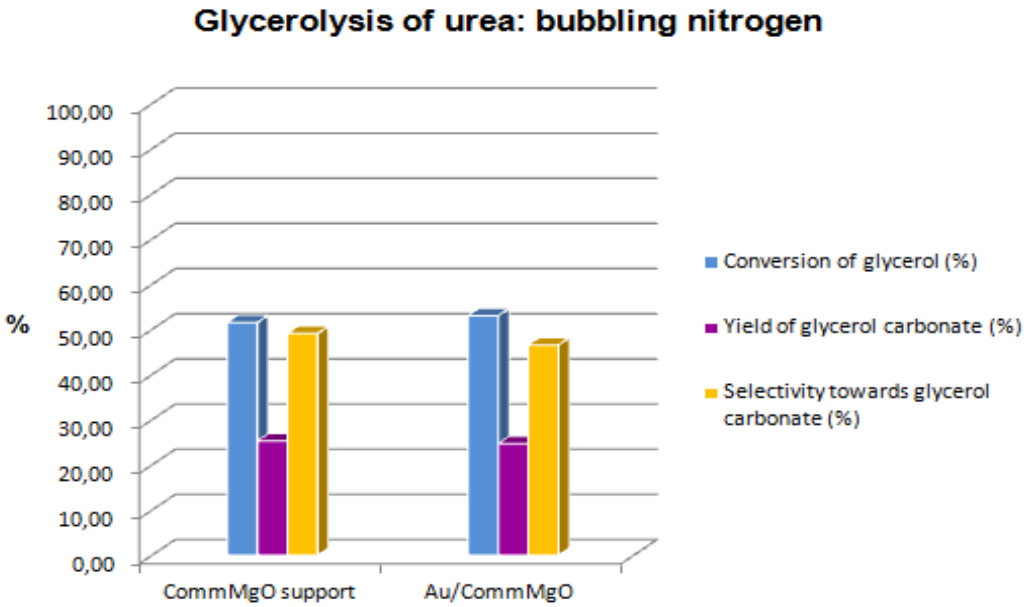

Fig. 53. Results of the reactions with the commercial MgO support and catalyst under bubbling nitrogen conditions.

There can be assumed that the procedure with the gas chromatograph went well. So there has to be something wrong about the reaction conditions. The practically equal percentages between the commercial MgO support and gold deposited on commercial MgO could be explained due to the fact that the reaction products can be entrained with the nitrogen flow (entrainment of a liquid with a gas).

6.3.3.2.2 X-ray diffraction

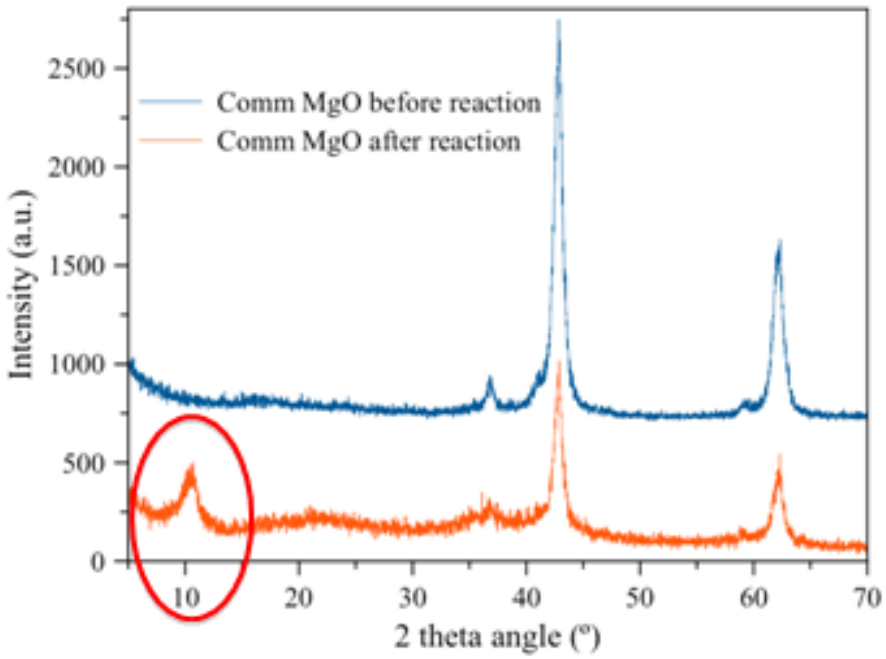

Fig. 54. XRD diffractogram of the commercial MgO support before and after reaction under nitrogen bubbling conditions.

The figure above (fig. 54) represents the XRD patterns of the commercial MgO support before and after catalytic reaction. Both patterns show that the material has the periclase structure. [72, 92]

Moreover, the patterns match quite well, but in the diffractogram after reaction there is one significant peak observed at the early angle of 10°. This may be caused by the glycerol. Because during the reaction it is possible that there is a partial reconstruction of the brucite crystal structure and this structure is layered. During reaction, intercalation of the glycerol can occur between those layers which increases the distance between the layers resulting in a peak at a very early angle.

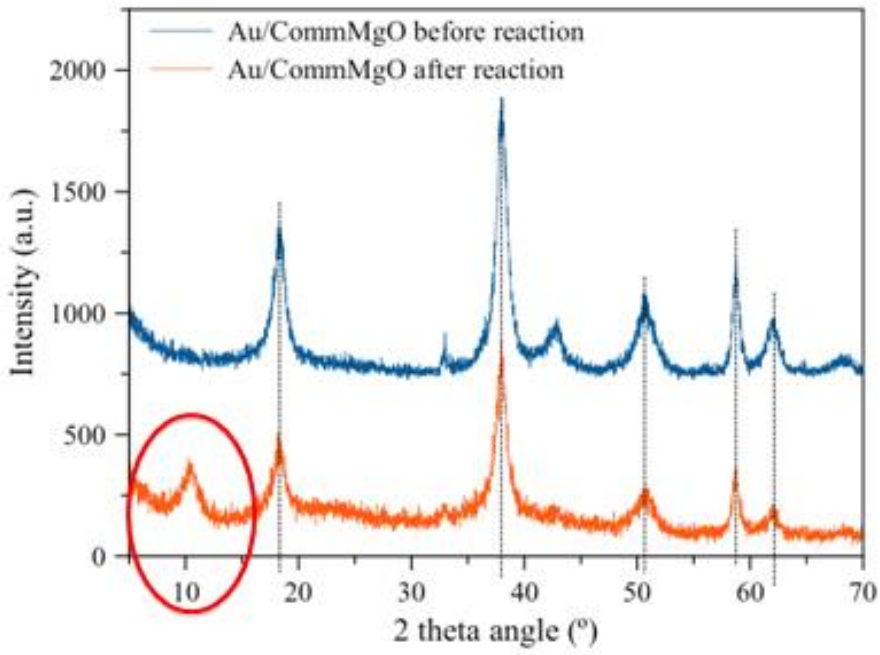

Fig. 55. XRD diffractogram of the commercial MgO gold catalyst before and after reaction under nitrogen bubbling conditions.

Completely the same phenomenon occurs with the XRD diffractograms of the gold on commercial MgO catalyst before and after reaction (fig. 55). The patterns represent the periclase as well as the brucite crystal stucture due to the partial rehydration of the periclase structure during the deposition process of gold. The patterns also coincide, but the only significant difference is the peak of the red diffractogram at a very little angle. This can repeatedly be explained by the intercalation of glycerol between the layers of the brucite structure.

6.3.3.2.3 X-ray fluorescence

XRF analysis is performed on the gold on commercial MgO catalyst before and after reaction in order to get some information about the loading of gold on the material. The quantity of leached gold can be calculated as well.
Sample preparation and calculations to determine the loading of gold on the commercial MgO support are done the same way as in subchapter 5.3.2.3. The loading of gold on commercial MgO before reaction has a value of 0,57%. Thus, considering a theoretical value of 1% loading of gold, it can be concluded that the deposition was not very efficient. However, after reaction, the loading of gold amounts 0,46%.
So, approximately 20% of gold has leached out during the glycerolysis of urea with the gold on commercial MgO catalyst. Further in this thesis, the catalysts synthesized using CTAB or P123 as surfactant, will also be examined regarding the loading of gold and analysed if their stability properties are improved.

6.3.4 Test reactions: implementation

To find what could be the problem, five test reactions with commercial ZnO as catalyst are exhibited in following list:

- Test reaction 1: nitrogen bubbling in reaction mixture – nitrogen flow of 60-70 ml/min – slow stirring
- Test reaction 2: nitrogen tube placed in head space – nitrogen flow of 60-70 ml/min
- Test reaction 3: vacuum pump – 500 mbar
- Test reaction 4: nitrogen bubbling in reaction mixture – nitrogen flow of 20-30 ml/min
- Test reaction 5: nitrogen bubbling in reaction mixture – nitrogen flow of 60-70 ml/min – fast stirring

A completely blanc reaction without catalyst is also performed under vacuum conditions. The results are represented in the bar graph below (fig. 56). Concerning the blanc reaction, it is important to mention that the reaction can proceed without a catalyst. Test reaction 3, the one with the vacuum pump, shows the best results concerning conversion of glycerol, yield of glycerol carbonate and selectivity towards glycerol carbonate.

Concerning the stirring rate, it can be decided that fast stirring results in higher conversions and yields causing a higher selectivity percentage (because of the improved diffusion). In addition, when the nitrogen tube is placed in the head space of the reactor (test reaction 2), the conversion is average, but the yield of glycerol carbonate is very low. This is probably because the formed ammonia cannot be removed well enough and the equilibrium is inadequately situated towards glycerol carbonate. Another conclusion is the lower the nitrogen flow, the lower the conversion and yield.

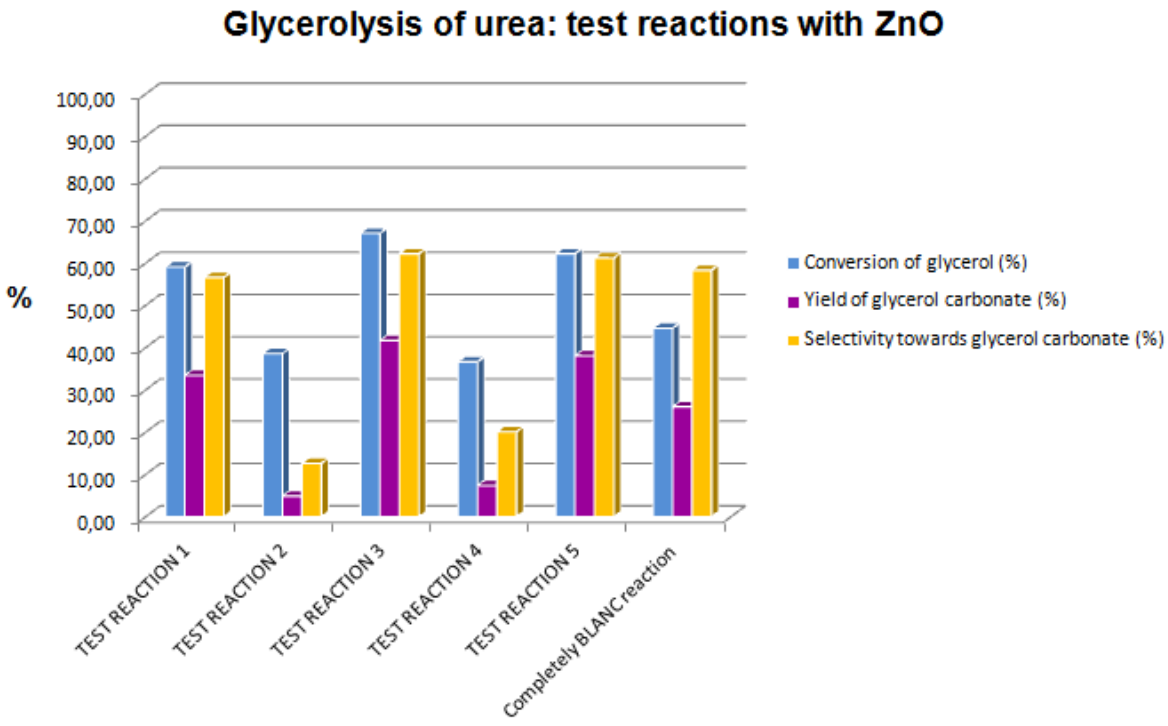

Fig. 56. Results of the test reactions with commercial ZnO as catalyst.

Thus, it is decided to do the rest of the reactions with the supports and the respective gold catalysts under vacuum conditions.

6.3.5 Glycerolysis of urea under vacuum: implementation

6.3.5.1 Results concerning the low surface area supports and catalysts

6.3.5.1.1 Conversion, yield and selectivity

Among the results of the reactions under vacuum conditions (fig. 57) there is absolutely a difference between the supports and their catalysts. The abbreviation 'LSA' stands for low surface area. It can be decided that with the catalyst gold supported on MgO prepared with the surfactant P123 the highest selectivity of 69% is obtained. Below, the results of this reaction are represented in table 10.

Table 10. Results of the catalyst with the highest selectivity: Au/MgO(P123) with low surface area.

Au/MgO(P123) with low surface area	
Conversion of glycerol	50%
Yield of glycerol carbonate	34%
Selectivity towards glycerol carbonate	69%

Although, the conversion of glycerol is not that much different in comparison to the blank reaction (conversion and selectivity of the blanc reaction is 45%, respectively 58%), but a great part of the converted glycerol is turned into glycerol carbonate and this proves that this kind of catalyst is actually working because the yield of the blanc reaction is only 26%. This is much lower than the yield of the best performing catalyst: 34%.

After a second run of the best scoring catalyst, the yield of glycerol decreases significantly from a value of 34% to a value of 19%, which results in a great loss of selectivity towards glycerol carbonate. Through several characterization techniques, this phenomenon will be explained as good as possible.

The reaction with the Au/CommMgO catalyst is also performed again under vacuum conditions. However, better results than the reaction with the same catalyst under bubbling nitrogen (conversion of 53% and a selectivity of 25%) are not acquired.

Another observation of fig. 57 is that the reaction with the Au/MgO(CTAB) catalyst scores average, but there is also a significant difference in comparison with its support. The

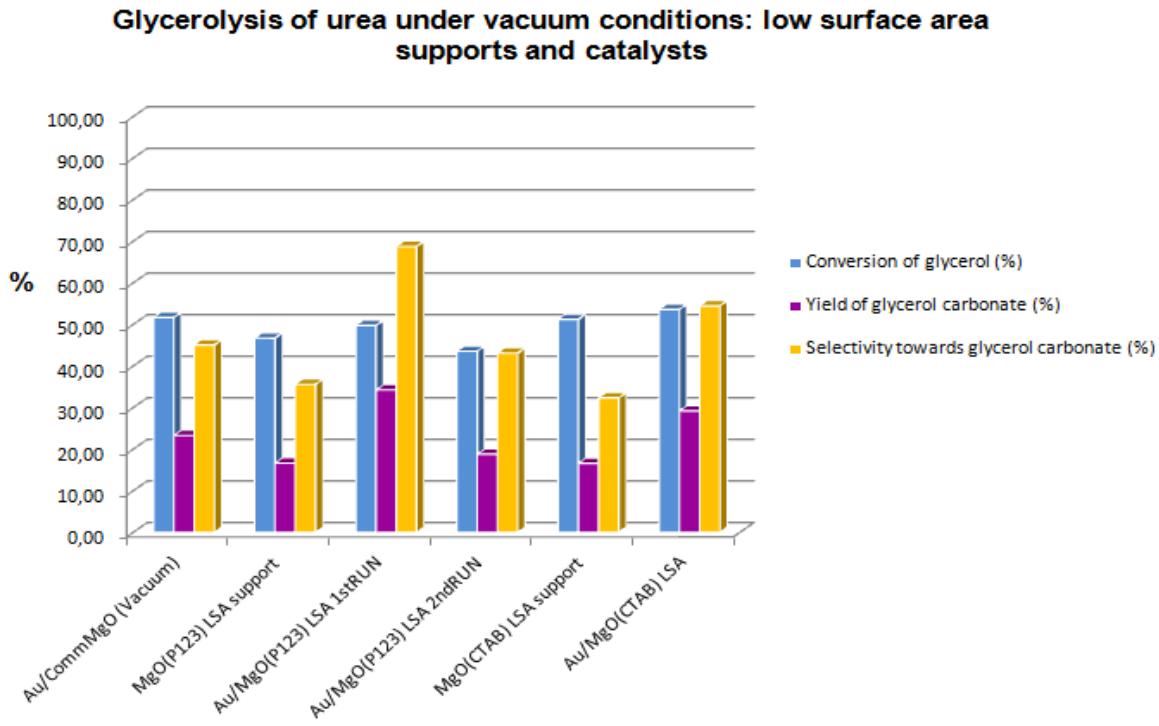

Fig. 57. Results of the reactions with the low surface area supports and catalysts under vacuum conditions.

conversions are practically the same, but in case of the catalyst, the yield doubles causing a selectivity twice as high as that of the reaction with the support.

6.3.5.1.2 Diffuse reflectance infrared Fourier transform spectroscopy

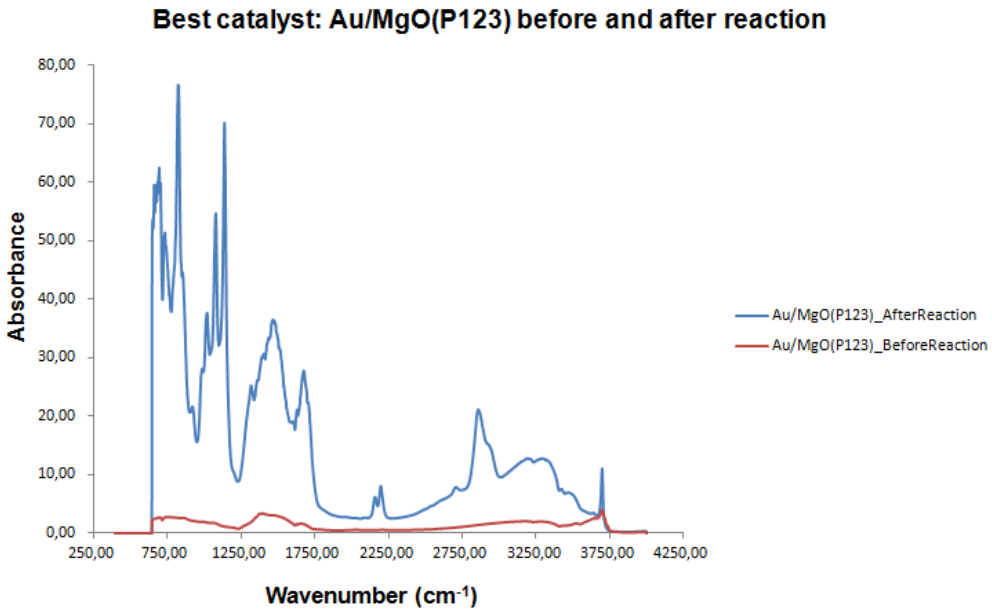

Fig. 58. DRIFT spectra of the best scoring catalyst regarding the selectivity: Au/MgO(P123) with low surface area before and after reaction.

Fig. 58 displays the DRIFT spectra of the Au/MgO(P123) low surface area catalyst which has the best selectivity towards glycerol carbonate, before and after reaction. There is a huge difference between the two spectra. The spectrum of the catalyst after reaction shows many and very sharp peaks in contrast to that of the catalyst before reaction. Carbonate stretches are observed in the Au/MgO catalyst after use, with bands at ~3500 cm^{-1}, ~1500 cm^{-1} and ~1100 cm^{-1}. [34]

This observation may indicate that the catalyst adsorbs a part of the reaction products on its surface during the reaction which can result in a significant decrease of its activity during the second run and causing a reduction in selectivity.

6.3.5.1.3 X-ray diffraction

Fig. 59 represents the XRD diffractograms of the Au/MgO(P123) low surface area catalyst before reaction, after a first run and after a second run. The peaks situated at the early angle of 10° occur again. A possible explanation is already clarified in a previous subchapter (6.3.3.2.2).

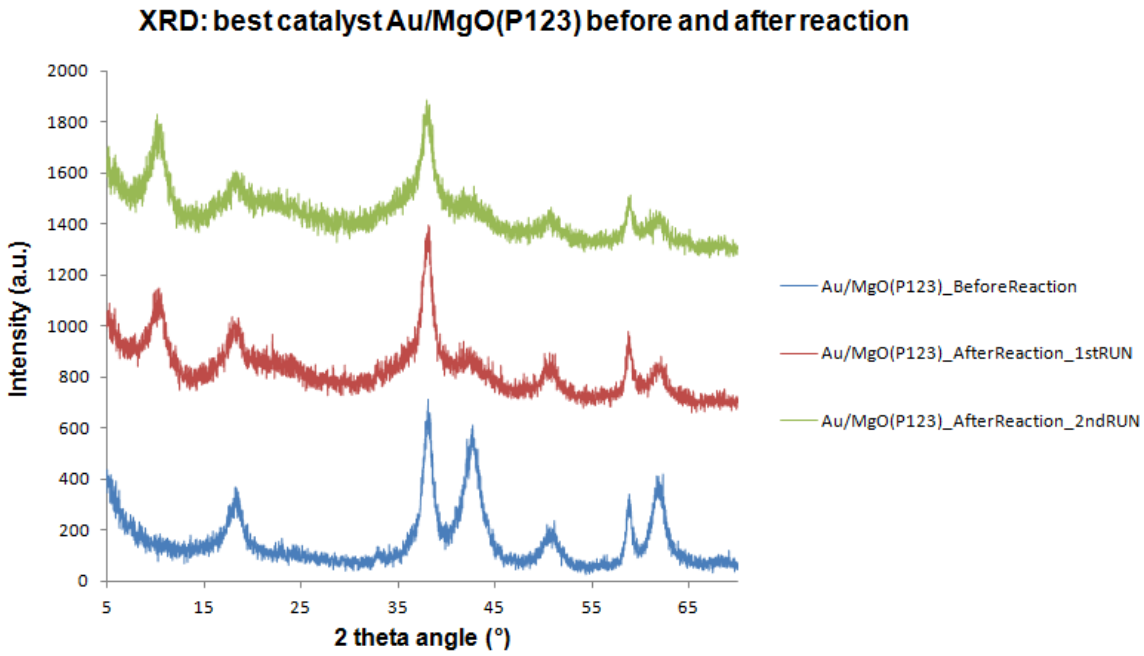

Fig. 59. XRD diffractograms of the best scoring catalyst concerning the selectivity (Au/MgO(P123)_LSA) before reaction (blue pattern), after reaction for the first run (red pattern) and after reaction for the second run (green patteren).

Another observation is the shrinkage of the peak right before an angle of 45° after a first run and after the second run. This peak is one which represents the periclase crystal structure of MgO. The shrinking of this peak could explain the partial reconstruction of the brucite phase of the support material. The same observation can be noticed in fig. 60 with the other low surface area catalyst: Au/MgO(CTAB).

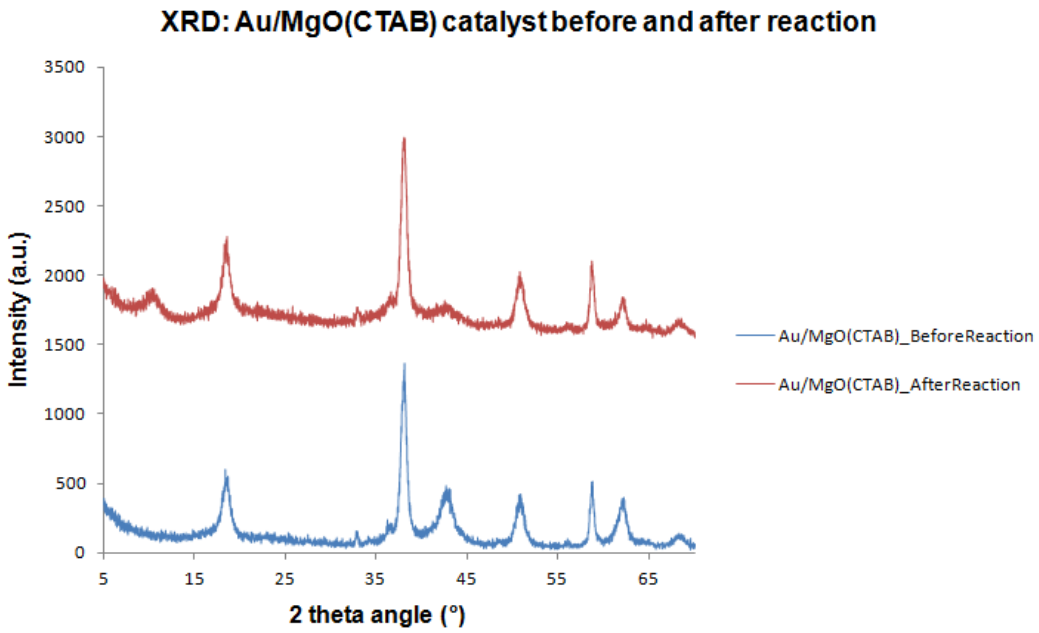

Fig. 60. XRD diffractograms of the Au/MgO(CTAB) low surface area catalyst before (blue pattern) and after (red pattern) reaction.

6.3.5.1.4 X-ray fluorenscence

Sample preparation and calculations to determine the loading of gold on the Au/MgO catalysts are done the same way as in subchapter 5.3.2.3.

Regarding the catalyst Au/MgO(P123) with the low surface area the experimental loading of gold on its surface is 0,75% before reaction which is not bad in comparison with the theoretical 1%. After reaction, the remaining loading of gold on the surface is only 0,41%. Thus, unfortunately there is a loss of gold nanoparticles on the surface of roughly 45%. The leaching of gold can explain the bad yield of glycerol carbonate in conjunction with the decrease in selectivity towards glycerol carbonate. After the second run of the best catalyst, the loading of gold is 0,36%. Thus, there is still leaching of gold out of the catalyst for approximately 35%. The gold catalyst of which the support is prepared with CTAB scores the best concerning the loading of gold before and after reaction with percentages of respectively 0,80% and 0,75%. This means that the catalyst is quite stable.

Table 11. Leaching percentages of the low surface area catalysts.

Low surface area catalyst	Loading of gold before reaction (%)	Loading of gold after reaction (%)	% leaching
Au/MgO(P123)_1stRUN	0,75	0,41	45
Au/MgO(P123)_2ndRUN	0,41	0,36	35
Au/MgO(CTAB)	0,80	0,75	6

6.3.5.1.5 Nitrogen adsorption

Table 12. BET surface area of the low surface area gold catalysts before gold deposition, before reaction and after reaction.

Catalyst	BET surface area (m²/g)		
	Before deposition of gold	Before Reaction	After reaction
Au/MgO(P123)_1stRUN	109	186	106
Au/MgO(P123)_2ndRUN	109	106	29
Au/MgO(CTAB)	50	115	49

In table 12 the BET surface area of the low surface area catalysts are represented before deposition, before reaction and after reaction. It can be noticed that, remarkably, for both samples Au/MgO(P123)_1stRUN and Au/MgO(CTAB) the surface area before deposition and after deposition (same as before reaction) is increased. This has not occurred before, but it could be explained by an error in the calcination program when transforming the magnesium hydroxide into magnesium oxide. When calcining again at 300°C after the deposition of gold, the temperature treatment could have fixed the MgO structure creating a material with a higher surface area.

After the use of the catalyst, the materials are becoming less porous and they lose approximately half of their surface area in the case of the used catalysts after a first run. After a second run, the surface area is reduced until more or less a fourth of its surface area before reaction.

In fig. 61 the nitrogen adsorption-desorption isotherms of the low surface area Au/MgO(P123) catalyst are shown before reaction and after a first and a second run. The same observations can be made as in 5.3.3.2. After gold deposition, the porous structure is partial re-hydrated into a layered, brucite material.

Furthermore, it is observed that after a first and a second run, a reduction of the hysteresis loop occurs. Less and less nitrogen is adsorbed by the material so desorption almost cannot take place. This may explain the contamination of the catalyst with the reaction products.

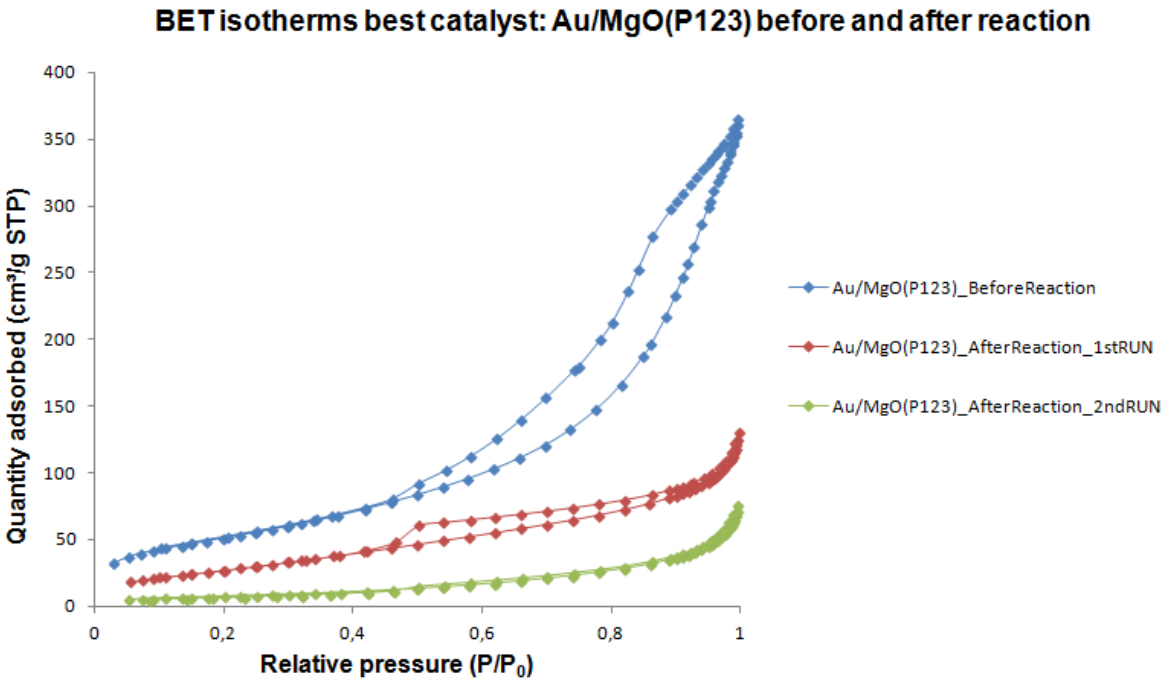

Fig. 61. Nitrogen adsorption-desorption isotherms of the best scoring catalyst concerning the selectivity towards glycerol carbonate (Au/MgO(P123)_LSA) before reaction (blue isotherm), after reaction for the first run (red isotherm) and after reaction for the second run (green isotherm).

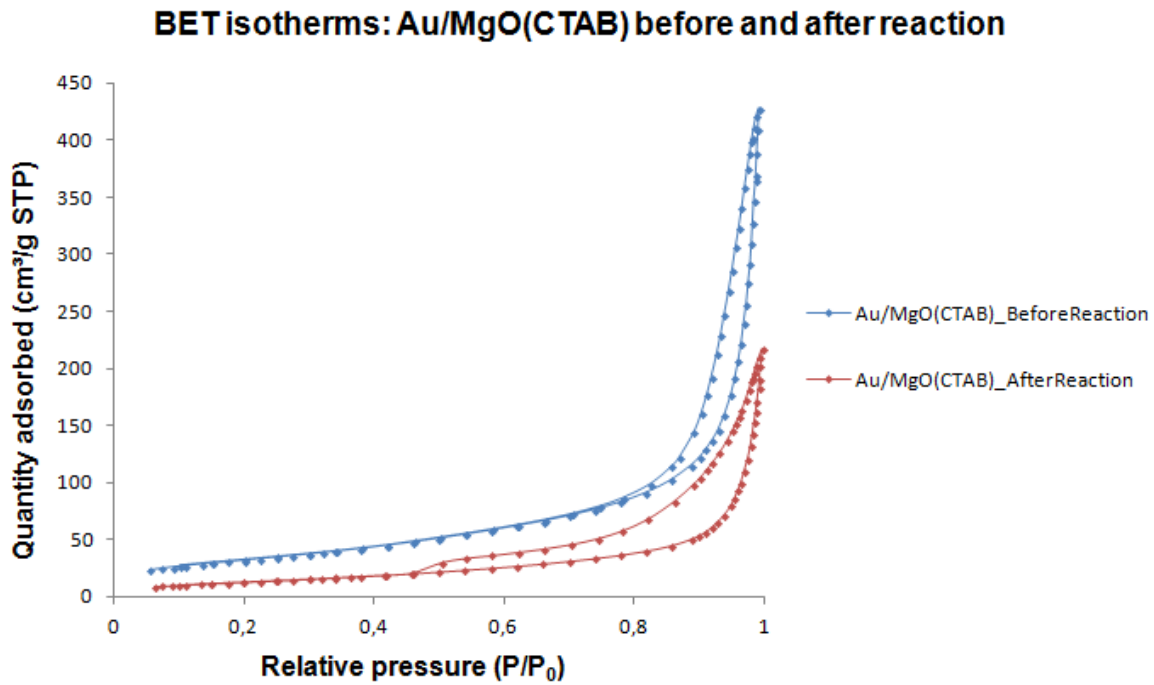

Fig. 62. Nitrogen adsorption-desorption isotherms of the Au/MgO(CTAB) low surface area catalyst before (blue isotherm) and after (red isotherm) reaction.

The same observation can be made with the isotherms of the low surface area catalyst Au/MgO(CTAB) in fig. 62. However, the hysteresis loop of the isotherm after reaction can be noticed. Thus, there still is some adsorption of nitrogen onto the material.

6.3.5.2 Results concerning the high surface area supports and catalysts

6.3.5.2.1 Conversion, yield and selectivity

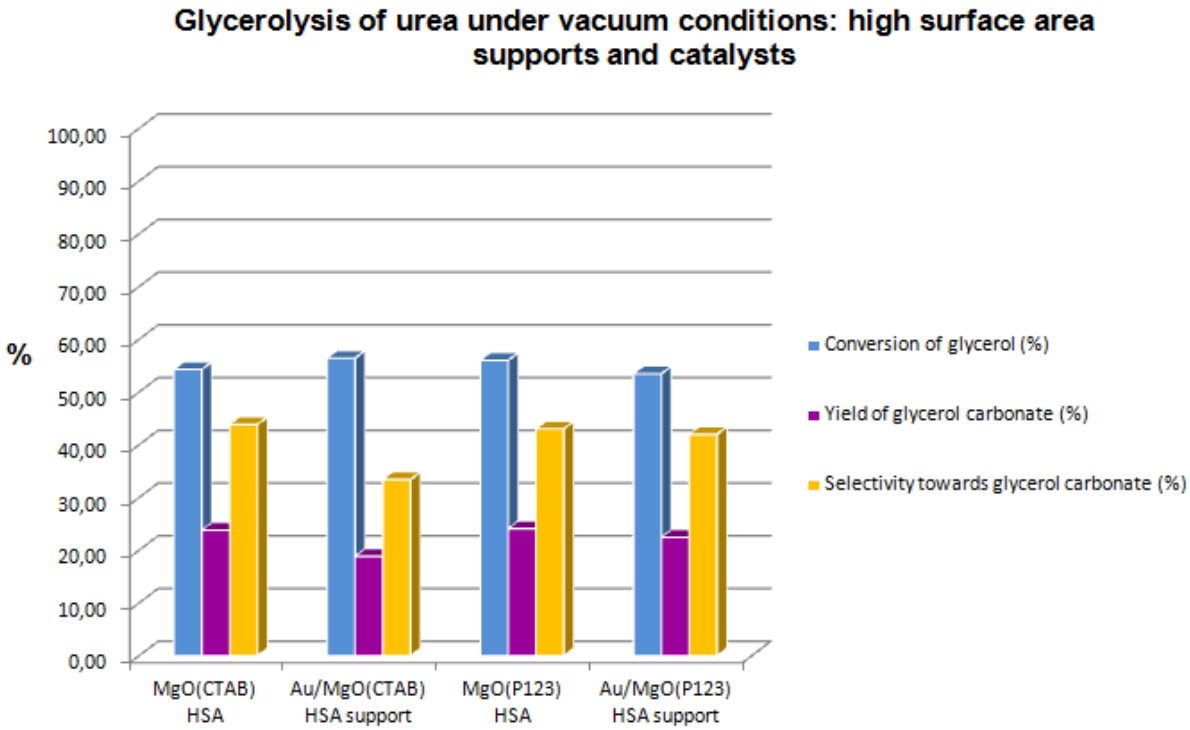

Fig. 63. Results of the reactions with the high surface area supports and catalysts under vacuum conditions.

In fig. 63, the results of the reactions with the high surface area catalysts are shown. Against the expectations, both of the high surface area catalysts do not perform very well. They both obtain conversions of around 50%, but the yield of glycerol carbonate is less than half of it causing a selectivity towards glycerol carbonate of only 40%.

6.3.5.2.2 X-ray diffraction

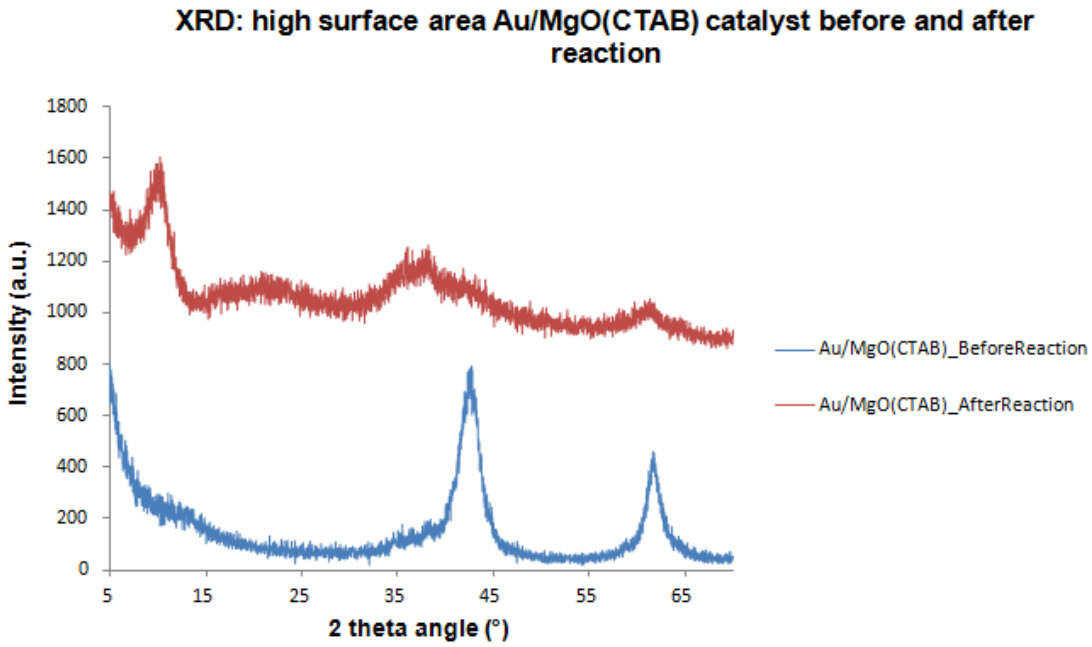

Fig. 64. XRD diffractograms of the Au/MgO(CTAB) high surface area catalyst before (blue pattern) and after (red pattern) reaction.

Fig. 64 represents the diffractograms of the high surface Au/MgO(CTAB) catalyst. The blue pattern (before reaction) suits quite well with that of periclase structured MgO. This means that after deposition of gold, a partial rehydration of the periclase phase to brucite may not have been occurred. Another observation is that there is a strong modification in the crystal structure of this high surface catalyst after reaction: the structure is converted into an almost amorphous structure. Remarkably, this phenomenon does not appear with the other catalysts. The peak situated at the early angle of 10° occurs again. The possible explanation is already clarified in a previous subchapter (6.3.3.2.2).

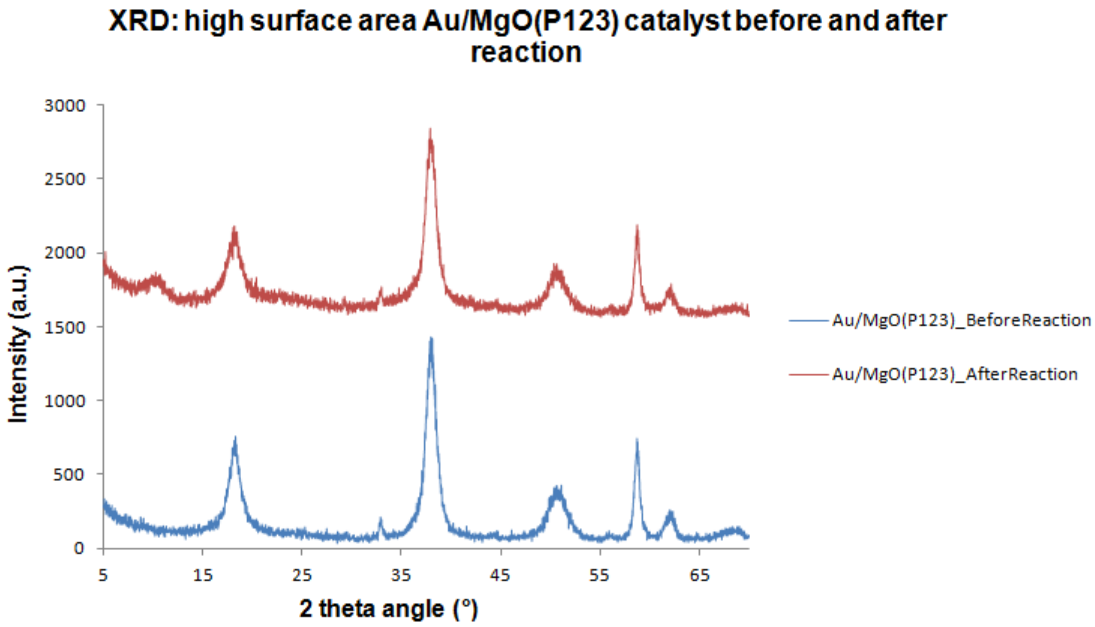

Fig. 65. XRD diffractograms of the Au/MgO(P123) high surface area catalyst before (blue pattern) and after (red pattern) reaction.

Fig. 65 shows the XRD patterns of the Au/MgO(P123) catalyst with a high surface area. The same observation can be made as in (5.3.3.1).

6.3.5.2.3 X-ray fluorescence

Sample preparation and calculations to determine the loading of gold on the Au/MgO catalysts are done the same way as in subchapter 5.3.2.3.

The deposition of gold on both high surface area support materials went very well since the gold percentages are situated very close to the theoretical value of 1%. However, leaching percentages are quite high. This could be due to the high surface area of the catalyst. Reaction products can precipitate onto the surface of the supports and either suffocate the gold nanoparticles, or drag the gold nanoparticles away with them during washing of the catalyst after reaction with acetone.

Table 13. Leaching percentages of the high surface area catalysts.

Low surface area catalyst	Loading of gold before reaction (%)	Loading of gold after reaction (%)	% leaching
Au/MgO(P123)_HSA	0,88	0,63	28
Au/MgO(CTAB)_HSA	0,98	0,38	61

6.3.5.2.4 Nitrogen adsorption

Table 14 shows the BET surface area of the high surface area catalysts. The same remark can be made as in 6.3.5.1.5 for the Au/MgO(CTAB) catalyst. After gold deposition, the surface area is higher than before. This is not the case with the Au/MgO(P123) catalyst. After use, the surface area decreases until approximately half of its value before reaction.

Table 14. BET surface area of the high surface area gold catalysts before gold deposition, before reaction and after reaction.

Catalyst	BET surface area (m^2/g)		
	Before deposition of gold	**Before Reaction**	**After reaction**
Au/MgO(P123)_HSA	187	140	67
Au/MgO(CTAB)_HSA	185	232	166

The nitrogen adsorption-desorption isotherms of the high surface area Au/MgO(P123) catalyst are shown in fig. 66. Remarkably, it is noticed that the hysteresis loop of the curve after reaction is bigger than that of the isotherm before reaction. This is not the case with the isotherms of the Au/MgO(CTAB) catalyst (fig. 67). After reaction, the quantity adsorbed nitrogen is very low and the hysteresis loop is very thin.

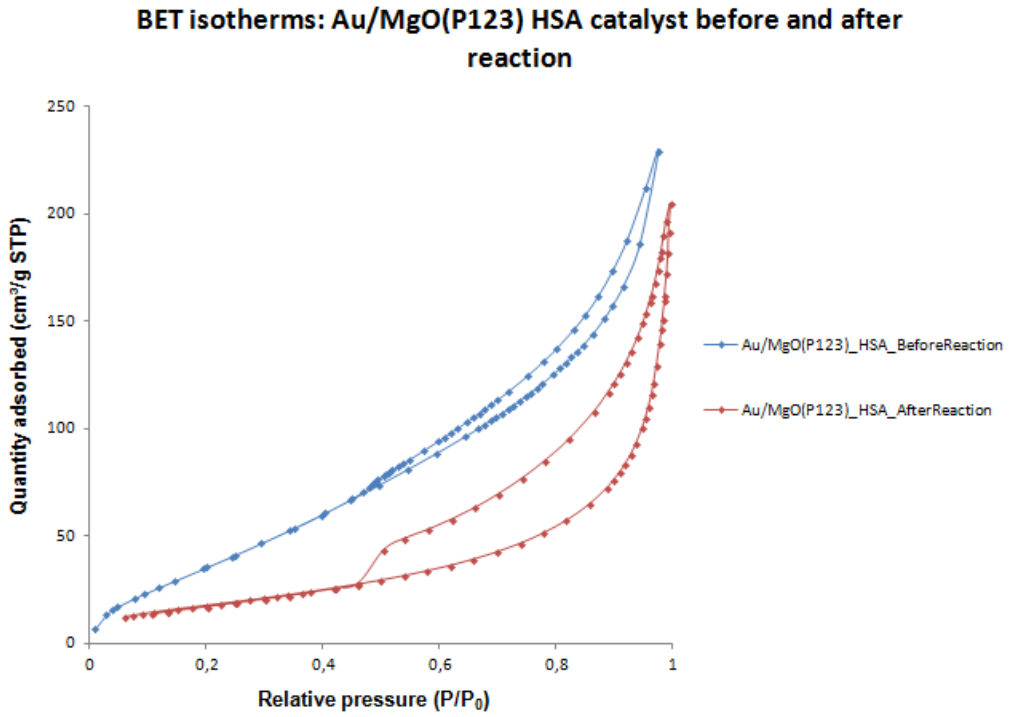

Fig. 66. BET isotherms of the Au/MgO(P123) high surface area catalyst before (blue isotherm) and after (red isotherm) reaction.

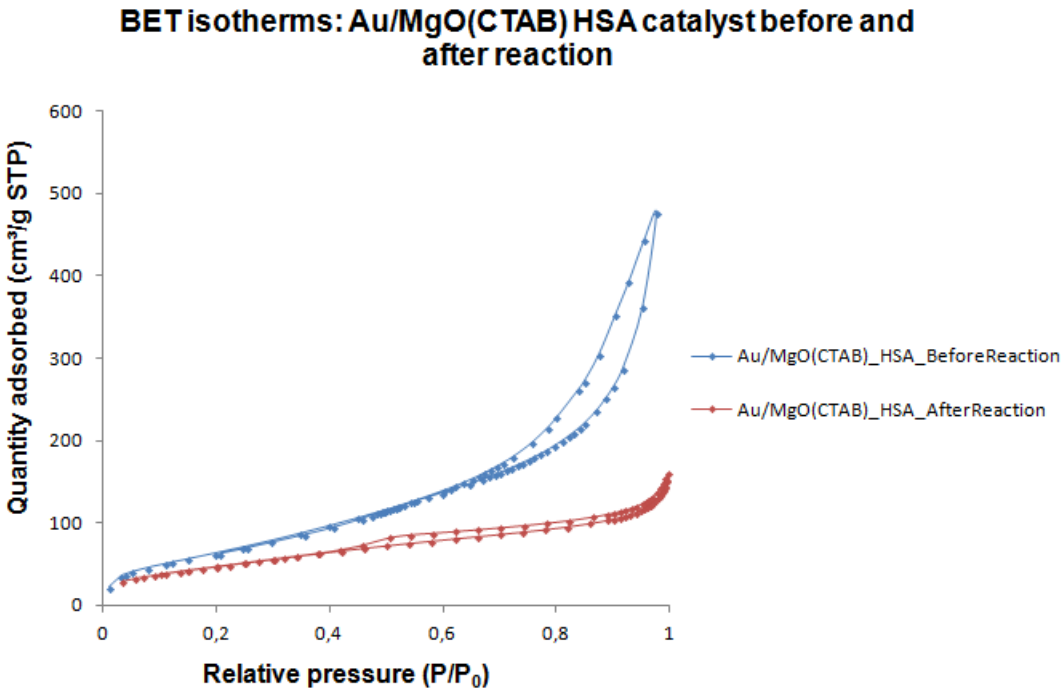

Fig. 67. BET isotherms of the Au/MgO(CTAB) high surface area catalyst before (blue isotherm) and after (red isotherm) reaction.

7 General conclusion

The goal of this thesis was to prepare suitable magnesium oxide supports and impregnate them with gold nanoparticles. Then, the Au/MgO catalysts were utilized for the catalysis of the glycerolysis of urea forming glycerol carbonate. Glycerol carbonate is an important glycerol derivative and a valuable chemical in many industries. This catalytic reaction is a sustainable way to produce glycerol carbonate, since glycerol is a by-product of the biodiesel production and urea represents an activated form of CO_2. Thus, both raw chemicals are affordable and easily available.

Magnesium oxide supports with different morphologies were made by a hydrothermal dissolution-recrystallization method. With this soft templating method two different kinds of surfactants were used as template: CTAB and P123. The two most promising MgO supports regarding their surface area were selected and deposited with gold.

The deposition of gold happened through a deposition-precipitation method using urea as precipitation agent. Small gold nanoparticles on the surface of the magnesium oxide support were obtained. After deposition it was observed with XRD that the MgO support partially regained the brucite structure.

As a result of an error in the synthesis method, low and high surface area gold catalysts were obtained. All the catalysts were used for the glycerolysis of urea producing glycerol carbonate. First, the reaction was executed with the Au/CommMgO catalyst and the respective support under bubbling vacuum condition in order to have a reference and to gain experience on the reaction procedure. However, conversion, yield and selectivity were practically the same for both the support and the catalyst. Thus, there was decided to do the rest of the reactions with the synthesized catalysts under vacuum conditions. Against the expectations, the low surface area catalysts performed better in terms of yield and selectivity than the high surface area catalysts. The best results were obtained by the Au/MgO(P123) low surface area catalyst with a conversion of 50%, a yield of 34% and a selectivity of 69%. According to the state of the art on the glycerolysis of urea with the Au/MgO catalyst, a conversion of 80% a yield of 55% and a selectivity of 70% are obtained under bubbling nitrogen conditions. [34]

So in this thesis, better results in comparison with the state of the art could not be achieved. However, nearly the same selectivity is obtained with the best catalyst.

8 Future prospects

If there was more time, I would really do some additional characterization and tests in order to improve the results concerning the catalytic reaction, the glycerolysis of urea.

To begin with, I would characterize the catalysts with temperature-programmed desorption to get information about the Lewis acid and basic places of the catalyst. Hence, more knowledge would be obtained about the activity of the gold catalyst.

Moreover, I would analyse the gold catalysts with X-ray photoelectron spectroscopy (XPS) in order to have knowledge regarding the oxidation state of the gold nanoparticles on the surface of the magnesium oxide support.

In addition, I could characterize the reaction mixture after catalysis with nuclear magnetic resonance (NMR) to find out the formed by-products during the glycerolysis of urea.

Furthermore, in order to remove all of the organic material out of the catalyst after reaction, I would wash the catalyst with acetone by means of a Soxhlet extraction and afterwards recalcine the material again at 300°C for three hours. In this way, the catalyst could regain some of its activity necessary for a successful second run. But, this procedure would only make sense if the leaching of the gold is reasonable.

Finally I would ‘play’ more with the reaction conditions such as the duration of the reaction, the reaction temperature and the glycerol/urea molar ratio. However, those parameters could lead to the formation of more by-products.

List of figures

List of tables

Reference list

1. Lertlukkanasuk, N., et al. (2013). "Reactive distillation for synthesis of glycerol carbonate via glycerolysis of urea." Chemical Engineering and Processing **70**: 103-109.
2. Hammond, C., et al. (2011). "Synthesis of glycerol carbonate from glycerol and urea with gold-based catalysts." Dalton Transactions **40**(15): 3927-3937.
3. Rubio-Marcos, F., et al. (2010). "Novel hierarchical Co_3O_4/ZnO mixtures by dry nanodispersion and their catalytic application in the carbonylation of glycerol." Journal of Catalysis **275**(2): 288-293.
4. Zheng, L., et al. (2014). "Transesterification of glycerol with dimethyl carbonate over Mg-Al hydrotalcites." Chinese Journal of Catalysis **35**(3): 310-318.
5. Climent, M. J., et al. (2010). "Chemicals from biomass: Synthesis of glycerol carbonate by transesterification and carbonylation with urea with hydrotalcite catalysts. The role of acid-base pairs." Journal of Catalysis **269**(1): 140-149.
6. Sonnati, M. O., et al. (2013). "Glycerol carbonate as a versatile building block for tomorrow: synthesis, reactivity, properties and applications." Green Chemistry **15**(2): 283-306.
7. Ochoa-Gomez, J. R., et al. (2012). "A Brief Review on Industrial Alternatives for the Manufacturing of Glycerol Carbonate, a Green Chemical." Organic Process Research & Development **16**(3): 389-399.
8. Li, J. and T. Wang (2011). "Chemical equilibrium of glycerol carbonate synthesis from glycerol." Journal of Chemical Thermodynamics **43**(5): 731-736.
9. Du, M., et al. (2012). "Synthesis of glycerol carbonate from glycerol and dimethyl carbonate catalyzed by K_2CO_3/MgO." Research on Chemical Intermediates **38**(3-5): 1069-1077.
10. Bai, R., et al. (2011). "Synthesis of glycerol carbonate from glycerol and dimethyl carbonate catalyzed by KF modified hydroxyapatite." Journal of Industrial and Engineering Chemistry **17**(4): 777-781.
11. Zhou, C. H., et al. (2013). "Recent Advances in Catalytic Conversion of Glycerol." Catalysis Reviews-Science and Engineering **55**(4): 369-453.
12. Xiang, X., et al. (2012). "Urea formation from carbon dioxide and ammonia at atmospheric pressure." Environmental Chemistry Letters **10**(3): 295-300.
13. Srinivas, B., et al. (2012). "Photocatalytic Synthesis of Urea from in situ Generated Ammonia and Carbon Dioxide." Photochemistry and Photobiology 88(2): 233-241.
14. Bruice, P. Y. (2011). Organic Chemistry, Pearson.
15. Verberckmoes, A. (2014). Fysicochemie II.
16. Verberckmoes, A. (2011). Aanvullingen Chemie II: Partim Organische Chemie.

17. Parlett, C. M. A., et al. (2013). "Hierarchical porous materials: catalytic applications." Chemical Society Reviews 42(9): 3876-3893.

18. Fujita, S.-i., et al. (2013). "Synthesis of glycerol Carbonate from glycerol and urea using zinc-containing solid catalysts: A homogeneous reaction." Journal of Catalysis **297**: 137-141.

19. Okutsu, M. and Kitsuki, T. (2000). Japanese Patent. No. 0001072.

20. Aresta, M., et al. (2009). "Valorization of bio-glycerol: New catalytic materials for the synthesis of glycerol carbonate via glycerolysis of urea." Journal of Catalysis **268**(1): 106-114.

21. Clearfie.A, et al. (1968). "New crystalline phases of zirconium phosphate possessing ion-exchange properties." Journal of Inorganic & Nuclear Chemistry **30**(8): 2249-&.

22. Yamanaka, S. and M. Tanaka (1979). "Formation region and structural model of gamma-zirconium phosphate." Journal of Inorganic & Nuclear Chemistry **41**(1): 45-48.

23. Clearfield, A. and Smith, S.D. (1968). “The Crystal Structure of Zirconium Phosphate and the Mechanism of Its Ion Exchange Behavior.” Journal of Colloid and Interface Science 28(2): 325-330.

24. Schroeder, S. and G., M (2002). Temperature-Programmed Desorption (TPD)/Thermal Desorption Spectroscopy (TDS). A. P. C. Laboratory. Berlin.

25. Rubio-Marcos, F., et al. (2013). "Control of the Interphases Formation Degree in Co3O4/ZnO Catalysts." Chemcatchem **5**(6): 1431-1440.

26. Wang, L., et al. (2011). "Efficient synthesis of glycerol carbonate from glycerol and urea with lanthanum oxide as a solid base catalyst." Catalysis Communications **12**(15): 1458-1462.

27. Valange, S., et al. (2007). "Lanthanum oxides for the selective synthesis of phytosterol esters: Correlation between catalytic and acid-base properties." Journal of Catalysis **251**(1): 113-122.

28. Zhang, F., et al. (2008). "Layered Double Hydroxides as Catalytic Materials: Recent Development." Catalysis Surveys from Asia **12**(4): 253-265.

29. Liu, P., et al. (2014). "Promotional effect of transition metal doping on the basicity and activity of calcined hydrotalcite catalysts for glycerol carbonate synthesis." Applied Catalysis B-Environmental **144**: 135-143.

30. Sun, Y., et al. (2014). "A Sustainable Preparation of Glycerol Carbonate from Glycerol and Urea Catalyzed by Hydrotalcite-Like Solid Catalysts." Energy Technology **2**(3): 263-268.

31. Kannan, S. (2006). "Catalytic applications of hydrotalcite-like materials and their derived forms." Catalysis Surveys from Asia **10**(3-4): 117-137.

32. Prescott, H. A., et al. (2005). "Application of calcined Mg-Al hydrotalcites for Michael additions: an investigation of catalytic activity-and acid-base properties." Journal of Catalysis **234**(1): 119-130.

33. Takehira, K. and T. Shishido (2007). "Preparation of supported metal catalysts starting from hydrotalcites as the precursors and their improvements by adopting "memory effect"." Catalysis Surveys from Asia **11**(1-2): 1-30.

34. Ab Rahim, M. H., et al. (2012). "Gold, palladium and gold-palladium supported nanoparticles for the synthesis of glycerol carbonate from glycerol and urea." Catalysis Science & Technology **2**(9): 1914-1924.

35. Stratakis, M. and H. Garcia (2012). "Catalysis by Supported Gold Nanoparticles: Beyond Aerobic Oxidative Processes." Chemical Reviews **112**(8): 4469-4506.

36. Wan, X., et al. (2013). “Magnesia-supported gold nanoparticles as efficient catalysts for oxidative esterification of aldehydes or alcohols with methanol to methyl esters.” Catalysis today **233**: 147-154.

37. Boronat, M., et al. (2011). "Mechanism of selective alcohol oxidation to aldehydes on gold catalysts: Influence of surface roughness on reactivity." Journal of Catalysis **278**(1): 50-58.

38. Carabineiro, S. A. C., et al. (2011). "Gold nanoparticles supported on magnesium oxide for CO oxidation." Nanoscale Research Letters **6**.

39. Okumura, M., et al. (2003). "Preparation of supported gold catalysts by gas-phase grafting of gold acethylacetonate for low-temperature oxidation of CO and of H_2." Journal of Molecular Catalysis a-Chemical **199**(1-2): 73-84.

40. Guzman, J. and B. C. Gates (2004). "Catalysis by supported gold: Correlation between catalytic activity for CO oxidation and oxidation states of gold." Journal of the American Chemical Society **126**(9): 2672-2673.

41. Yoon, B., et al. (2005). "Charging effects on bonding and catalyzed oxidation of CO on Au-8 clusters on MgO." Science **307**(5708): 403-407.

42. Minico, S., et al. (1997). "FT-IR study of Au/Fe_2O_3 catalysts for CO oxidation at low temperature." Catalysis Letters **47**(3-4): 273-276.

43. Hao, Z. P., et al. (2000). "Mechanism of gold activation in supported gold catalysts for CO oxidation." Reaction Kinetics and Catalysis Letters **70**(1): 153-160.

44. Haruta, M. (2002). "Catalysis of gold nanoparticles deposited on metal oxides." Cattech **6**(3): 102-115.

45. Geoffrey C. Bond, C. L., David T. Thompson (2006). Catalysis by gold. London, Imperial College press.

46. Stocker, M. (1996). "X-ray photoelectron spectroscopy on zeolites and related materials." Microporous Materials **6**(5-6): 235-257.

47. Huang, X.-S., et al. (2009). "Morphology effects of nanoscale ceria on the activity of Au/CeO_2 catalysts for low-temperature CO oxidation." Applied Catalysis B-Environmental **90**(1-2): 224-232.

48. Gluhoi, A. C. (2005). Fundamental studies focused on understanding of gold catalysis. The Netherlands, Leiden University. **Doctor:** 205.

49. Samodi, A., et al. (2013). "Effects of surfactants, solvents and time on the morphology of MgO nanoparticles prepared by the wet chemical method." Materials Letters **109**: 269-274.

50. Sun, R.-Q., et al. (2008). "Synthesizing nanocrystal-assembled mesoporous magnesium oxide using cotton fibres as exotemplate." Microporous and Mesoporous Materials **111**(1-3): 314-322.

51. Margitfalvi, J. L., et al. (2002). "Au/MgO catalysts modified with ascorbic acid for low temperature CO oxidation." Catalysis Today **72**(1-2): 157-169.

52. Koo, K. Y., et al. (2014). "A highly dispersed Pt/gamma-Al2O3 catalyst prepared via deposition-precipitation method for preferential CO oxidation." International Journal of Hydrogen Energy **39**(11): 5696-5703.

53. Costa, V. V., et al. (2012). "Gold nanoparticles supported on magnesium oxide as catalysts for the aerobic oxidation of alcohols under alkali-free conditions." Journal of Catalysis **292**: 148-156.

54. Pradeep, T. and Anshup (2009). "Noble metal nanoparticles for water purification: A critical review." Thin Solid Films **517**(24): 6441-6478.

55. Pradeep, T. and Nair, A. (2007). Indian Patent. No. 200767.

56. Tang, C., et al. (2014). "Efficient fabrication of active CuO-CeO_2/SBA-15 catalysts for preferential oxidation of CO by solid state impregnation." Applied Catalysis B-Environmental **146**: 201-212.

57. Chen, C. L., et al. (2001). "Direct impregnation method for preparing sulfated zirconia supported on mesoporous silica." Microporous and Mesoporous Materials **50**(2-3): 201-208.

58. Sun, J., et al. (2014). "Comparative study on the catalytic CO oxidation properties of CuO/CeO_2 catalysts prepared by solid state and wet impregnation." Chinese Journal of Catalysis **35**(8): 1347-1358.

59. Xiong, H., et al. (2014). "Comparison of impregnation and deposition precipitation for the synthesis of hydrothermally stable niobia/carbon." Applied Catalysis a-General **471**: 165-174.

60. Koo, K. Y., et al. (2014). "A highly dispersed Pt/gamma-Al_2O_3 catalyst prepared via deposition-precipitation method for preferential CO oxidation." International Journal of Hydrogen Energy **39**(11): 5696-5703.

61. Park, H., et al. (2009). "Surface passivation of highly ordered TiO_2 nanotube arrays and application to dye-sensitized solar cells using the concept of isoelectric point." Journal of the Ceramic Society of Japan **117**(1365): 596-599.

62. Estrada, M., et al. (2014). "Aerobic oxidation of benzyl alcohol in methanol solutions over Au nanoparticles: $Mg(OH)_2$ vs MgO as the support." Applied Catalysis a-General **473**: 96-103.

63. Zhang, R., et al. (2012). "Mesoporous titania: From synthesis to application." Nano Today **7**(4): 344-366.

64. Vivero-Escoto, J. L., et al. (2012). "Recent progress in mesoporous titania materials: adjusting morphology for innovative applications." Science and Technology of Advanced Materials **13**(1).

65. Villar-Rodil, S., et al. (2005). "Activated carbon materials of uniform porosity from polyaramid fibers." Chemistry of Materials **17**(24): 5893-5908.

66. Mohamed, M. M., et al. (2007). "Synthesis of micro-mesoporous TiO_2 materials assembled via cationic surfactants: Morphology, thermal stability and surface acidity characteristics." Microporous and Mesoporous Materials **103**(1-3): 174-183.

67. Yokoi, T. and T. Tatsumi (2007). "Synthesis of mesoporous silica materials by using anionic surfactants as template." Journal of the Japan Petroleum Institute **50**(6): 299-311.

68. Wan, Y., et al. (2007). "Designed synthesis of mesoporous solids via nonionic-surfactant-templating approach." Chemical Communications(9): 897-926.

69. Wei-Dong, X., et al. (2008). "Preparation of mesoporous silica using amphoteric surfactant potassium and sodium N-dodecyl glycine template." Journal of the American Ceramic Society **91**(5): 1517-1521.

70. Pal, N. and A. Bhaumik (2013). "Soft templating strategies for the synthesis of mesoporous materials: Inorganic, organic-inorganic hybrid and purely organic solids." Advances in Colloid and Interface Science **189**: 21-41.

71. Gu, D. and F. Schueth (2014). "Synthesis of non-siliceous mesoporous oxides." Chemical Society Reviews **43**(1): 313-344.

72. Chen, D. and R. A. Caruso (2013). "Recent Progress in the Synthesis of Spherical Titania Nanostructures and Their Applications." Advanced Functional Materials **23**(11): 1356-1374.

73. Mahoney, L. and R. T. Koodali (2014). "Versatility of Evaporation-Induced Self-Assembly (EISA) Method for Preparation of Mesoporous TiO_2 for Energy and Environmental Applications." Materials **7**(4): 2697-2746.

74. Nagappa, B. and G. T. Chandrappa (2007). "Mesoporous nanocrystalline magnesium oxide for environmental remediation." Microporous and Mesoporous Materials **106**(1-3): 212-218.

75. Rezaei, M., et al. (2011). "Preparation of nanocrystalline MgO by surfactant assisted precipitation method." Materials Research Bulletin **46**(10): 1632-1637.

76. Simanjuntak, F. S. H., et al. (2014). "Surfactant-assisted synthesis of MgO: Characterization and catalytic activity on the transesterification of dimethyl carbonate with glycerol." Applied Catalysis a-General **484**: 33-38.

77. Wang, G., et al. (2008). "P123-assisted hydrothermal synthesis and characterization of rectangular parallelepiped and hexagonal prism single-crystalline MgO with three-dimensional wormholelike mesopores." Inorganic Chemistry **47**(10): 4015-4022.

78. Callister, W. D. and D. G. Rethwisch (2009). Materials Science and Engineering: An Introduction, John Wiley & Sons Canada, Limited.

79. Schaubroeck, J. (2012). Instrumentele analyse I.

80. Jones, F.W., (1937). "The measurement of particle size by the X-ray method."

81. KD, V.-P. (2000). "Scanning Electron Microscopy: an introduction." Elsevier science Ltd.

82. Joy, D. C. (1991). "The theory and practice of high-resolution scanning electron-microscopy." Ultramicroscopy **37**(1-4): 216-233.

83. Joy, D. C. and J. B. Pawley (1992). " high-resolution scanning electronmicroscopy." Ultramicroscopy **47**(1-3): 80-100.

84. FEI (2010). An introduction to electron microscopy.

85. KD, V.-P. (2000). "TEM: an introduction." Elsevier science Ltd.

86. Leofanti, G., et al. (1998). "Surface area and pore texture of catalysts." Catalysis Today **41**(1-3): 207-219.

87. ."Fundamentals and Practice of XRF Analysis." 2013, from http://www.scribd.com/doc/130346648/Introduzione-alla-Spettrometria-XRF-pdf#scribd

88. Owen, T. (2000). Fundamentals of UV-visible spectroscopy. Germany, Agilent Technologies.

89. Mitchell, M. B. (1993). "Fundamentals and applications of diffuse-reflectance infrared fourier-transform (DRIFT) spectroscopy." Advances in Chemistry Series(236): 351-375.

90. Suzuki, E. M. and W. R. Gresham (1986). "Forensic-science applications of diffuse reflectance infrared fourier-transform spectroscopy (DRIFTS). 1. Principles, sampling methods and advantages." Journal of Forensic Sciences **31**(3): 931-952.

91. Schaubroeck, J. (2012). Analytische Chemie, Chemische Analyse.

92. Yan, L., et al. (2002). "Formation of rod-like $Mg(OH)_2$ nanocrystallites under hydrothermal conditions and the conversion to MgO nanorods by thermal dehydration." Materials Chemistry and Physics **76**(2): 119-122.

93. Dhaouadi, H., et al. (2011). "$Mg(OH)_2$ Nanorods Synthesized by A Facile Hydrothermal Method in the Presence of CTAB." Nano-Micro Letters **3**(3): 153-159.

94. Cui, H., et al. (2014). "Synthesis and characterization of mesoporous MgO by template-free hydrothermal method." Materials Research Bulletin **50**: 307-311.

95. Ding, Y., et al. (2001). "Nanoscale magnesium hydroxide and magnesium oxide powders: Control over size, shape, and structure via hydrothermal synthesis." Chemistry of Materials **13**(2): 435-440.

96. Lee, S.-D., et al. (2014). "Catalytic performance of ion-exchanged montmorillonite with quaternary ammonium salts for the glycerolysis of urea." Catalysis Today **232**: 127-133.

Appendix

Annex 1: X-ray fluorescence calibration curve

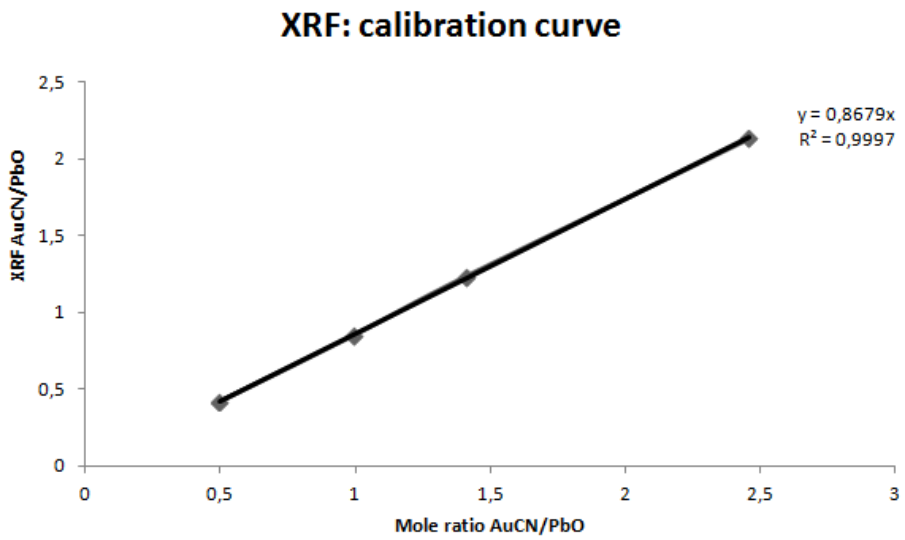

Fig. 68. Calibration curve XRF.

Annex 2: Gas chromatography calibration curve for glycerol

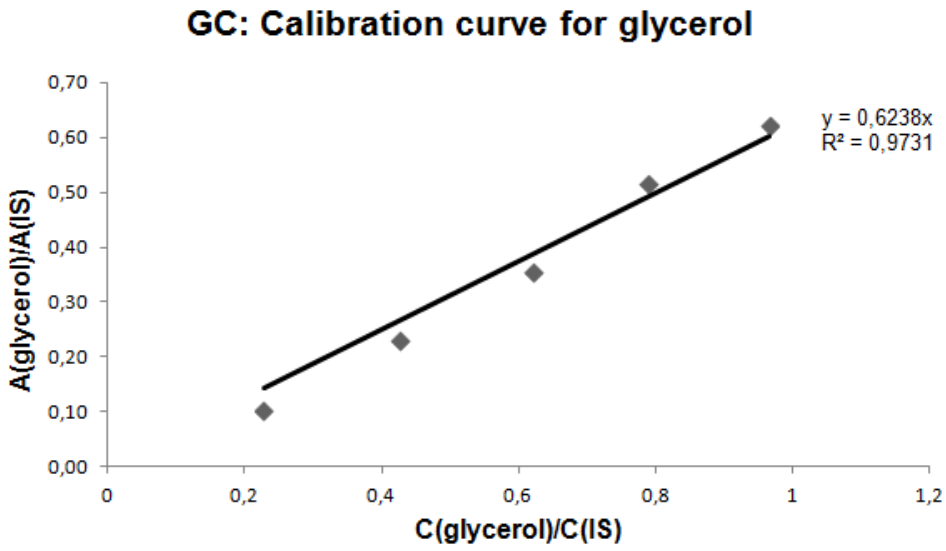

Fig. 69. Calibration curve for glycerol.

Annex 3: Gas chromatography calibration curve for glycerol carbonate

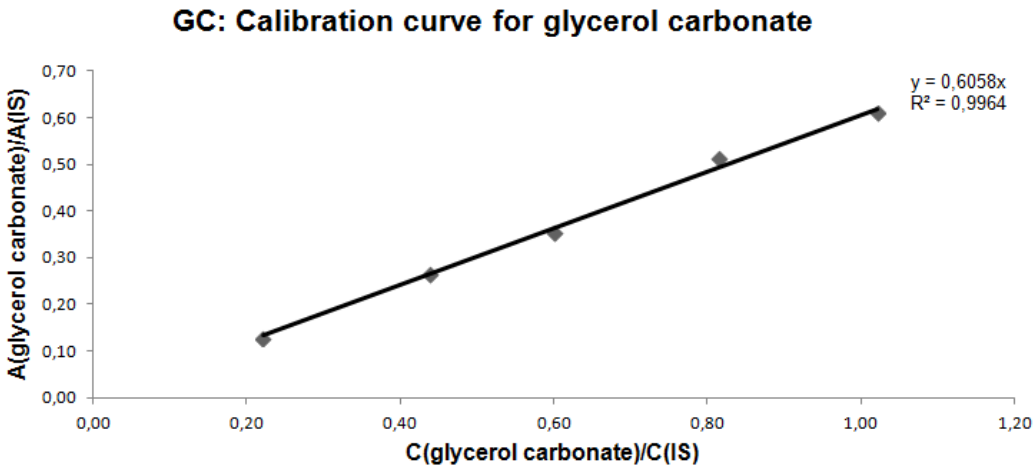

Fig. 70. Calibration curve for glycerol carbonate.

Annex 4: GC-MS

GC-MS analysis is executed in order to try to identify the possible side products which can be formed during the glycerolysis of urea (fig. 71).

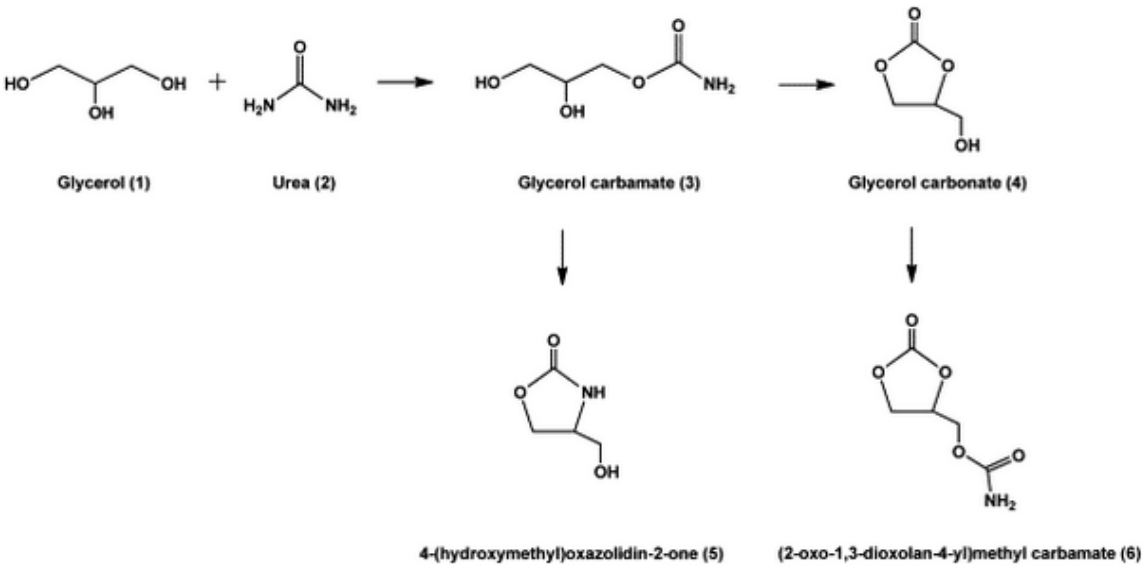

Fig. 71. Possible reaction steps for the glycerolysis of urea. [96]

Peak 1 at Retention Time 8.51

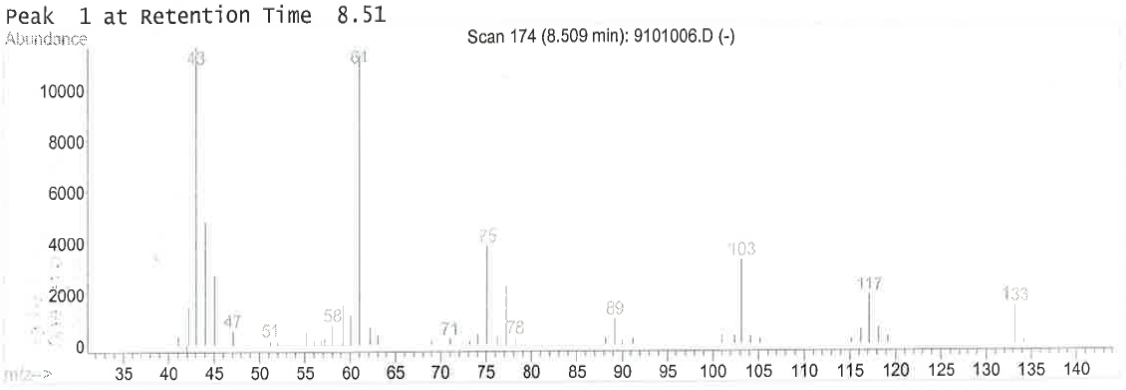

Peak 2 at Retention Time 9.36

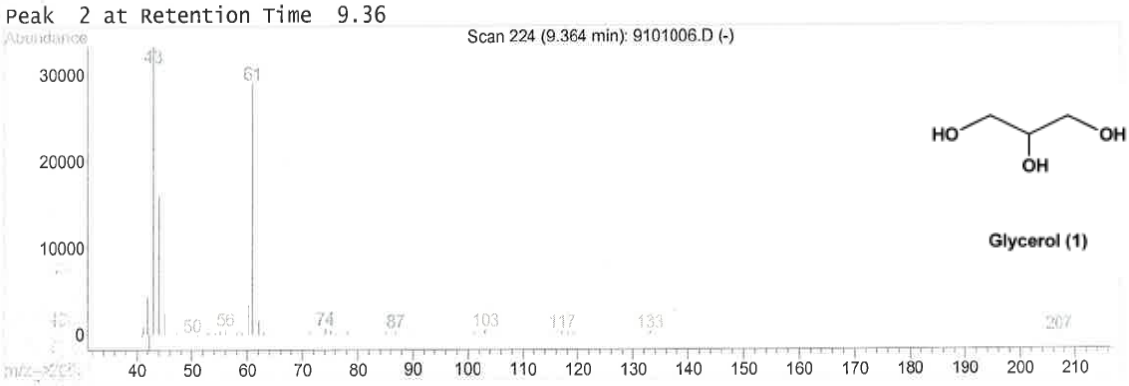

Glycerol (1)

Peak 3 at Retention Time 11.60

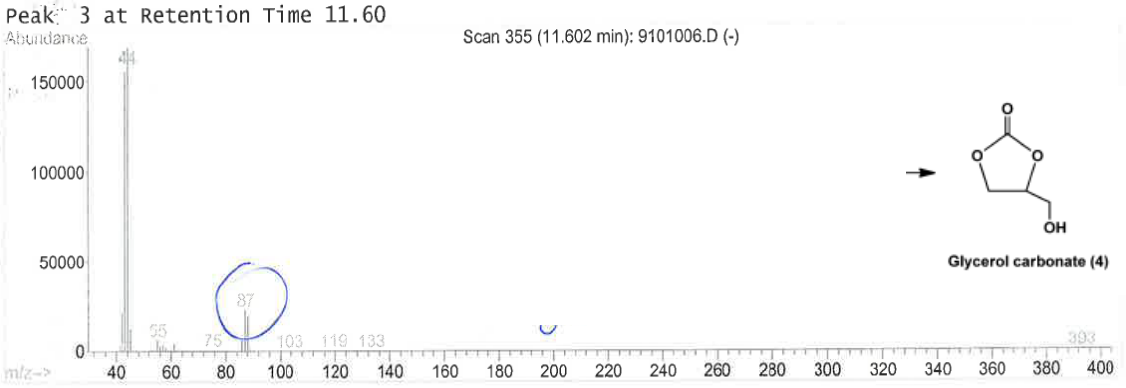

Glycerol carbonate (4)

Peak 4 at Retention Time 13.07

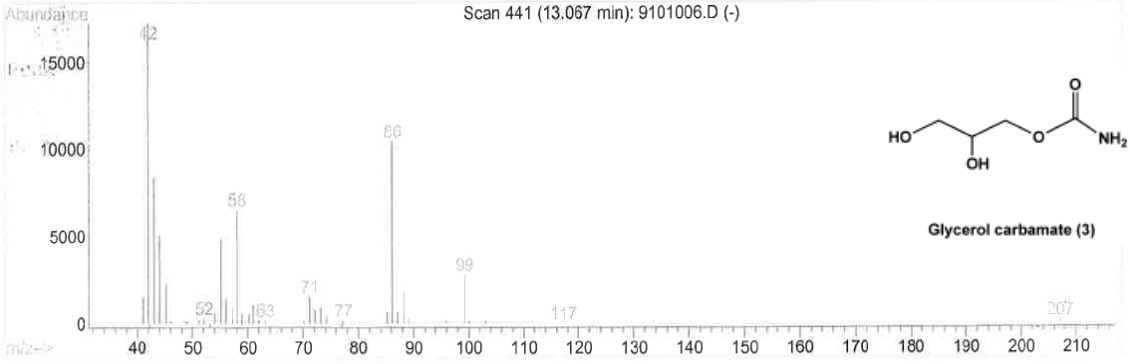

Glycerol carbamate (3)

Peak 5 at Retention Time 13.41

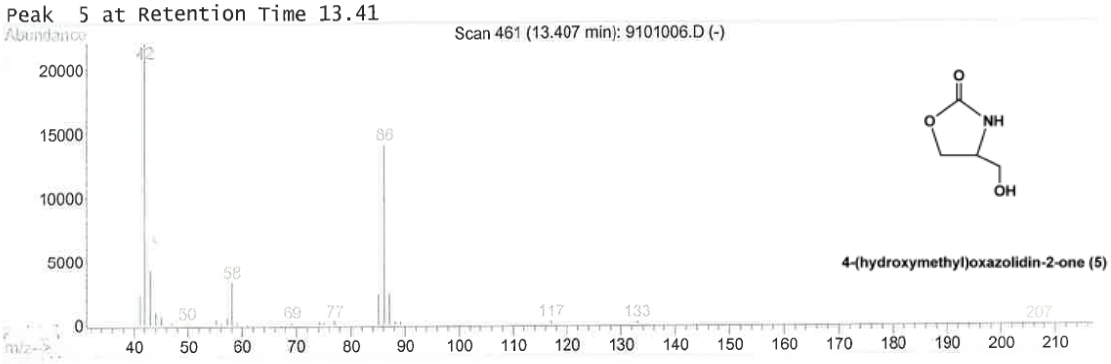

Peak 6 at Retention Time 13.65

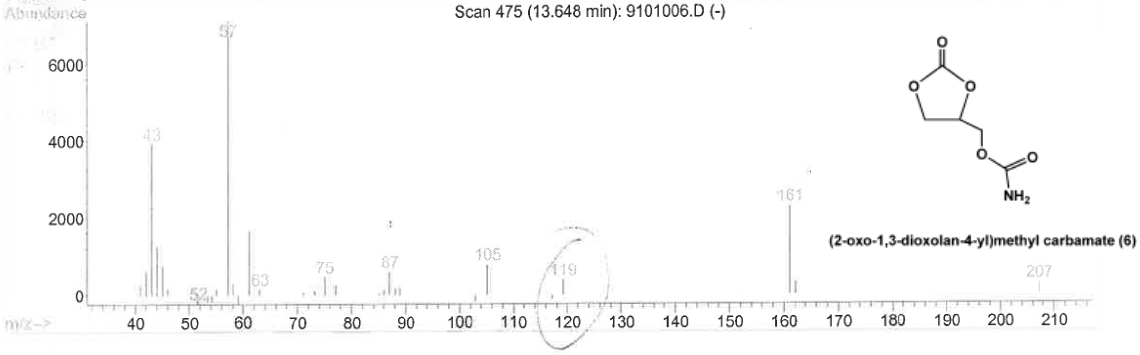

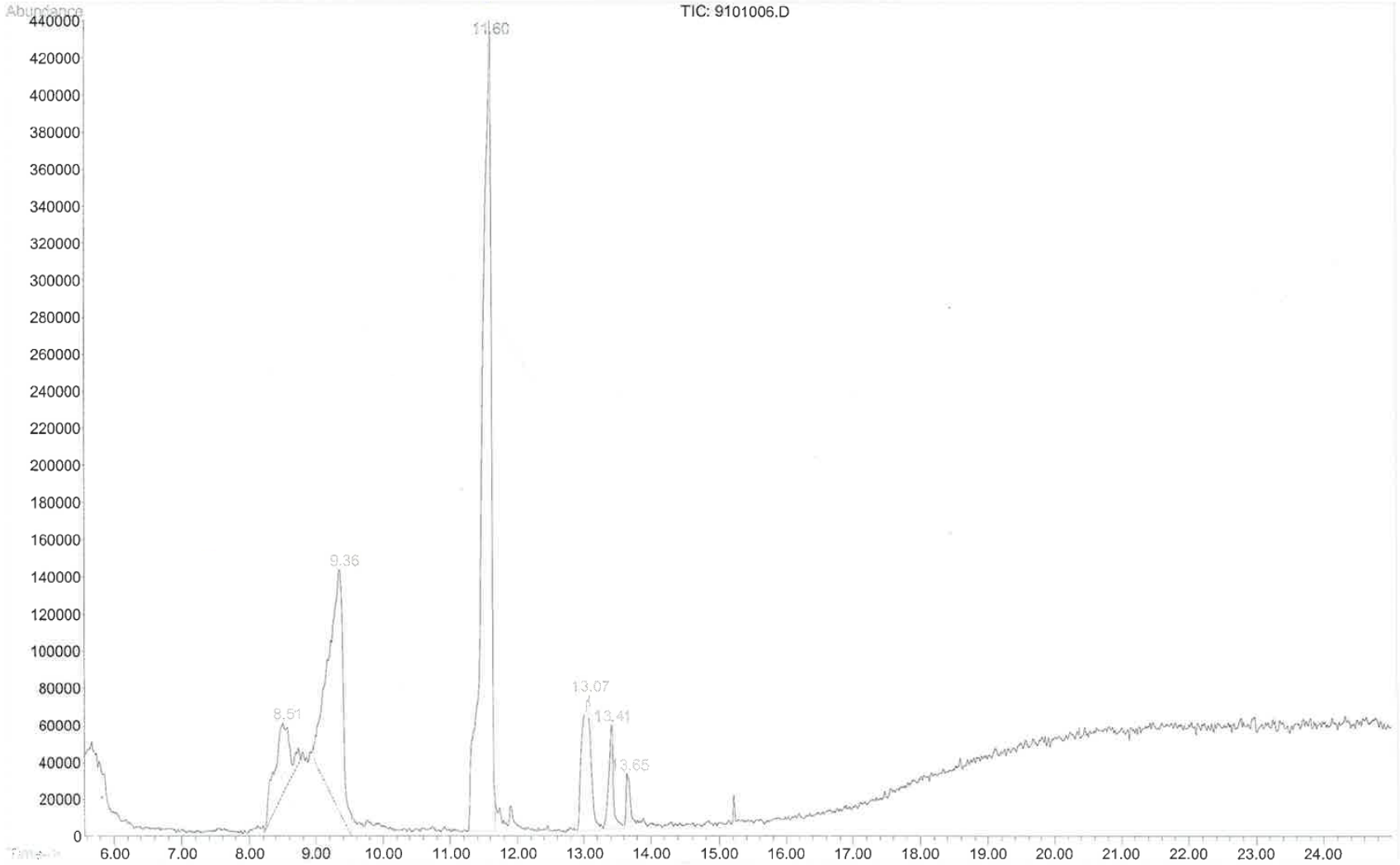
TIC: 9101006.D
Abundance
440000
420000
400000
380000
360000
340000
320000
300000
280000
260000
240000
220000
200000
180000
160000
140000
120000
100000
80000
60000
40000
20000
0
11.60
9.36
8.51
13.07
13.41
13.65
6.00
7.00
8.00
9.00
10.00
11.00
12.00
13.00
14.00
15.00
16.00
17.00
18.00
19.00
20.00
21.00
22.00
23.00
24.00